RESEARCH TECHNICAL REPORT

Experimental Data for Model Validation of Smoke Transport in Data Centers

FM Global®

Experimental Data for Model Validation of Smoke Transport in Data Centers

by

Sai Thumuluru, Benjamin Ditch, Prateep Chatterjee and Marcos Chaos

September 2014

FM Global
1151 Boston-Providence Turnpike
Norwood, MA 02062

Project ID 0003048373

DISCLAIMER

The research presented in this report, including any findings and conclusions, is for informational purposes only. Any references to specific products, manufacturers, or contractors do not constitute a recommendation, evaluation or endorsement by Factory Mutual Insurance Company (FM Global) of such products, manufacturers or contractors. FM Global makes no warranty, express or implied, with respect to any product or process referenced in this report. FM Global assumes no liability by or through the use of any information in this report.

EXECUTIVE SUMMARY

A large-scale experimental study was conducted to provide data on the smoke transport in data centers involving high airflow rates and the corresponding response of multiple types of smoke detectors. The primary objective of this study was to provide an experimental dataset for validation of computational fluid dynamics (CFD) models. This report describes testing conducted in a representative data center involving a characteristic confined cold aisle design. The experiments included a) characterization of airflow with detailed velocity measurements and b) smoke concentration measurements and response of smoke detectors to various smoke sources. All testing was conducted at the FM Global Research Campus in West Glocester, Rhode Island, USA.

This study was conducted in partnership with the National Fire Protection Association's (NFPA) Fire Protection Research Foundation (FPRF)[i]. Hughes Associates Inc. (HAI) was selected as the FPRF project contractor on CFD modeling of smoke transport. The principal objective was to provide recommendations to code standards on placement of smoke detectors in data centers. The project was divided into two phases: Phase I involved identifying a suitable CFD model developed and validated to meet the overall project objectives[ii] and Phase II involved the following five tasks:

- Task 1 – Select CFD Model(s)
- Task 2 – Fire Source Characterization
- Task 3 – Detector Response Characterization
- Task 4 – Full-Scale Model Verification and Validation
- Task 5 – Perform CFD Simulations

FM Global partnered with FPRF on Task 4 to provide the first-of-its-kind experimental dataset for full-scale model validation.

---

[i] "Validation of Modeling Tools for Detection Design in High Airflow Environments, Phase 2," Project Summary prepared by the Fire Protection Research Foundation, Quincy, MA.

[ii] Gottuk, D., Floyd, J., Dinaburg, J., and Williamson, J., "Validation of Modeling Tools for Detection Design in High Airflow Environments – Final Phase I Report," prepared for Fire Protection Research Foundation, Quincy, MA, August 2012.

Current guidance for the placement of smoke detectors in large data centers can be found in FM Global Property Loss Prevention Data Sheet 5-32[iii], "Data Centers and Related Facilities," and NFPA Standard 75[iv], "Standard for the Fire Protection of Information Technology Equipment." To date, optimization of smoke detector placement in high airflow environments such as data centers has not been possible due to limited analysis on the relationship between smoke transport and smoke detector response.

The data center mock-up was developed by FM Global and agreed upon by the FPRF project panel. The mock-up consisted of three main sections: a subfloor from which the inlet air was drawn, a server room which was comprised of server cabinets separating a hot aisle and a confined cold aisle, and the ceiling plenum through which the outlet air and smoke were exhausted. The overall interior room dimensions were 7.3 m long x 4.9 m wide x 4.9 m tall (24 ft x 16 ft x 16 ft). The rationale behind choosing this facility design was to provide experimental data under a challenging scenario for model validation. Donated server cabinets were uniformly refurbished and installed to represent the airflow conditions in a real data center.

The data center was instrumented to measure the temperature and velocity of air movement, as well as the static pressure in each section of the enclosure. Measuring low levels of local smoke concentrations was a considerable challenge and for this purpose three aspirated smoke concentration meters were developed at FM Global. These smoke concentration meters used laser light extinction and gravimetric filtering methods at one location each in the subfloor, server room and the ceiling plenum.

Nine clusters of smoke detectors were placed at three locations each in the subfloor, server room, and ceiling plenum. Each cluster consisted of one aspirated smoke detector and two spot smoke detectors, for an overall twenty-seven detectors. The placement of the detectors was chosen with the objective of providing benchmark data for model validation.

[iii] "Data Centers and Related Facilities", FM Global Property Loss Prevention Data Sheet 5-32, July, 2012, Norwood, MA.
[iv] "Standard for the Fire Protection of Information Technology Equipment," National Fire Protection Association Standard 75, 2013, Quincy MA.

Testing was divided into two series. First the airflow inside each section of the test enclosure was characterized at air exchange rates of 78 and 265 air changes per hour (ACH). Over 200 airflow characterization tests were conducted with the application of an advanced three-component velocity measurement technique (sonic anemometer) at over 100 locations within the test enclosure. Pressure measurements within the enclosure were acquired to aid CFD model validation. The acquired dataset is important for establishing the baseline airflow pattern and, therefore, the smoke transport in the test setup.

The second test series involved measurements of smoke concentrations and smoke detector responses at various locations. Ten tests, involving the following four smoke sources, were conducted:

- 10 kW propylene flame (located in the hot aisle and subfloor)
- Polyethylene foam packaging material (located in the cold aisle)
- Printed circuit boards (located inside the cabinets)
- Cables (located in the subfloor)

The test results are summarized as follows:

1. Airflow measurements
   - Detailed quasi-steady airflow measurements were provided as baseline flow conditions for the validation of CFD airflow modeling.

2. Smoke concentration measurements
   - Time-dependent local smoke concentration measurements, with a well characterized propylene burner as the smoke source, were collected for validation of CFD models.
   - A novel aspirated smoke concentration meter, developed as part of this project, was shown to be effective as a point source measurement of smoke concentration with a minimum light extinction measurement limit of 2 %/m (0.61 %/ft) corresponding to a concentration of 2 mg/m^3, characteristic of smoke production in flaming combustion.
   - Good quantitative agreement was obtained between the overall smoke concentration measured by the aspirated laser system and the gravimetric samples.

- It was confirmed that different values of extinction coefficient should be used in the interpretation of light extinction data depending on the nature of the smoke being measured (i.e., smoke generated from flaming combustion versus pyrolysis).
- On a comparative basis, the propylene burner produced the highest amount of smoke followed by the cables, foam material and circuit boards. The smoke concentrations produced by the foam material and circuit boards were below the measurement threshold of the laser system.

3. Smoke detector response
    - The responses from the three types of smoke detectors at the same location showed similar trends.
    - The smoke detectors closest to the smoke source and in the direction of the exhaust flow showed the fastest response and the highest concentration. This reemphasizes the principal role of airflow in determining smoke detector response.
    - In general, a detector response does not provide information on the location of the fire source.
    - The exhaust (ceiling plenum) of the setup was the most reliable location in detecting the smoke. The detectors in the exhaust (ceiling plenum) of the test setup always showed a response irrespective of the location of the smoke source. However, they activated later than the detectors in the other sections of the setup.
    - In all cases, the increase of the air exchange rate reduces the overall magnitudes of smoke obscuration. This is mainly due to the higher mixing and dilution of the smoke from the sources at the higher air exchange rates.

In conclusion, the airflow distribution, smoke concentration and detector obscuration measurements were quantified to provide a benchmark dataset for validation of computational models designed for evaluating smoke transport and detector response in data centers.

ABSTRACT

This report details the findings of the characterization of airflow, smoke concentration and response of smoke detectors to smoke sources in data centers for model validation through large-scale tests conducted at the FM Global Research Campus in West Glocester, Rhode Island, USA. The study was conducted in partnership with the National Fire Protection Association's (NFPA) Fire Protection Research Foundation (FPRF).

A test facility of dimensions 7.3 m long x 4.9 m wide x 4.9 m tall (24 ft x 16 ft x 16 ft) representing a mockup of a data center was constructed in the Small Burn Laboratory at the FM Global Research Campus. The facility consisted of three main sections: a subfloor from which the inlet air was drawn, a server room containing two rows of server cabinets in a hot and confined cold aisle design, and the ceiling plenum through which the exhaust air was drawn. Extensive instrumentation involving bi-directional velocity probes, thermocouples, and pressure measurements was provided in the setup. A unique aspirated smoke concentration meter consisting of an Aspirated Laser and Gravimetric Filter system (developed and calibrated by FM Global) was also used to measure the smoke concentrations at locations in the subfloor, server room and ceiling plenum. Nine clusters of smoke detectors, each consisting of an aspirated detector and two spot detectors, were used to evaluate the response to four different representative smoke sources that were placed in the different sections. The selected smoke sources were a propylene burner, foam material, printed circuit boards and cables. The sources were placed at sample locations involving the subfloor, cold aisle, and hot aisle and server cabinets.

The airflow throughout the test enclosure was characterized using a 3-D sonic anemometer at over 100 locations and air exchange rates of 78 and 265 air changes per hour (ACH). A series of 10 smoke tests were then conducted at the two air exchange rates to measure evolution of smoke concentration in the facility and the smoke detector response from the four smoke sources. The results of the tests provided benchmark data for validation of computational models and emphasized the importance of the airflow pattern in the smoke transport and the smoke detector response.

ACKNOWLEDGEMENTS

The authors thank Rich Chmura, Jeff Chaffee, Mike Skidmore, Chris Labutti, Jason Tucker, Mark Bardol, Myles Silva and the entire FM Global Research Campus crew for their efforts in the construction of the setup and the successful running of the tests. The diligent oversight of project safety and hazardous material disposal by Janine Pitocco ensured personnel safety throughout this project.

The authors gratefully acknowledge the technical discussion and input from the other members of FM Global Research including Yi Wang, Christopher Wieczorek, Jeff Newman and Sergey Dorofeev.

The authors would like to thank the Fire Protection Research Foundation for providing the opportunity to work on this project as well as for the continuous collaboration over the past several years. Special thanks to Verizon Communications, Honeywell International Inc. and Simplex for the donated equipment.

Finally, the authors would like to take this opportunity to especially thank Amanda Kimball from the Fire Protection Research Foundation, and Jason Floyd, Josh Dinaburg and Dan Gottuk from Hughes Associates Inc. for their valuable input and timely discussions.

TABLE OF CONTENTS

LIST OF FIGURES

LIST OF TABLES

1 INTRODUCTION

Disruptions in data center operations due to fires have become a frequent occurrence. In March 2008, a fire destroyed 75 servers, routers and switches in a Wisconsin data center [1] causing a disruption of more than 10 days to customers. The municipal operations in Calgary, Alberta, Canada, [2] were disrupted due to a fire in July 2012, severely limiting many services and forcing area hospitals to delay surgeries. Macomb County, Michigan, declared a state of emergency after its IT service went offline following a fire that damaged the building that houses the county's data centers [3]. Such fires clearly demonstrate the need for better detection and fire protection. Proper placement of smoke/fire detectors in data centers is not only very important but also challenging due to the unique conditions [46] of high ventilation and the multitude of structural configurations.

This project was initiated to assess the response of smoke detectors in data center environments. Specifically, it provides large-scale experimental data on smoke transport in a high airflow environment and subsequent smoke detector response to different smoke sources. With increasing size of the data centers along with increased loading (per square feet) and cooling requirements, improvements to building codes and standards are required. Due to the multitude of designs it is difficult to design a series of tests that could identify all potential scenarios. Instead, the first step to address this gap would be to develop computational models that could potentially address these different scenarios. These models are foreseen to be able to:

1. Use experimentally determined smoke generation rates of typical fire sources as an input;
2. Simulate smoke concentration distribution as a function of time in a high-airflow environment;
3. Model response of various types of smoke detectors to dynamic changes of smoke concentration.

Prior to any application of such models to improve engineering codes and standards, they need experimental validation on a large scale. This study is aimed at providing validation data for items 2) and 3) in the list above. This report describes the experimental setup, instrumentation details, results of the airflow characterization, smoke concentration measurements and the response time from smoke detectors placed at various locations. All the testing described in this report was conducted at the FM Global Research Campus in Rhode Island, USA.

The current study was conducted in partnership with the National Fire Protection Association's (NFPA) Fire Protection Research Foundation (FPRF). Hughes Associates Inc. (HAI) was selected as the project contractor with the main objective of providing recommendations to improving NFPA code standards for placement of smoke detectors in data centers. The FPRF project was divided into two phases. Phase I involved identifying suitable computer models that could be developed/validated to meet the overall project objectives. Phase II of the project involved the following five tasks:

- Task 1 – Select CFD Model(s)
- Task 2 – Fire Source Characterization
- Task 3 – Detector Response Characterization
- Task 4 – Full-Scale Model Verification and Validation
- Task 5 – Perform CFD Simulations

Providing experimental data for model validation has always been a challenge especially at large scale. Considering the ongoing multiyear effort at FM Global on smoke damage and transport modeling, FM Global partnered with FPRF to complete Task 4 and provide validation data from large-scale tests.

1.1 BACKGROUND

1.1.1 Data Center Design

Increased data processing and storage needs by industry, governments and a rapid growth in communication volumes and speeds all have contributed to the rapid rise in the building of data centers. With a fast rise in the adoption of cloud computing [7], companies and government organizations are scrutinizing data centers to a higher degree in areas such as security, availability, environmental impact and adherence to standards [8]. Well-known operational metrics for data center availability can be used to evaluate the business impact of a disruption. The report entitled *2013 Cost of Data Center Outages* [9] "quantifies the costs of an unplanned data center outage at slightly more than $7,900 per minute." Currently, considerable innovation

and development are taking place to improve operations, availability and also in designing environmentally friendly data centers. Recent fires in data centers such as the ones in Calgary (2012) [2] and Michigan (April 2013) [3] have demonstrated the significance of damage caused to physical property, business interruption and the health of people involved.

Figure 1-1 shows sample pictures of a typical data centers. One of the typical designs involves a raised floor through which cold air flows into the facility, a server room that consists of the computer servers along with hot and cold aisles, and a dropped ceiling through which the hot air is extracted from the space. Smoke detection in data centers is a challenge due to the unique room configuration and high air exchange rates involved. Typical smoke detection involves either Spot-Type detectors (ion/photoelectric) or aspirated detectors that sample air from the room. The detectors can be placed throughout the data center or only in select and specific locations, such as the subfloor, server room, ceiling plenum or in the server cabinets themselves. The intelligent placement of smoke detectors is critical in detecting fires.

Typical data centers have air exchange rates measured in units of Total Air Changes per Hour (ACH) and current NFPA/ASHRAE standards [10, 11] specify the maximum ACHs to be 60. The smoke detectors currently used in data centers include spot and aspirated detectors. Current guidance for the placement of smoke detectors in large data centers can be found in FM Global Property Loss Prevention Data Sheet 5-32 [12, 13], “Data Centers and Related Facilities,” and the National Fire Protection Association (NFPA) Standard 75 [11], “Standard for the Fire Protection of Information Technology Equipment.” These building codes and standards specify horizontal spacing between the smoke detectors based on ceiling heights. To date, optimization of smoke detector placement has not been possible due to limited research [14] on the relationship between smoke transport and smoke detector response in high airflow environments, especially on the technical issues of airflow and dilution effects. There are no reliable data available for validation of computational models for smoke transport, and thorough analysis of smoke detector placement in data centers has not yet been attempted.

Figure 1-1: Sample pictures of a typical data center with arrangements of server cabinets.

1.1.2 Previous Literature

A number of studies have focused on the airflow within a data center environment [15-21]. Most of these studies mainly address the airflow distribution and heat transfer within a data center environment and not on smoke transport. A few experimental studies have been conducted in the past to evaluate smoke detector response to flaming and nonflaming fires in simpler test configurations. Aggarwal and Motevalli [22] conducted experimental studies in an enclosure with smoldering fires and noted that the detector response depends on the type of detector and smoke characteristics as two decoupled phenomena. Milke et al. [23], in a research study for FPRF, measured the obscuration levels from transient and steady state fires in a ventilated room with air exchange rates varying from 0 to 12 ACH. Miller [24] conducted a study on characterizing the effect of smoke detector response in a ventilated duct. All these studies have been limited to studying the smoke detector response in simpler test configurations and under less complex airflow patterns. Specifically, there have been no experimental studies on the impact of the complex airflow patterns, resulting from the high ventilation rates typically observed in a data center environment, on the smoke transport and subsequent smoke detector response.

1.1.3 Measurement of Smoke Concentration

Since this project aims to provide large-scale experimental data on smoke transport in a high airflow environment and subsequent smoke detector response for validation of computational models, of primary importance is the characterization of the smoke concentration in the vicinity of the smoke detectors. As such, the smoke concentration measurement must be non-intrusive in the test space and also represent a point source to aid in providing accurate resolution for model validation, e.g., of the order or less than 25 mm (1 in.) diameter area. Smoke concentration measurements are typically accomplished using a light extinction technique based on the attenuation of a concentrated light source (e.g., laser or white light) across a volume [25]. The subsequent measurement can be related to the average smoke concentration in the volume and the sensitivity of the system is dependent on the optical path length and the type of smoke being measured. To achieve smoke concentration levels in the range of 1.0% obscuration often require the instruments to be located within the test volume with path lengths of 0.9 m to 1.5 m (3 ft to 5 ft).

It is important to note that any measurement of light extinction, or obscuration, is highly dependent on the measuring device, local gas/smoke conditions, and smoke morphology (i.e., type).

In the present study, laser light extinction is used as an independent measurement of smoke concentration. This was done in an effort to obtain a quantitative measure of smoke that could be related to the response of the smoke detectors tested in this project. Therefore, the following discussion reviews the fundamental background of light extinction measurements, which was used herein to interpret data obtained in this study.

1.1.3.1 Governing Principles of Light Extinction Smoke Measurements

Bouguer's law (i.e., the Beer-Lambert law) relates the transmission of monochromatic light through a medium to the absorption and scattering (i.e., extinction) properties of the medium:

$$\frac{I}{I_o} = \exp\left(-\kappa_e L\right) \tag{1}$$

Where I_o is the initial light intensity, I is the transmitted intensity, κ_e is the extinction coefficient (m^{-1}), and L is the optical path length (m). In the general context of smoke measurements, the extinction coefficient is related to smoke concentration through:

$$\kappa_e = m_s''' \sigma_e^m \tag{2}$$

Where m_s''' is the smoke mass concentration (kg/m^3) and σ_e^m is the mass-specific extinction coefficient (m^2/kg). The mass-specific extinction coefficient is expected to be a function of the morphology of smoke particles (i.e., size distribution and structure) as well as the wavelength of light interacting with the medium. However, it is generally assumed that smoke particles conform to the Rayleigh (i.e., small particle) limit of Mie theory given by $\alpha < 0.1$, where α is a size parameter ($\alpha = \pi d_p/\lambda$, where d_p is the smoke particle diameter and λ is the wavelength of light). In this case, σ_e^m is independent of size distribution and:

$$\sigma_e^m = \frac{c}{\lambda \rho_s} \tag{3}$$

Where c is a dimensionless coefficient of particulate extinction and ρ_s is the density of smoke particles (kg/m^3). The coefficient of particulate extinction at the small particle limit can be assumed to be exclusively due to light absorption (i.e., negligible scattering) and given by [26]:

$$c = 6\pi \,\mathrm{Im}\left(\frac{m^2-1}{m^2+2}\right) = \frac{36\pi nk}{\left(n^2-k^2+2\right)^2+4n^2k^2} \tag{4}$$

Where $m = n+ik$ is the complex index of refraction of smoke particles.

The preceding discussion indicates that σ_e^m is constant and universal for carbonaceous smoke if the small particle limit assumption is satisfied. In the case of post-flame (or overfire) smoke generated from over ventilated flames, this assumption may be justified by considering that smoke produced from all flames basically consists of carbon particles generated in the fuel-rich areas of the flame that become small as they oxidize upon passing through the flame sheet [27]. This assumption will be challenged below; nonetheless, in the Rayleigh limit, smoke concentration can be determined from the measurement of transmitted light intensity by combining Equations 1 and 2:

$$m_s''' = \frac{1}{\sigma_e^m L}\ln\left(\frac{I_o}{I}\right) \tag{5}$$

Consequently, with knowledge of the smoke transport conditions, the smoke mass flow rate can be calculated as follows:

$$\dot{G}_s = m_s'''\dot{V}_{gas} = \frac{\dot{V}_{gas}}{\sigma_e^m L}\ln\left(\frac{I_o}{I}\right) \tag{6}$$

Here, $\dot{G}_s$ is the smoke mass flow rate (kg/s), and $\dot{V}_{gas}$ is the volumetric flow rate (m^3/s) of the smoke-laden gas medium being measured.

The value of σ_e^m warrants further discussion, which is provided below. It is noted, however, that results presented herein regarding smoke mass measurements, given the nature of Equations 5 and 6, can be expressed in terms of other values for σ_e^m by simple linear scaling.

1.1.3.2 Extinction Coefficient: Flaming Combustion

A typical value for the index of refraction of flame-generated smoke particles (i.e., soot) is $m = 1.57\text{-}0.57i$, which has been widely attributed to Dalzell and Sarofim [26], although the actual average value they reported was $m = 1.56\text{-}0.46i$ over the wavelength range spanning 4.358×10^{-7} to 8.065×10^{-7} m [28]. Using $m = 1.57\text{-}0.57i$ in Equation 4 yields $c = 4.9$. Considering a wavelength of 6.328×10^{-7} m (of relevance to the present study) and a smoke particle density of ~1,800 kg/m^3 [29, 30], one obtains, from Equation 3, $\sigma_e^m = 4{,}295$ m^2/kg. This value is considerably lower than those experimentally measured (8,700±1,100 m^2/kg) [31] and indicates that the Rayleigh limit assumption made above is not valid for smoke particles. This conclusion is reasonable considering that smoke particles are aggregates composed of hundreds of primary particles and the average aggregate dimension can be of the same order of magnitude as the light source wavelength [32]. In this case scattering becomes an important process in light extinction [33], which is neglected in the Rayleigh limit assumption. Experimental measurements of σ_e^m, however, exhibit nearly constant values for overfire smoke for a wide range of fuels [31, 34]. This observation is thought to be a result of the low fractal dimension (less than 2) of smoke agglomerates [32]. Therefore, although derived based on the Rayleigh limit assumption, use of Equation 5 is justified for smoke concentration measurements using light extinction techniques.

In the present study, a value of $\sigma_e^m = 10{,}056\pm1{,}011$ m^2/kg for $\lambda = 6.328\times10^{-7}$ m is used for flame-generated smoke based on the measurements of Newman and Steciak [25], who determined $c = 7\pm0.3$ and $\rho_s = 1{,}100\pm100$ kg/m^3. The value for σ_e^m lies on the upper range of those determined in the review of Mulholland and Croarkin [31]. Furthermore, the smoke density, ρ_s, is lower than values reported in the literature, which are typically based on measurements for particulate carbon black, e.g., [35]. The selected smoke density includes the mass of both carbon agglomerates and absorbed non-particulates, e.g., volatile organic compounds (VOCs), which are prevalent in flaming combustion.

1.1.3.3 Extinction Coefficient: Nonflaming Combustion

Nonflaming phenomena (i.e., pyrolysis and smoldering) generate aerosol particles that are considerably larger than those produced through flaming combustion [36]. In this case, light

scattering becomes a major contributor to overall light extinction, and light absorption is considerably decreased [37]; this contrasts with the observations made above for flame-generated smoke. Therefore, the mass-specific extinction coefficient will be dependent on the scattering properties of the nonflaming smoke, which, in turn, are bound to be strongly influenced by the size and structure of particle aggregates. Nonetheless, typical σ_e^m values reported in the literature for nonflaming smoke are on the order of 4,000-5,000 m^2/kg [38, 39]. In this report a value of σ_e^m=4,670 m^2/kg has been used for nonflaming smoke sources, corresponding to the recent study of Perera and Litton [39].

1.1.3.4 A Note on Detector Sensitivity

The standard measure of the sensitivity of smoke detectors has been usually defined by "obscuration" which is the fractional reduction in light intensity provided by a smoke-laden medium per unit length and is given by [40, 41]:

$$O_L = 1 - T^{\frac{1}{L}} \tag{7}$$

Where O_L is the obscuration (m^{-1}), T is the light transmissivity, and L is the optical path length (m), as given above. Sensitivity values are often reported in %/m, which can be simply represented by 100 O_L. Another measure of obscuration typically found in the smoke detector literature is the optical density, OD, which stems from the following relationship:

$$T = 10^{-OD} \tag{8}$$

Note that for low obscuration levels ($T \to 1$), which are of relevance to most smoke detector applications, Equation 7 can be expanded via a Taylor series around $T = 1$ to yield

$$O_L \approx \frac{1}{L}(1 - T); \text{ for } T \to 1 \tag{9}$$

which is perhaps a more physically intuitive definition for obscuration.

In standard tests [40, 41], the sensitivity of a given smoke detector is tested in a "smoke box" in which the obscuration level is determined using a tungsten filament automotive-type white light source over a path length of 1.52 m (5 ft). Note that this light source is spectrally broad (i.e., non-

monochromatic). In this case Bouguer's law (Equation 1) does not apply [42]; for example, the studies of Clark [43] and Chow and Lai [44] have shown that smoke optical density measurements obtained with monochromatic and "white light" sources can be considerably different. This is the reason why in Equations 7 and 8, for the sake of clarity and differentiation, T is used rather than I/I_0. Therefore, due consideration should be given to comparisons between extinction results obtained using monochromatic sources, such as that used in the smoke concentration meter described in this report, and smoke detector obscuration/sensitivity data.

1.2 PROJECT SCOPE AND TEST RATIONALE

The primary objectives of this work were to:

- Characterize the airflow in a typical data center for a range of representative air exchange rates
- Provide large-scale experimental data on evolution of smoke concentration and detector response for validation of computational models of smoke transport for
    - Two air exchange rates
    - Four typical fire sources
    - Four representative fire locations in the data center
    - Multiple representative locations of smoke measurements and detectors in the data center

Following these objectives, a multi-level test facility involving a confined cold-aisle configuration was chosen. The rationale for the design was to provide experimental data under challenging scenarios for model validation. The results provided from this research study are aimed at providing model validation data. Any direct implications of the results on detector response times are limited to this test configuration due to the unknown impact of changes in smoke detector response to variations in smoke sources and facility configuration. Due to the multitude of layouts found in real life data centers, it is not possible to conduct tests under all the scenarios, and hence it is important to note that placement of the smoke detectors was strictly chosen to provide data for model validation.

Experiments were conducted in the following order: First, the airflow velocities were characterized using a 3-D sonic anemometer and, second, the full-scale smoke concentration measurements and detection tests were performed in the presence of smoke sources placed at various locations in the enclosure. The details of the test setup are provided in the next chapter.

2 EXPERIMENTAL SETUP

The experiments were conducted in the Small Burn Laboratory at the FM Global Research Campus in West Glocester, Rhode Island, USA. The laboratory had dimensions of 14 m long x 14 m wide, with an 8 m high ceiling (47 ft x 47 ft x 27 ft). The air emissions control system (AECS) for the laboratory consists of four exhaust ducts, one located near each corner of the laboratory ceiling, with a maximum exhaust rate of nominally 24 m^3/sec. (50,000 ft^3/min.).

The test enclosure was constructed by an outside contractor, R&R Wolf Construction, Inc. of North Attleboro, Massachusetts, using standard construction industry practices. The dimensions and general layout of the enclosure were selected to represent a portion of a larger data center. Figure 2-1 shows a section of a typical data center with hot and cold aisles and server cabinets. Also shown in the same figure is the test section for this study with the dotted lines representing planes of symmetry.

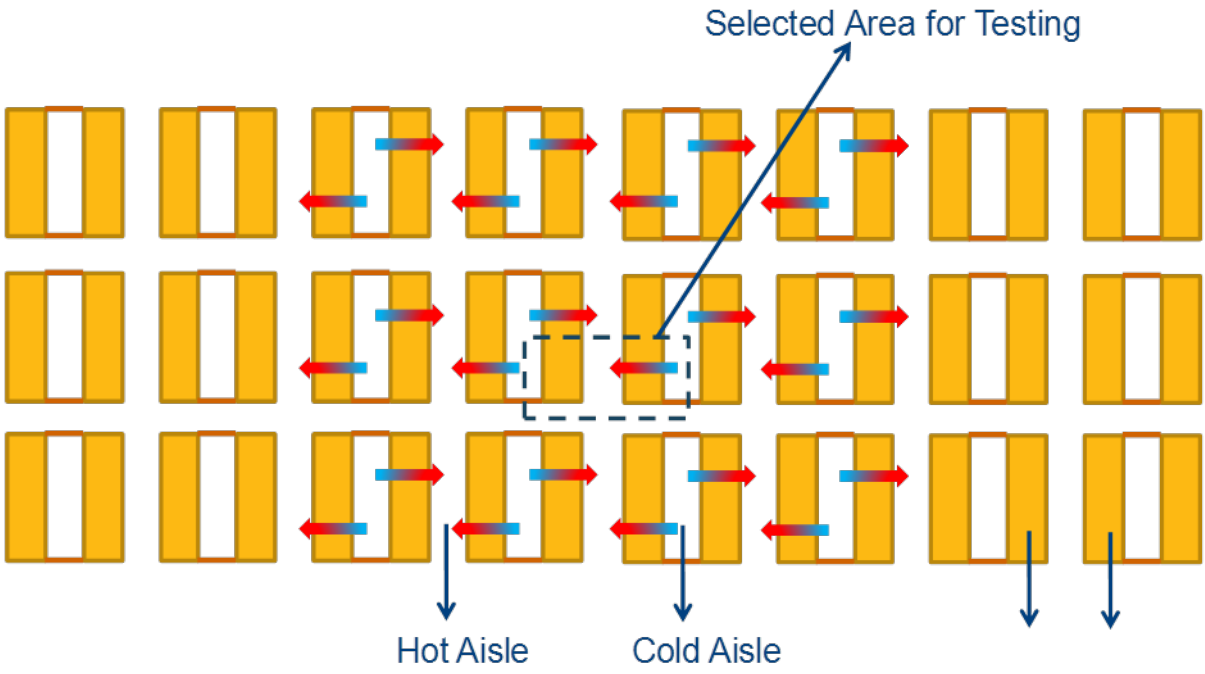

Figure 2-1: Plan view of a section of a data center with 2 cold aisles and four rows of server cabinets.

The overall interior room dimensions were 7.3 m long x 4.9 m wide x 4.9 m high (24 ft x 16 ft x 16 ft). Figure 2-2 and Figure 2-3 show the enclosure consisting of three levels, including a 1)

subfloor, 2) server room and 3) ceiling plenum. The server room was further separated into three sections, 2_i) one hot aisle and 2_{ii}) two enclosed cold aisles, and contained two rows of server cabinets and cable trays. The floor of the test enclosure indicated as Segment A-A, was smooth, flat and horizontal. A raised floor, indicated as Segment B-B, provided a subfloor level with a nominal height of 1.0 m (3 ft) and a suspended ceiling, indicated at Segment C-C, provided a plenum with a nominal height of 1.0 m (3 ft). The ceiling of the enclosure, indicated as Segment D-D, was smooth, flat and horizontal.

Figure 2-4 shows a plan view of the server room portion of the test enclosure. The north, south and west walls of the enclosure represent planes of symmetry (mirror images). For instance, the cold aisles have dimensions of 5.3 m long (17.5 ft) by 0.6 m wide (2 ft). Assuming symmetry in the north-south direction, the width of the cold aisles represents a typical 1.2 m (4 ft) width.

Figure 2-5 and Figure 2-6 present a general overview of the airflow path within the test enclosure. Cooling air was provided into the test enclosure via the open east side of the subfloor and entered the cold aisle through the vents in the subfloor. The air then passed through the server cabinets (where cooling of the hot data servers would have occurred if present), and into the hot aisle. The air then entered the ceiling plenum through the vents in the suspended ceiling and was exhausted out of the enclosure via the open east side of the ceiling plenum.

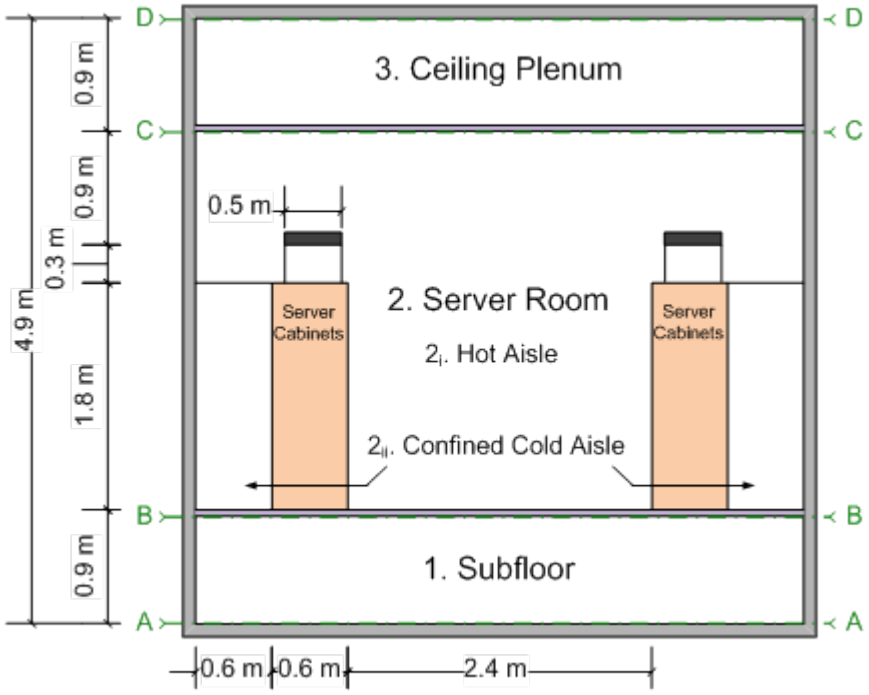

Figure 2-2: Front elevation view of the test enclosure.

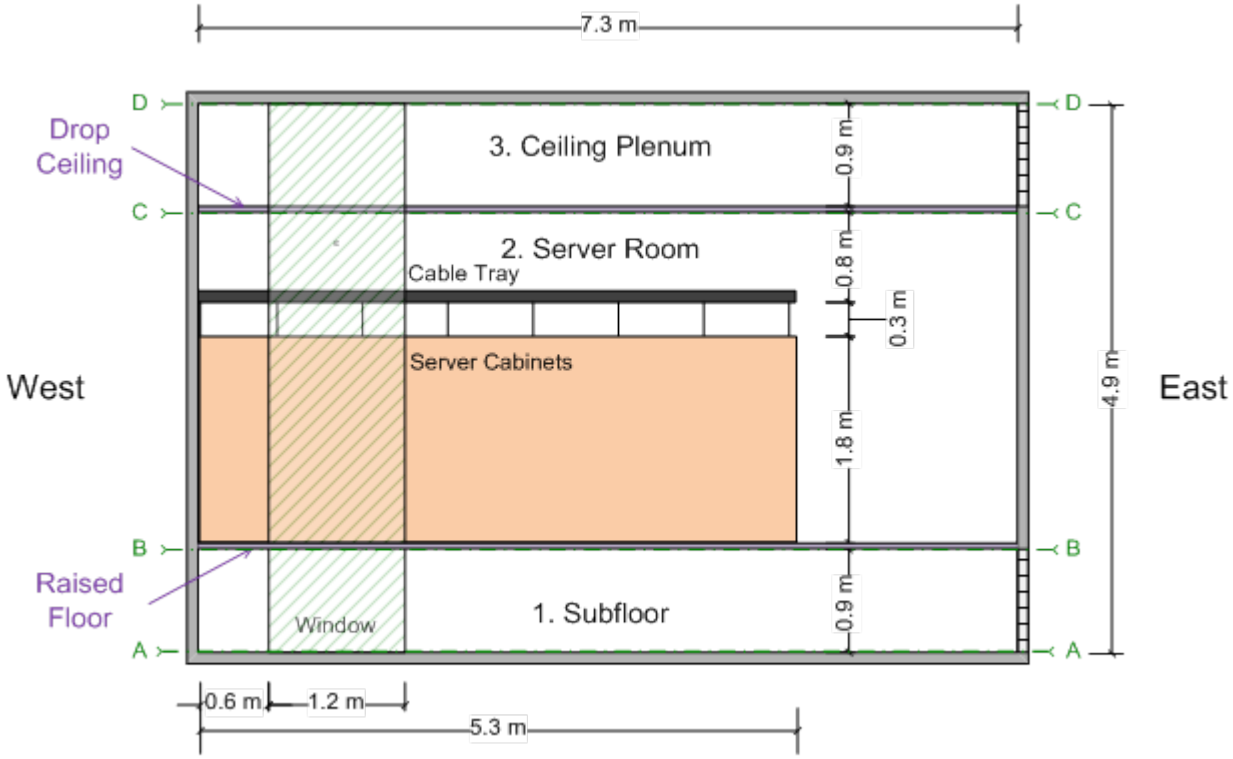

Figure 2-3: Side elevation view of test enclosure.

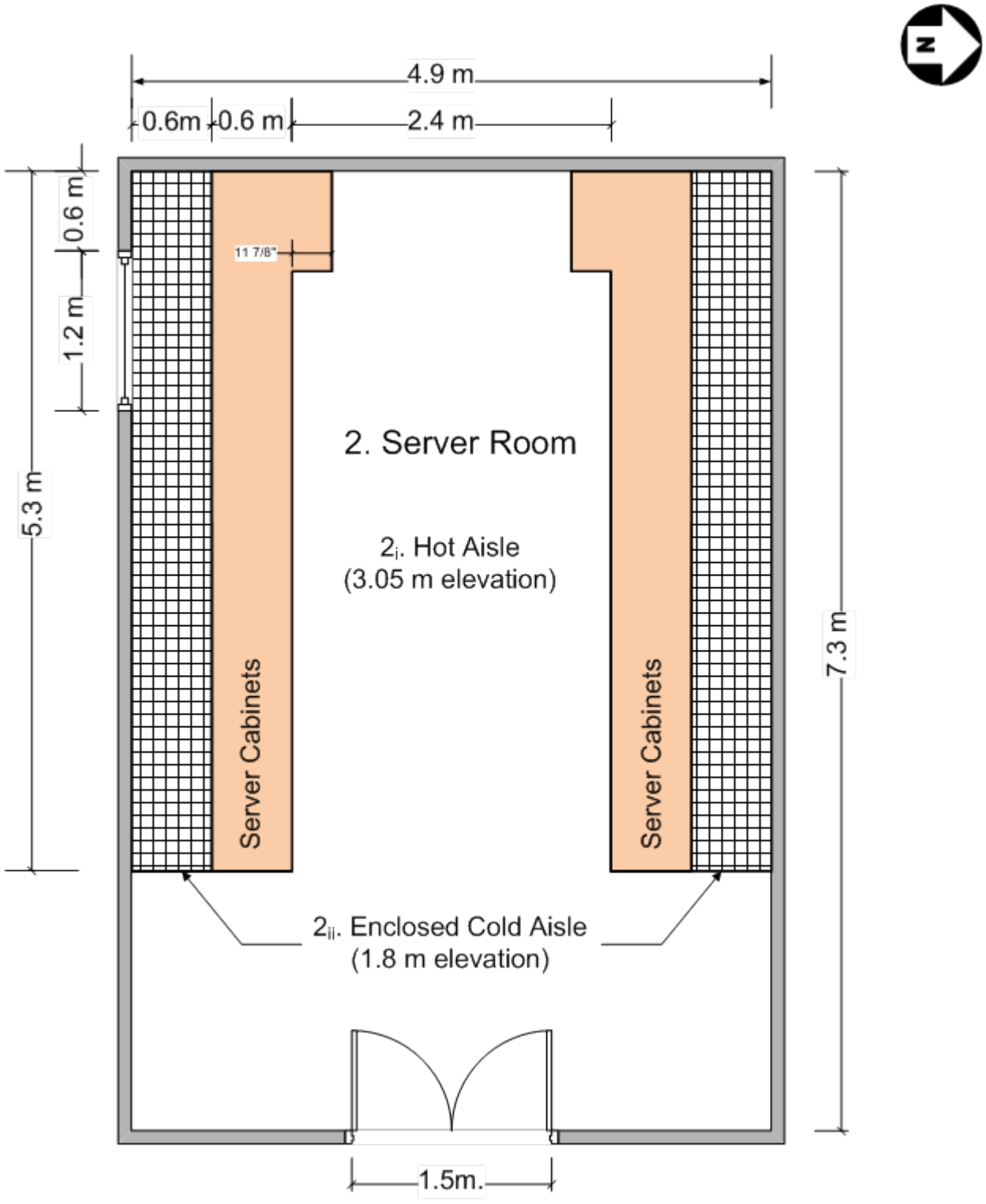

Figure 2-4: Overview of server room portion of test enclosure.

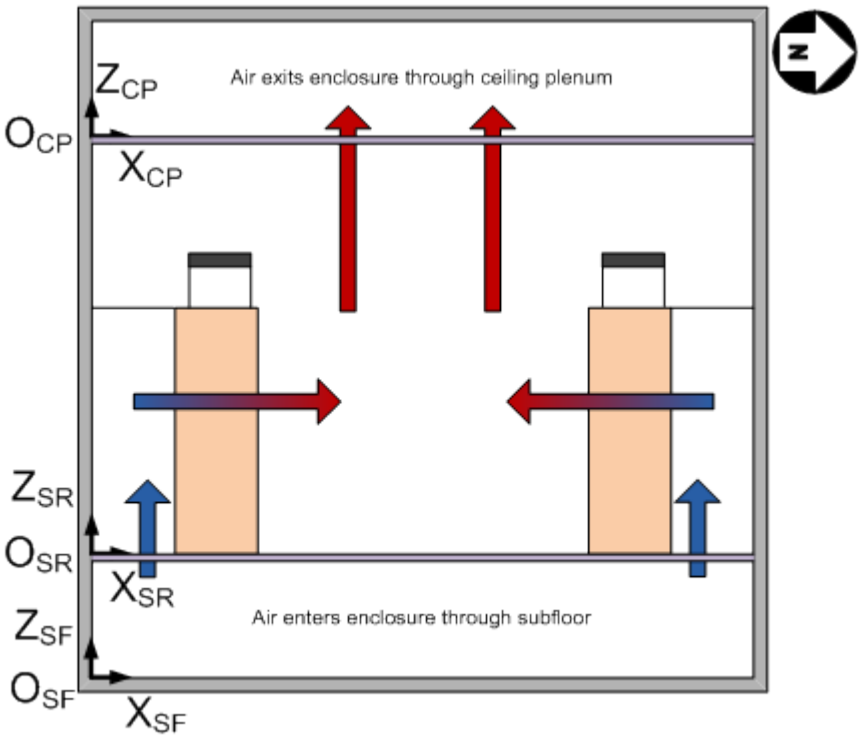

Figure 2-5: Side elevation view (from east wall) of test enclosure showing general airflow and axes for coordinate system.

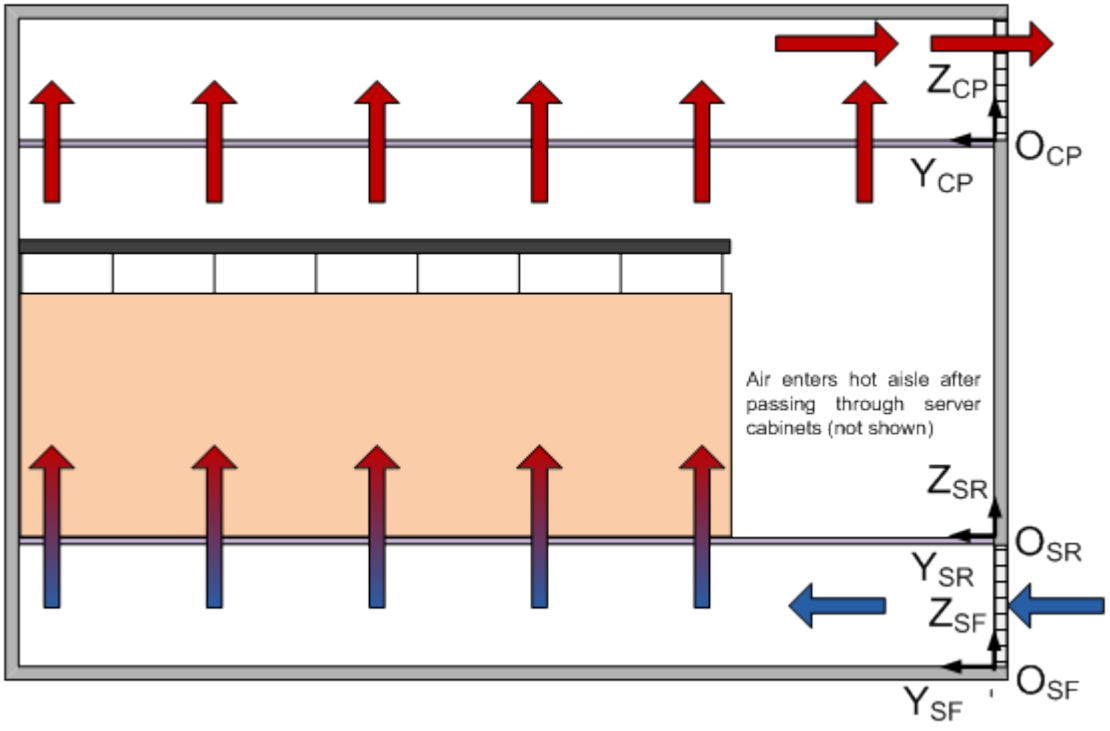

Figure 2-6: Front elevation view (from south wall) of test enclosure showing general airflow and axes for coordinate system.

2.1 COORDINATE SYSTEM

The test enclosure consisted of three main sections: 1) subfloor (SF) 2) server room (SR) and 3) ceiling plenum (CP). As shown in Figure 2-5 and Figure 2-6, for each section the following coordinate system is followed: x is the lateral distance from the south wall and its direction is positive in the north direction; y is the horizontal distance from the east wall (inlet) and is positive in west direction; z is the vertical distance from the floor and is positive in the upward direction. Locations within the subfloor are with respect to the origin in the subfloor O_{SF}, while locations in the server room (hot and cold aisles) are with respect to the origin O_{SR} and locations in the ceiling plenum are with respect to the location O_{CP}. The only factor differentiating these origins is their vertical (y) location. The origin O_{SF} is located at the floor of the subfloor and on the intersection of the east and south wall of the test setup. Similarly, O_{SR} and O_{CP} are at the intersection of the east and south walls and on the floor of the server room and ceiling plenum, respectively. The origins O_{SR} and O_{SF} are separated by a vertical height of 0.91 m (3 ft) and the origins O_{CP} and O_{SR} are separated by a vertical height of 3 m (10 ft).

2.2 EXTERIOR CONSTRUCTION DETAILS

Figure 2-7 shows an overall view of the test enclosure. The walls of the enclosure were constructed with 50.8 mm x 102 mm (2 in. x 4 in.) wood studs spaced 406 mm (16 in.) on center. The inside walls were finished with 15.9 mm (5/8 in.) thick gypsum board that was taped, spackled and painted bright white. The south wall contained a window that extended the full height of the enclosure and was comprised of two vertically stacked 1.22 m wide x 2.44 m tall x 6.4 mm thick (48 in. x 96 in. x 1/4 in.) clear polycarbonate panels (Figure 2-8). The window was mounted flush with the interior gypsum board. The east wall contained a 1.52 m wide x 2.13 m tall (5 ft x 7 ft) double door at the elevation of the raised floor to provide access to the server room level. The double door opened into the enclosure so the doors closed flush to the interior wall. A flat astragal was installed on the double doors to seal the gap between the doors.

Air inlet and outlet for the enclosure was accomplished with two large penetrations that extended the entire width of the east wall, with dimensions of 4.88 m wide by 1.0 m tall (16 ft x 3 ft). These penetrations were located at the lower and upper extent of the enclosure to coincide with

the subfloor and ceiling plenum, respectively. The subfloor penetration was filled with a 25.4 mm (1 in.) thick general purpose polyester air filter to minimize unwanted particulates from entering the enclosure. A channel was constructed to bring fresh outside air directly into the enclosure to mitigate smoke recirculation in the laboratory that was observed during a preliminary test (Figure 2-9). The channel was approximately 6.10 m long (20 ft) with dimensions of 4.88 m wide by 1.0 m tall (16 ft x 3 ft) at the inlet of the enclosure subfloor and tapered out to 4.27 m x 1.22 m (14 ft x 4 ft) at the exterior rollup door to the laboratory. No floor decking was provided; the exterior walls sat directly on the polished concrete floor of the laboratory with a foam gasket to provide an airtight seal.

The ceiling was constructed using 50.8 mm x 254 mm (2 in. x 10 in.) lumber spaced 406 mm (16 in.) on center. Since no perimeter boxing was necessary, the joists were toed-in to the wall header plates. The ceiling was finished with 19.9 mm (5/8 in.) fire-rated sheetrock that was taped, spackled and painted bright white.

Figure 2-7: Photograph of the overall test enclosure viewing the east wall.

Figure 2-8: Photograph of the test enclosure south wall (left) and a close-up of full height window (right).

Figure 2-9: Photograph of inlet channel into the enclosure subfloor.

2.3 INTERIOR CONSTRUCTION DETAILS

Figure 2-10 shows the design of the raised floor, which is constructed of 0.6 m x 0.6 m (2 ft x 2 ft) panels on metal support rods. The floor system (Aluminum 1500 Series) was purchased from Maxcess Aluminum Floor Inc., located in Taunton, MA. The floor panels in the cold aisle were comprised of grated vents with an open area of 54%. The floor panels in the hot aisle were solid, and the entire floor perimeter was sealed to the enclosure walls.

Figure 2-11 shows the design of the suspended ceiling, which was constructed of 0.6 m x 0.6 m (2 ft x 2 ft) panels suspended with metal channel. The ceiling was comprised of a combination of solid stipple panels and ventilated return grates suspended on metal channel. Stipple panels are constructed from 15.9 mm (5/8 in.) thick gypsum board with a white decorative veneered surface. The return grates (McMaster-Carr, part number 2532K5) had a perforated face with 6.4 mm (1/4 in.) diameter holes and a 50% open area. The number of vents was based on standard industry practice and selected to provide an open area equivalent to or greater than the floor grates. The perimeter of the suspended ceiling was sealed to the enclosure walls.

Figure 2-10: Photograph of the raised-floor during enclosure construction (top), close-up of floor panel support rods and underside floor grates (bottom-left), and top view of floor grates in the cold aisle (bottom-right).

Figure 2-11: Photograph of ventilation return grates in the suspended ceiling.

2.4 VENTILATION AND AIRFLOW

Ventilation from the enclosure was accomplished by extracting air through the ceiling plenum using a large duct exhaust fan. To allow for accurate measurement of the exhaust flow rate, a duct system was design which included multiple straighteners and flow stabilizers, as well as an instrumentation section to measure the flow velocity. A plan view of the exhaust system is shown in Figure 2-12 and includes the following design features:

A. Duct reducer: Exhaust air enters the duct system via a reducer section that tapers from a 4.88 m wide x 1.0 m tall (16 ft x 3 ft) opening at the connection to the test enclosure to 1.5 m wide x 1.5 m tall (4.8 ft x 4.8 ft) opening, over a 2.9 m (9.5 ft) length. The length of the reducer was selected to maintain a reduction angle of less than 30^{o}. The remainder of the duct had a square cross section with dimensions of 1.5 m wide x 1.5 m tall (4.8 ft x 4.8 ft) and an overall length of 4.6 m (15 ft).
B. Flow straightener: A flow straightener was located at the entrance to the square section of duct and was fabricated with 20 gauge sheet steel and provided 50.8 mm wide x 50.8 mm tall x 254 mm deep (2 in. x 2 in. x 10 in.) channels.
C. Flow stabilization screen: A flow stabilization screen (McMaster-Carr, part number 9219T207) was installed 0.64 m (25 in.) downstream from the end of the flow straightener. The purpose of the stabilization screen was to create a uniform air velocity distribution along the duct cross section.
D. Instrumentation section: Five pitot tubes were installed within the exhaust duct to measure distribution of flow velocity along two cross sections. The cross-sectional layout of the pitot tubes is shown in Figure 2-13. Temperature of the airflow within the duct is measured with a single type K thermocouple (same as in the enclosure and described below in Section 2.6.2) adjacent to the central pitot tube. The pitot tubes were securely fastened to 9.5 mm (3/8 in.) diameter support rods that traversed the duct to mitigate measurement error due to shaking of the instrument.
E. Coarse hash stabilizer: An additional coarse flow stabilizer was located approximately 0.3 m (1 ft) upstream of the exhaust fan. The coarse straightener was fabricated with 20 gauge sheet steel and provided 0.4 m wide x 0.4 m tall x 0.3 m deep (1.3 ft x 1.3 ft x 1 ft)

channels. The purpose of this straightener was to minimize rotational air current from the exhaust fan that may disturb the airflow in the vicinity of the measurement section.

F. Exhaust fan: Ventilation was provided by a 1.5 m (5 ft) diameter medium-duty exhaust fan (Dayton, model number 7M872) with an operational range up to 1,400 m^3/min. (50,000 ft^3/min.) under minimal pressure drop, which would be equivalent to more than 800 ACH within the test enclosure. However, the effective flow volume range was reduced due to the pressure drop induced by the test enclosure.

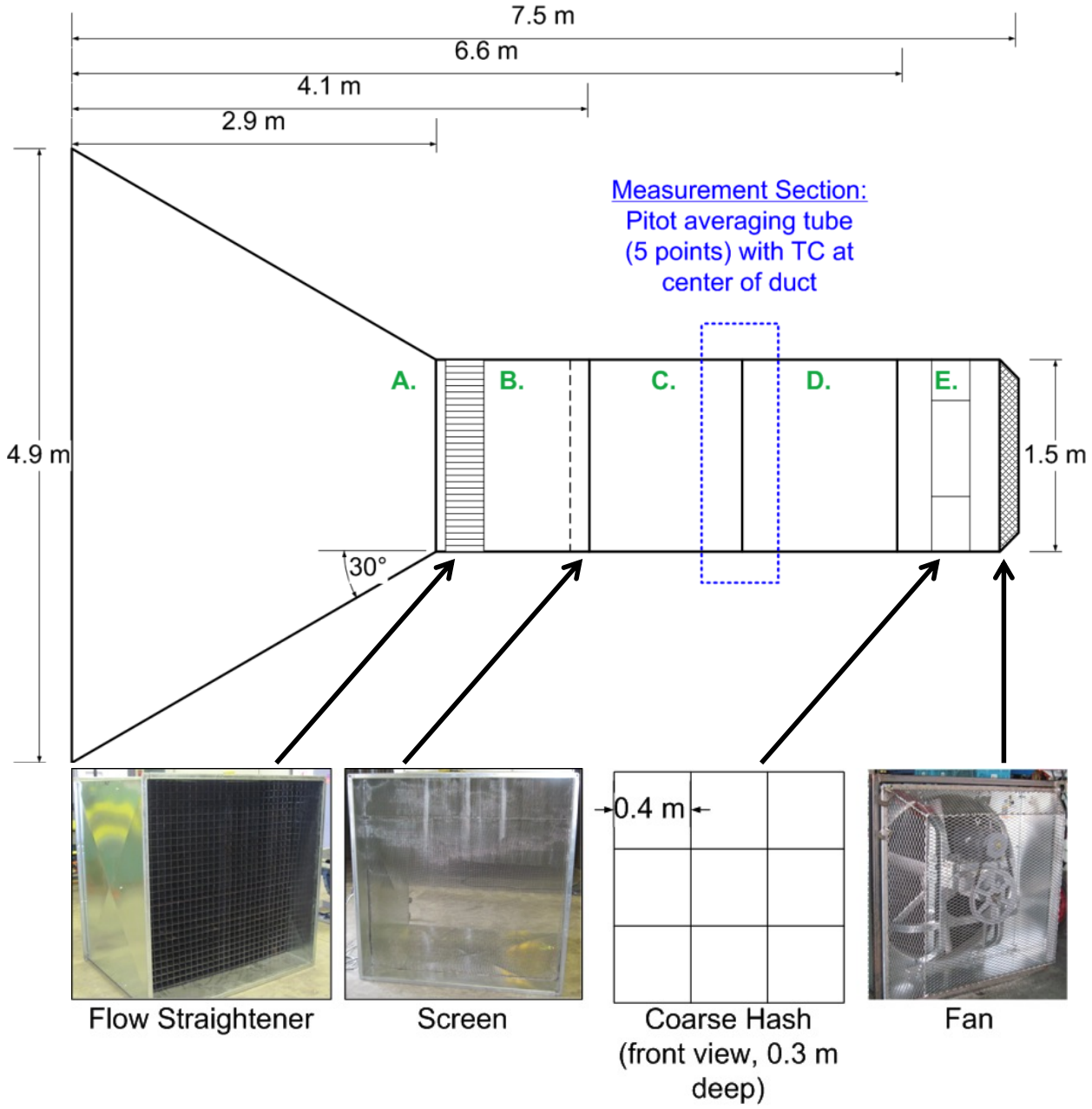

Figure 2-12: Plan view of exhaust duct system showing key construction components; A) duct reducer, B) flow straightener, C) flow stabilization screen, D) measurement section, E) coarse hash, and F) exhaust fan.

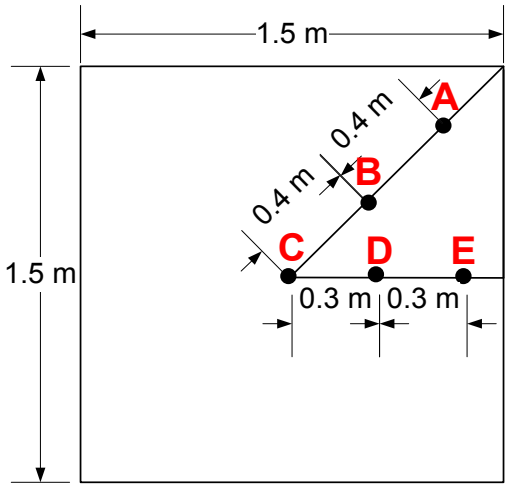

Figure 2-13: Cross-sectional view of flow measurement instrumentation in exhaust duct. Measurement plane can be referenced as item D) in Figure 2-12.

2.5 SERVER CABINETS

The server room contained two 5.3 m (17.5 ft) long rows of server cabinets placed adjacent to the grated floor panels, as shown in Figure 2-4. The cabinet dimensions were 0.76 m wide x 0.61 m deep x 1.8 m tall (2.5 ft x 2.0 ft x 6 ft), and each row contained seven cabinets abutted side-by-side (Figure 2-14). The cabinets located against the west wall of the enclosure had an increased depth of 0.76 m (2.5 ft). The cold aisle was enclosed on all sides with plywood sealed to the enclosure walls, ensuring that all the airflow was directed through the cabinets.

The server cabinets were donated by Verizon Communications, Inc. and were designed for telecom switches. For the purpose of this project, the telecom switches and all other internal components were removed. The cabinet doors contained perforations with 0.41 mm (0.016 in.) diameter holes resulting in an average open area of 92%. To simulate deposition that would normally occur as the smoke-laden air passes through servers within a cabinet, a screen was installed against the frame of each cabinet, nominally 25.4 mm (1 in.) inside the doors facing the hot aisle. The screen was made from steel woven wire cloth (McMaster Carr, Part # 9219T207), with an opening size of 0.38 mm (0.015 in.) and a wire diameter of 0.254 mm (0.01 in.), resulting in an open area of 36%.

In addition, an open-top cable tray was installed parallel to, and centered 0.3 m (1 ft) above, the entire length of the server cabinets. The cable tray had dimensions of 0.46 m x 0.10 m (18 in. x 4 in.) and is shown in Figure 2-15. The cable tray was placed to simulate obstructions in airflow common in modern-day data centers.

Figure 2-14: Picture showing the server cabinets in the hot aisle.

Figure 2-15: Picture showing the cable trays installed above the server cabinets.

2.6 INSTRUMENTATION

The test facility was instrumented with thermocouples, bi-directional velocity probes and pitot probes for flow rate measurements. Three smoke concentration meters were used to measure the smoke concentrations. All instrumentation was calibrated in accordance with ISO 17025 [45].

Figure 2-16 shows a schematic layout of the measurement clusters used in Figure 2-18 through Figure 2-20. A photo of a detector cluster is shown in Figure 2-17. Each cluster consists of at least two spot-type smoke detectors, one aspirated smoke detector, and one bi-directional probe and thermocouple. One cluster location per elevation in the enclosure (i.e., Segment B-B, Segment C-C, and Segment D-D – see Figure 2-2 and Figure 2-3) also included a smoke concentration meter extraction point.

Figure 2-18 shows the measurement cluster locations, grated floor panel layout, and inlet air direction in the subfloor, i.e., Segment B-B of Figure 2-2 and Figure 2-3. The measurement clusters were aligned parallel to the grated floor vents below the cold aisle. Also shown is the smoke source location in the subfloor, which was placed on the enclosure floor nominally 0.6 m (2 ft) below the measurement clusters, i.e., Segment A-A of Figure 2-2 and Figure 2-3. The smoke sources used in the subfloor were the propylene burner and electrical cables.

Figure 2-19 shows the instrumentation locations and the layout of ventilation return grates in the suspended ceiling, i.e., Segment C-C of Figure 2-2 and Figure 2-3. The measurement clusters are located diagonally from south-west to north-east under the suspended ceiling. Also shown are the smoke source locations in the server room, which were placed on top of the raised floor nominally 6.1 m (10 ft) below the measurement clusters. The smoke sources used in the server room were the propylene burner, which was located in the hot aisle, the foam blocks, which were located in the cold aisle, and the circuit boards, which were located in a server cabinet.

Figure 2-20 shows the instrumentation locations and outlet air direction in the ceiling plenum, i.e., Segment C-C of Figure 2-2 and Figure 2-3. The measurement clusters were located diagonally from south-west to north-east under the enclosure ceiling directly above the locations at the suspended ceiling. No smoke sources were located in the ceiling plenum.

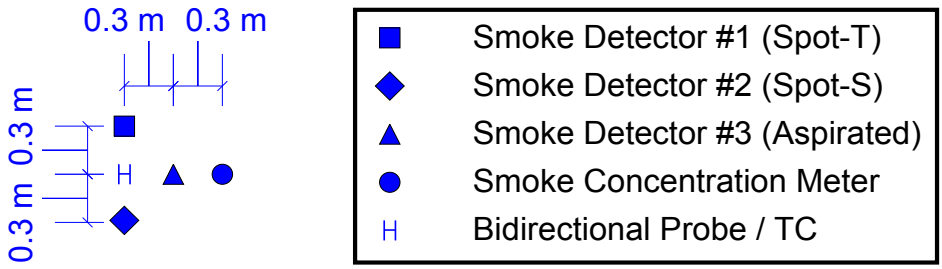

Figure 2-16: Instrumentation layout for measurement clusters in the test enclosure.

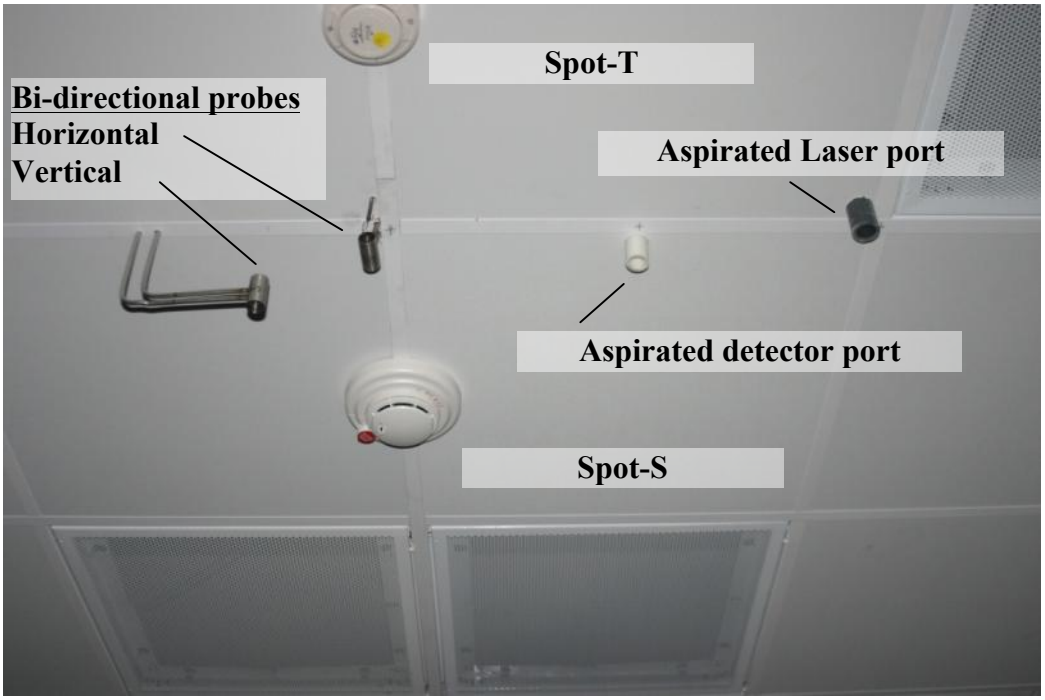

Figure 2-17: Close-up image of instrumentation and detector cluster underneath the suspended ceiling in the server room.

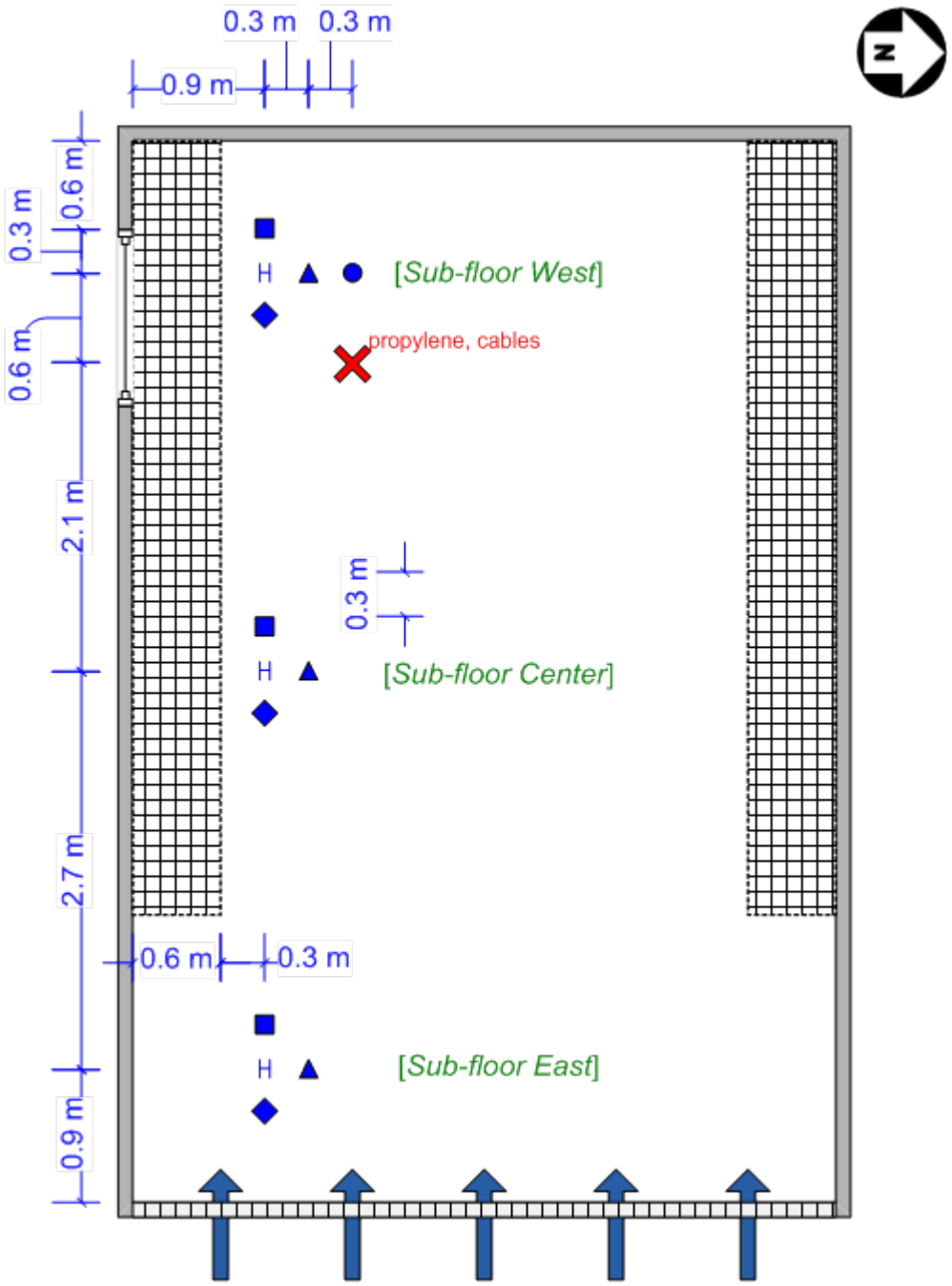

Figure 2-18: Plan view of the instrumentation layout and smoke source location (propylene burner and electrical cables) at Segment B-B of Figure 2-2 and Figure 2-3 (raised floor). Also shown is the air inlet direction into the subfloor.

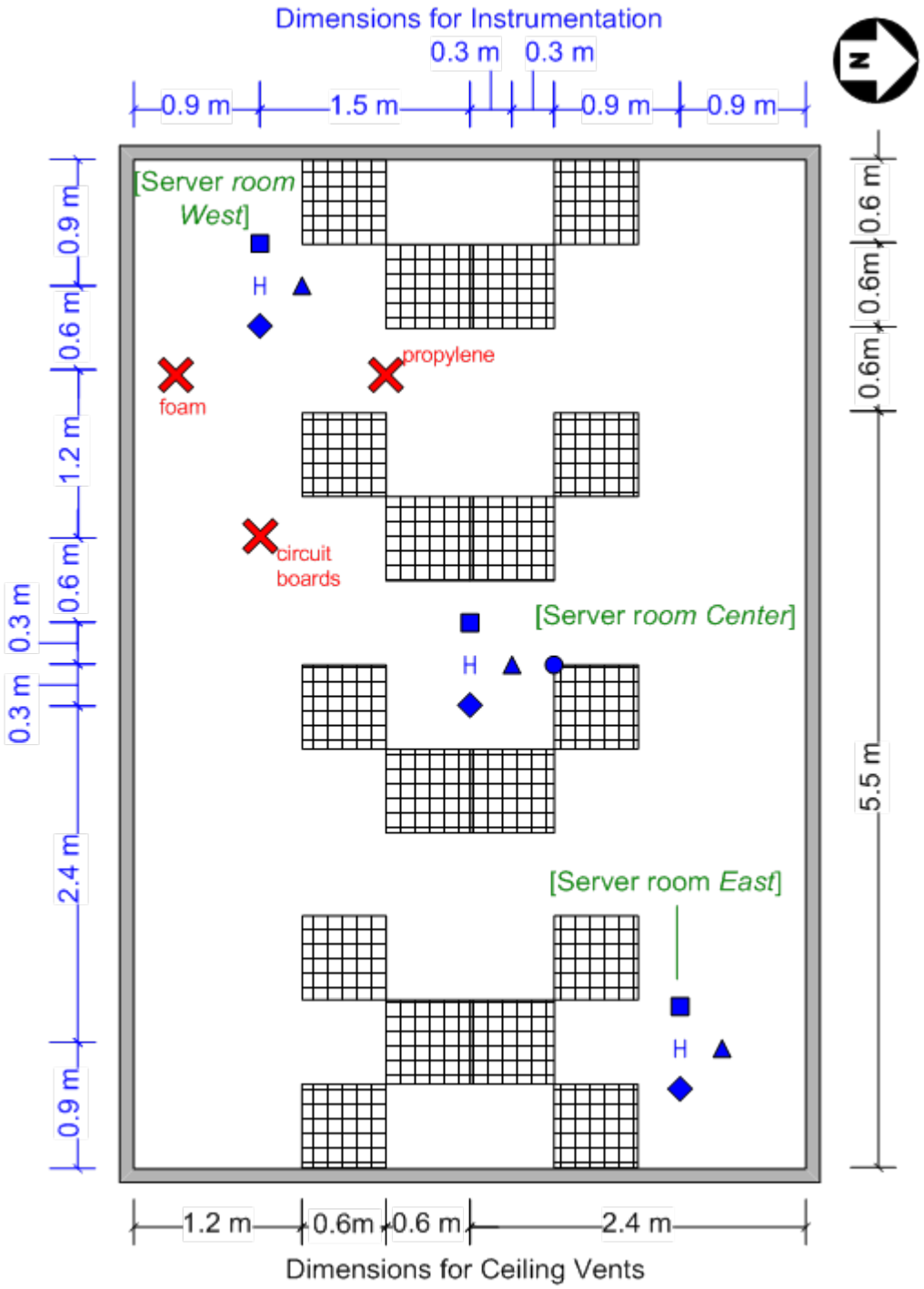

Figure 2-19: Plan view of the ceiling vents, instrumentation and smoke source location at Segment C-C of Figure 2-2 and Figure 2-3 (suspended ceiling) in the server room. Smoke source in the cold aisle (foam) and hot aisle (propylene) were placed on the floor while the circuit boards were placed at an elevation of 0.9 m (39 in.) in the server cabinet.

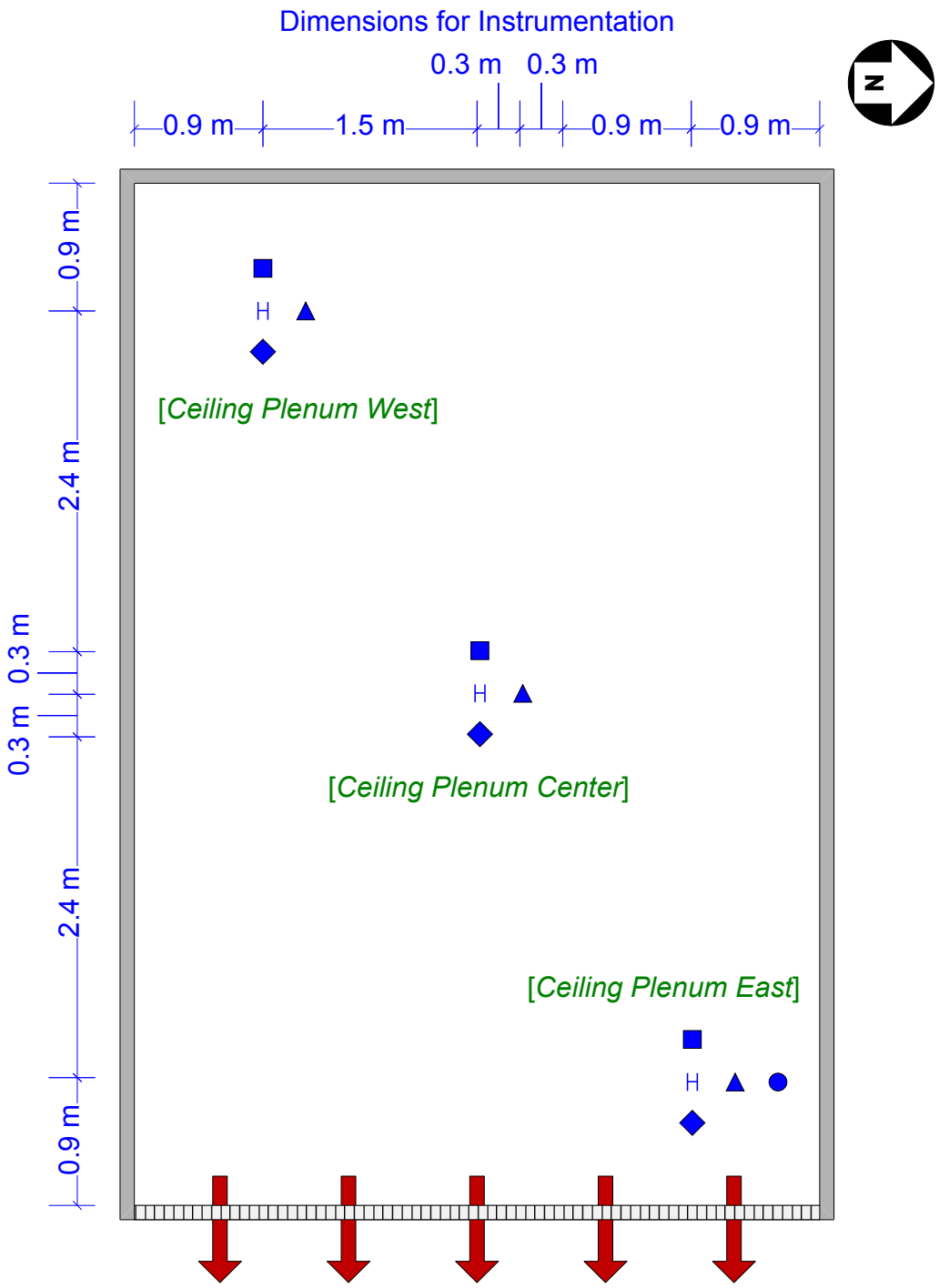

Figure 2-20: Plan view of the instrumentation and airflow direction at Segment C-C of Figure 2-2 and Figure 2-3 (suspended ceiling) in the ceiling plenum.

2.6.1 Smoke Detectors

Three clusters of smoke detectors were installed in each level of the test enclosure: the subfloor, server room and ceiling plenum. Each cluster contained two spot detectors and tubing for one aspirated smoke detector. Table 2-1 lists the location of each cluster in the enclosure. For reference, a sample picture of the detector placement underneath the suspended ceiling in the server room is shown in Figure 2-17.

Table 2-1: Locations of smoke detector clusters*.

Location of smoke detector clusters	Coordinates (m, [ft])	Schematic
Subfloor East	$(0.9, 0.9, 0.9)_{SF}$, $[(3.0, 3.0, 3.0)_{SF}]$	Figure 2-18
Subfloor Center	$(0.9, 3.6, 0.9)_{SF}$, $[(3, 11, 3.0)_{SF}]$	
Subfloor West	$(0.9, 6.3, 0.9)_{SF}$, $[(3, 19.1, 3.0)_{SF}]$	
Server Room East	$(3.9, 0.9, 3.0)_{SR}$, $[(0.9, 3.0, 0.9)_{SR}]$	Figure 2-19
Server Room Center	$(2.4, 3.6, 3.0)_{SR}$, $[(0.9, 11, 0.9)_{SR}]$	
Server Room West	$(0.9, 6.3, 3.0)_{SR}$, $[(3.0, 19.1, 0.9)_{SR}]$	
Ceiling Plenum East	$(3.9, 0.9, 0.9)_{CP}$, $[(0.9, 3.0, 3.0)_{CP}]$	Figure 2-20
Ceiling Plenum Center	$(2.4, 3.6, 0.9)_{CP}$, $[(0.9, 11, 3.0)_{CP}]$	
Ceiling Plenum West	$(0.9, 6.3, 0.9)_{CP}$, $[(3.0, 19.1, 3.0)_{CP}]$	

* The cluster locations are with respect to the bi-directional velocity probes. The detectors are offset from the probes by 0.3 m (1 ft) and are as shown in Figure 2-16.

2.6.1.1 Aspirated Smoke Detector (Aspirated Detector)

Figure 2-21 shows a picture of the aspirated smoke detector, hereafter referred to as the Aspirated detector. Each detector was attached to the outside of the test enclosure, and air from within the test enclosure was sampled from a port inside the enclosure. The sampling ports inside the room were connected to the inlet of the Aspirated detectors through PVC tubing, with a ~ 2.54 cm (1 in.) inner diameter, while the outlets were exhausted into the laboratory. The

Aspirated detector has a manufacturer specified obscuration range of 0.0015 to 21.7 %/m (0.00046 to 6.6 %/ft). The five user-selectable alarm thresholds were set to 0.039, 0.16, 0.33, 3.28 and 9.84 %/m (0.012, 0.05, 0.1, 1.0 and 3.0 %/ft). For each user-selected threshold, the detector provided a continuous analog measurement with a resolution equivalent to 1% of the adjacent thresholds. More details about the Aspirated detector are provided in Appendix A.1.

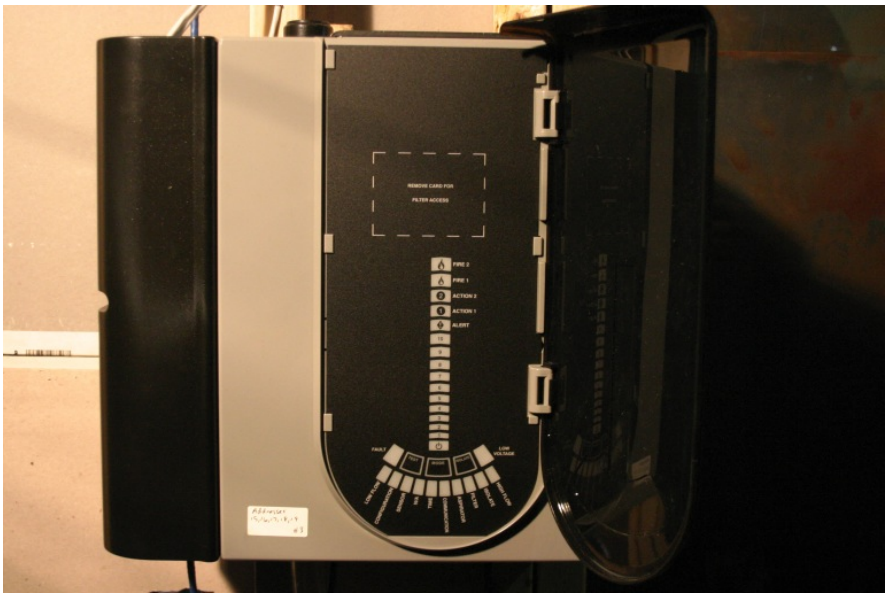

Figure 2-21: Aspirated smoke detector (Aspirated)

2.6.1.2 Combination Photoelectric Smoke Detector (Spot-S)

Figure 2-22 shows a picture of the first spot detector, hereafter referred to as Spot-S. This was a combination addressable photoelectric and heat multi-sensor detector. For the purpose of this project, only the light obscuration measurement from the photoelectric smoke detector was recorded (the heat detector response was not recorded). The manufacturer specified range was 0.66 – 14.11 %/m (0.2 – 4.3 %/ft) with nine preset discrete levels of 0.66, 1.65, 3.28, 4.92, 6.56, 8.20, 9.84, 11.48 and 13.12 %/m (0.20, 0.50, 1.00, 1.50, 2.00, 2.50, 3.00, 3.50 and 4.00 %/ft). No additional resolution beyond these seven discrete levels was available. Additional information regarding the smoke detector and data recording requirement can be found in Appendix A.2.

The Spot-S detector recorded data on separate hardware provided by Simplex. Unfortunately, it was not possible to sync the timing of the Spot-S detector with those of the Aspirated and Spot-T detectors. This did not affect the obscuration levels, but for the activation times, an average time difference with the Aspirated/Spot-T and FM Global's DAQ system was used in all calculations. This only impacted comparisons across each type of detector and did not impact comparisons for the Spot-S detector across each detector location for any given test.

Figure 2-22: Combination photoelectric smoke detector (Spot-S)

2.6.1.3 Spot-Type Smoke Detector (Spot-T)

Figure 2-23 shows a picture of the second spot detector, hereafter referred to as Spot-T. This was an addressable photoelectric detector which provided measurements within the manufacturer specified range of 0.066 to 6.56 %/m (0.02 to 2 %/ft) at seven preset discrete alarm thresholds, of 0.066, 0.098, 0.328, 1.64, 3.28, 4.92 and 6.56 %/m (0.02, 0.03, 0.1, 0.5, 1.0, 1.5 and 2.0 %/ft). No additional resolution beyond these seven levels was available. More details about the thresholds and its conversion into obscuration (%/m) can be found in Appendix A.3.

Figure 2-23: Photoelectric smoke detector (Spot-T)

2.6.2 Thermocouple Measurements

At the nine instrumentation cluster locations, the temperature was measured using a 20-gauge Type K, bare-bead, 6.4 mm (0.25 in.) sheathed, chromel-alumel thermocouple (Omega KQXL300E). A similar thermocouple was also located adjacent to the pitot tubes in the exhaust duct. These thermocouples have a response time index (RTI) of 8 ± 1 $m^{1/2}s^{1/2}$ (14.5 ± 1.8 $ft^{1/2}s^{1/2}$).

2.6.3 Velocity Measurements

Within the test enclosure, air velocity measurements were acquired at each instrumentation cluster as shown in Figure 2-18 through Figure 2-20. Each measurement was derived from the combination of a 19 mm (¾ in.) diameter bi-directional probe [46] and a 20-gauge bare-bead thermocouple. The bi-directional probes were connected to pressure transducers (Setra Model 2641R25WB2DT1F), which have a range of ± 62.5 Pa (0.25 in. H_20) and 0.25% accuracy (full scale). This method is consistent with FM Global Large Burn Lab practices for near-ceiling gas velocities and the method described by Ingason [47] for fire plume gas velocities within a rack storage array. Only horizontal measurements were taken in the subfloor and ceiling plenum, while both horizontal and vertical measurements were acquired in the server room.

Within in the exhaust duct, air velocity measurements were acquired at five locations, as shown in Figure 2-13. Each measurement was derived from the combination of a pitot tube (Dwyer Instruments, Model 160-18) and a 20-gauge exposed bead thermocouple (Omega KQXL300E).

In addition, the airflow within the test enclosure was separately characterized using a 3-D sonic anemometer (Campbell Scientific Inc., CSAT3 [48]) at over 100 locations throughout the enclosure. A picture of the anemometer head with dimensions is shown in Figure 2-24.

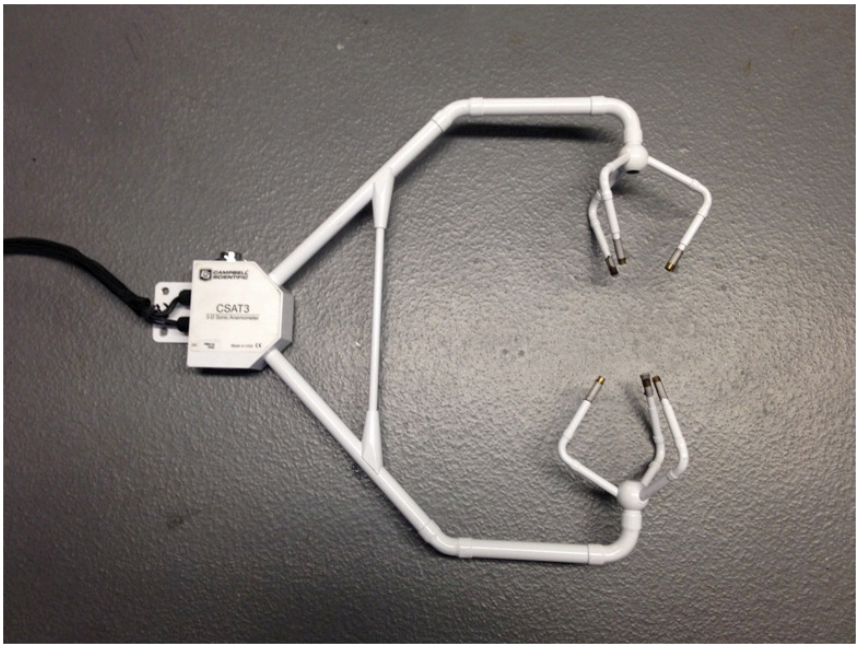

Figure 2-24: Picture of the 3-D sonic anemometer head.

2.6.4 Pressure Measurements

The static pressure difference from the ambient was recorded at four sections in the room (subfloor, cold aisle, ceiling of the server room and ceiling plenum) using differential pressure transducers (Setra Model 2641R25WB2DT1F). These transducers had a range of ± 62.5 Pa (0.25 in. H_20) and 0.25% (full scale) accuracy. Figure 2-25 shows the layout of pressure transducers and thermocouple connection boards on the outside of the test enclosure.

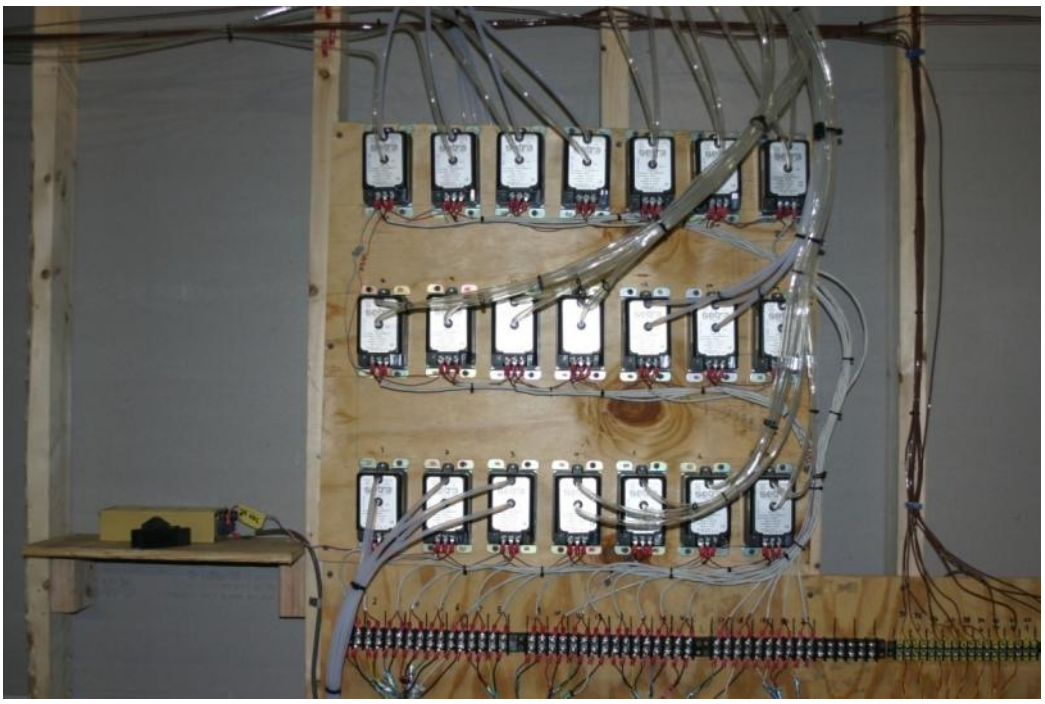

Figure 2-25: External layout of pressure transducers and thermocouple connections

2.6.5 Smoke Concentration

Smoke concentrations (g/m^3) at the select locations within the test enclosure were measured with a custom-designed aspirated laser system and a gravimetric system (Figure 2-26) [49]. Measurements were acquired in the vicinity of the smoke detectors at three instrumentation clusters (*Subfloor West*, *Server Room Center*, and *Ceiling Plenum East*) as shown in Figure 2-18 through Figure 2-20. The laser-based system provided a temporal measurement of the local smoke concentration (i.e., point source measurement). A 2.54 cm (1 in.) tube was used to collect the smoke at each location. The smoke was then passed through a beam extension chamber where laser light was reflected multiple times (to increase the optical path length and measurement sensitivity while maintaining a small measurement volume) and the incident and output intensities were measured. The reduction in intensity is used to compute the extinction, which is then converted into smoke concentration according to the principles outlined in Section 1.1.3. A thorough discussion of the design, governing principles, and calibration for the smoke concentration meter (SCM) can be found in Appendix B. Complementary gravimetric measurements, using smoke deposition on quartz filters, at the same locations provided a time-

averaged measurement of the smoke concentration and a means of validating the laser-based system measurement.

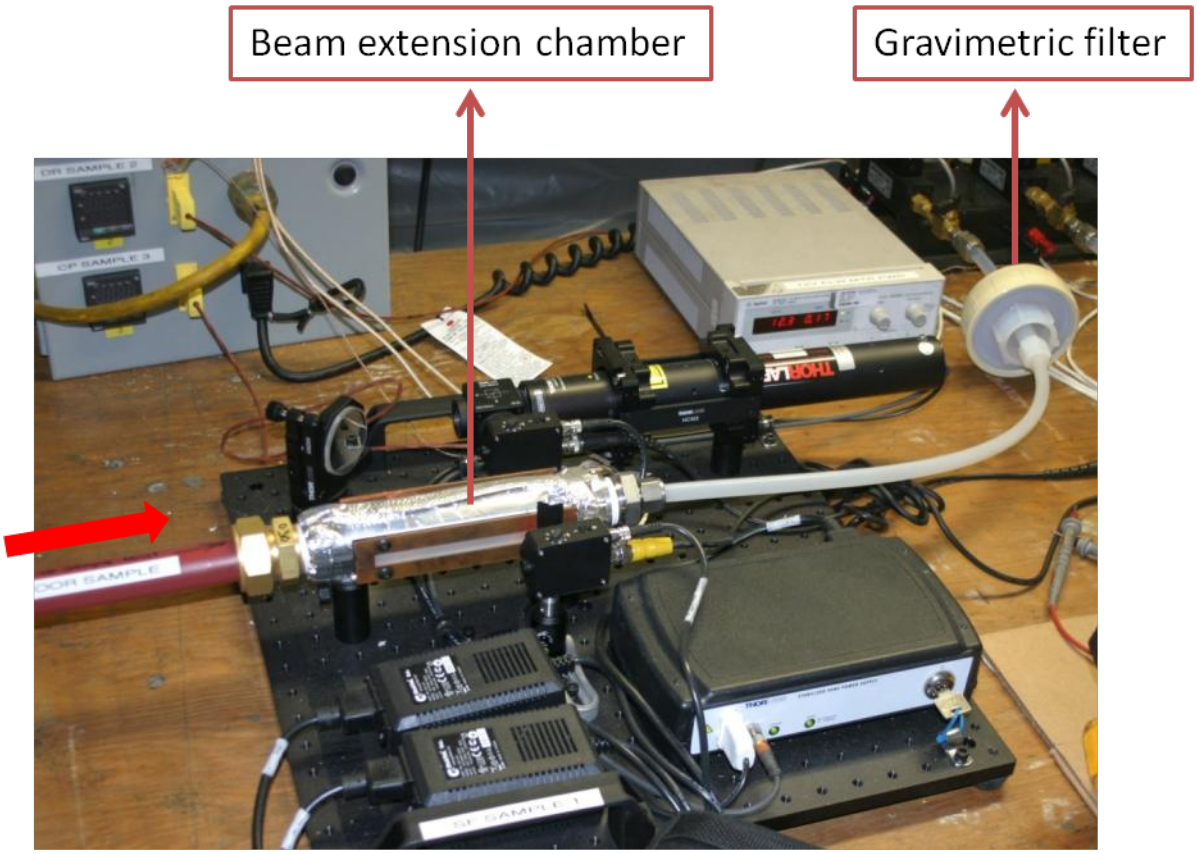

Figure 2-26: Smoke concentration meter (SCM) consisting of the Aspirated Laser and Gravimetric Filter

2.6.6 Cameras

Three high-definition video cameras were each placed in the hot aisle, subfloor and overlooking the cold aisle from the west wall. A micro camera was also placed in one of the server cabinets (with the smoke source) to record the smoke transport from the circuit boards.

2.6.7 Other Instrumentation

Building system instrumentation for measuring fan rotational speed, propylene flow rate, lab space exhaust, ambient temperature and pressure were also used during the tests to record the respective variables.

2.7 SMOKE SOURCES

Four smoke sources were selected for testing in this project. The propylene burner represented a steady-state smoke source produced from flaming combustion. The foam material, circuit boards and electrical cables represented transient smoke sources using combustible materials common to data centers. Heater cartridges were used for the circuit boards and electrical cables to produce smoke by overheating of the combustible content. The foam material produced smoke through flaming combustion, while no flames were observed from the circuit boards and the electrical cables. The smoke yield as a function of time for all the above sources was characterized by Hughes Associates Inc. as a part of Task 2 of the overall project. The characterization conditions were different from the large-scale tests at FM Global, and the effect of the change in ventilation on the smoke yield is unknown. For the propylene smoke source, Sivathanu and Faeth [50] estimated soot yields of 6% (by mass). However, it should be noted that this estimate was also under different conditions from the current tests, and deviations from this value are possible due to the change in flow conditions.

2.7.1 Propylene Burner

A 0.1 m (4 in.) ring burner was used with flow rates corresponding to a heat output of 10 kW and is shown in Figure 2-27. The fuel flow was provided using a standard tank, and the flow rate was maintained steady to yield a steady heat release rate output. Ignition was accomplished with an electrical arc. The advantage of using the propylene burner was that it acts as a steady, easily reproducible and well characterized smoke source that could also be easily scaled. This is highly desirable, especially for modeling purposes. The propylene burner was placed at two locations: in the hot aisle and in the subfloor.

Figure 2-27: Propylene ring burner

2.7.2 Packaging Foam

The foam smoke source consisted of two sets of solid anti-static polyethylene foam blocks (Grainger 5GDC0) separated by 0.3 m (12 in.) and is shown in Figure 2-28. Each block of foam consisted of two vertically stacked smaller blocks of dimension 150 mm x 410 mm x 50 mm (6 in. x 16 in. x 2 in.). Two 2.54 mm (1 in.) holes were drilled 25.4 mm (1 in.) deep in the center of each half of the block. The holes were filled with 20 mL (1.2 $in.^3$) of isopropyl alcohol and ignited with a propane torch. Each of the blocks was placed on a thin sheet of metal to allow for liquefaction and pool collection.

Figure 2-28: Foam material

2.7.3 Circuit Boards

Two Nortel Networks NTGB06CA60 circuit boards were attached to each other by drilling 9.4 mm (0.37 in.) holes at the factory stamping locations in the center of the board. A metal X-shaped bracket was removed from one of the two boards by loosening the four screws holding it in place. The drill locations and bracket screws are shown in Figure 2-29. The bracket was removed to allow a heat cartridge to be inserted between the two boards. The boards were connected using 9.4 mm (0.37 in.) bolts, washers and nuts. The boards were attached facing the same way such that the front plates and plugs were aligned. The aligned boards and heat cartridge placement (in a burned board) are shown in Figure 2-30.

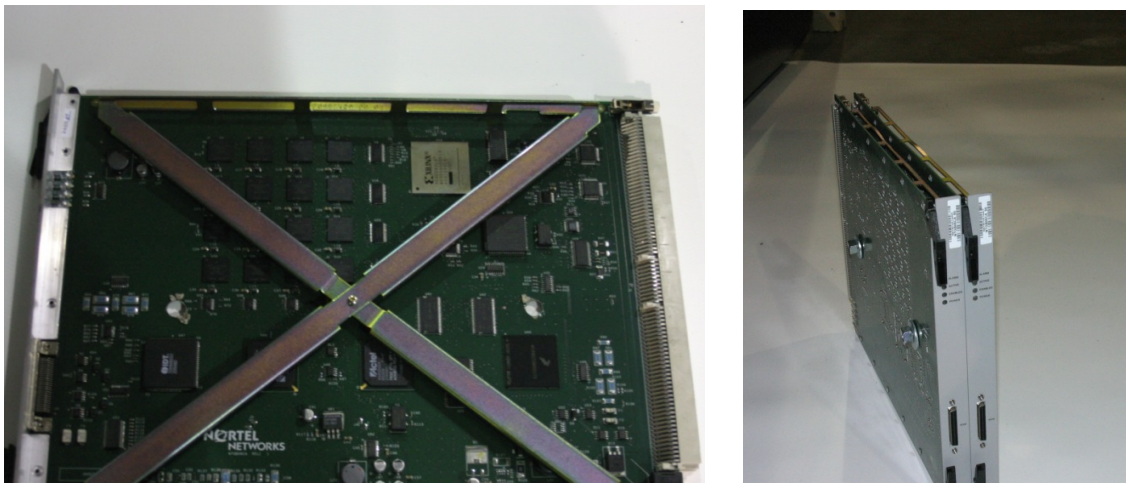

Figure 2-29: Printed circuit boards; top view (left) and side view of two boards sandwiched together (right).

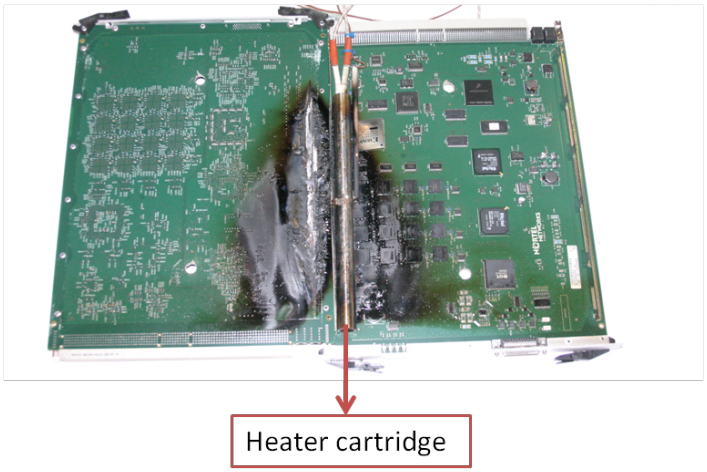

Figure 2-30: Circuit boards after completion of smoke test.

A 24-gauge, type K thermocouple bead was welded to the center of a 2,000 W, 240 V AC heat cartridge, 0.25 m (10 in.) long and 0.019 m (0.75 in.) in diameter. The cartridge was then placed between the two boards at the base along the rail. The temperature of the heat cartridge was controlled using a temperature controller and solid-state relay at a steady 515°C (959°F) until the boards stopped producing smoke. The heat caused the pyrolysis of the circuit board in contact with and surrounding the heater elements yielding smoke. There were no flames observed from this source, and all smoke was only due to pyrolysis.

2.7.4 Electrical Cables

The electrical cable smoke source consisted of five 0.2 m (8 in.) pieces of cables (16 gauge, 3 conductor-shielded continuous multiflex cable: McMaster part number 9700T45). The cables were bundled around a 120 V, 500 W Vulcan cartridge heater. The heater was operated using a custom-built controller with the ability to control multiple heat cartridges at a fixed temperature or setting. In the current test series, it was found that a single cartridge was sufficient to produce enough smoke for the purposes of testing. A 24-gauge thermocouple was spot welded to the outside of the cartridge heater at the center of its long dimension. The heater cartridge and thermocouple inside a cable bundle are shown in Figure 2-31. The cables were evenly spaced concentrically around the heater and tightened into place with fiberglass-sheathed thermocouple wire. The cartridge was maintained at a fixed temperature of 600°C (1,100°F).

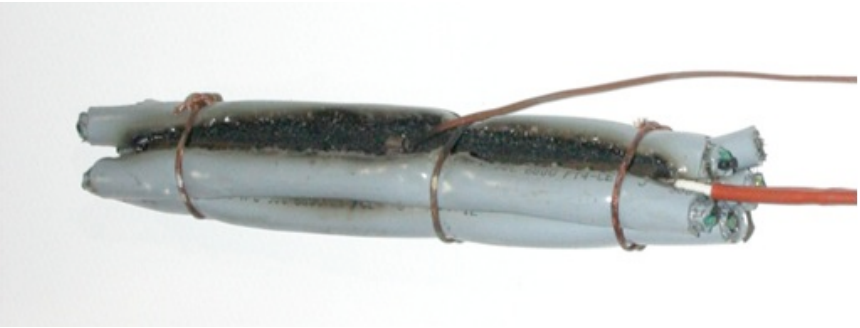

Figure 2-31: Electrical cable bundle after completion of smoke test.

3 AIRFLOW CHARACTERIZATION

Before conducting the smoke transport tests, extensive mapping of airflow velocities within the test setup was conducted. A three-component sonic anemometer [48] was used to measure the x, y and z velocity components at several locations in the subfloor, the cold aisle, the hot aisle and inside the ceiling plenum (see Section 2.1, Figure 2-5, and Figure 2-6). The velocity measurements are critical in the understanding of airflow patterns. These airflow patterns are responsible for smoke transport inside the enclosure. The velocity measurements were not expected to change in the presence of smoke due to the small energy contribution from the source fires and the moderately heated smoke particulates. Over 200 tests were conducted, and sonic anemometer measurements were taken for both the low (78 ACH) and high (265 ACH) flow rates. The air exchange rates are based on the volume of the entire test setup. In addition to the discussion provided below, a complete tabulation of the sonic anemometer velocity measurements can be found in Appendix D. Besides the sonic anemometer measurements, velocities at the aspirated smoke detector locations were measured using bi-directional probes, and pitot tube measurements were taken in the square duct upstream of the fan location (see Figure 2-12 and Figure 2-13 for details of the duct geometry and measurement locations). The bi-directional probe data are not presented in this section, but are included in Appendix D.

A schematic with the airflow pattern in the enclosure is shown in Figure 3-1. The x = 0, y = 0 location is in the southeast corner and the orientation axis is shown next to this location. It should be noted that the z = 0 location is specific to the test section. For example, for measurements in the cold aisle, z = 0 is located at the southeast bottom corner of the server room (see Figure 2-5 and Figure 2-6 for details). The flow in the enclosure is induced by a fan extracting air downstream of the ceiling plenum. The resulting flow enters the enclosure through the inlet on the east side into the subfloor. It then turns upwards (z-direction) and enters the cold aisle through perforated floors. In the cold aisle, the flow again turns in the x-direction and enters the server cabinets and then exits into the hot aisle. In the hot aisle, the flow generally turns vertically (z-direction), although large recirculation regions near the middle and near the east wall were observed and are described later, and enters the ceiling plenum through ceiling vents (not shown in Figure 3-1). The flow inside the ceiling plenum turns towards the negative y-direction, i.e., towards the outlet on the east, and exits into the fan duct.

Along with the overall pressure gradient due to the fan suction, significant pressure drops occur across the cold aisle perforated floor, the server cabinets and the ceiling vents. Differential pressure measurements across the perforated floor and ceiling vents were taken in order to provide guidance for modeling. The differential pressure data are reported in Table 3-1 for both flow rate cases.

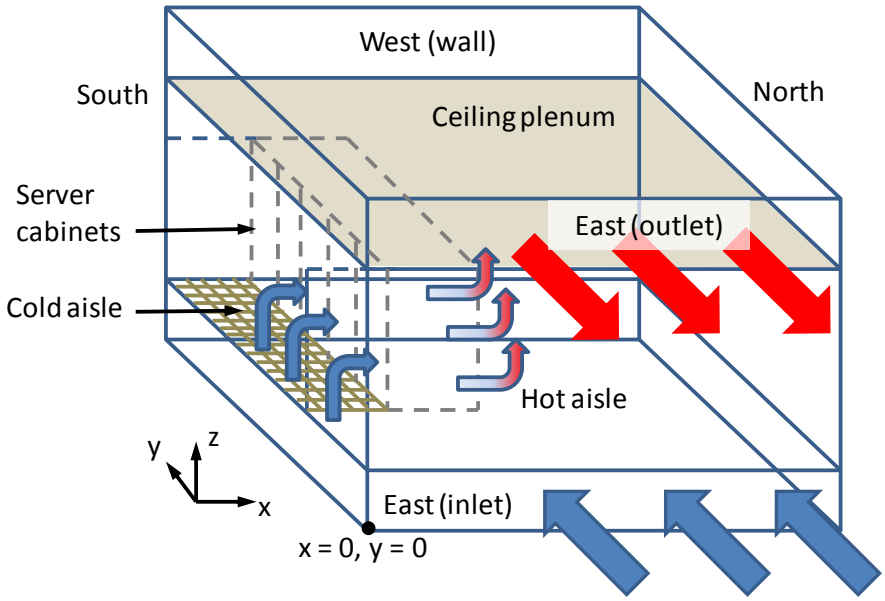

Figure 3-1: Test setup schematic showing airflow direction in the enclosure sections. Only one set of server cabinet location is shown by the dashed lines.

Table 3-1: Differential pressure measurements across cold aisle perforated floor and ceiling vents for two flow rate cases.

Pressure drop across	Flow rate	Mean (Pa)	RMS (Pa)
Subfloor and cold aisle	265 ACH	20.9	0.70
	78 ACH	1.74	0.11
Server room and ceiling plenum	265 ACH	17.3	0.33
	78 ACH	2.18	0.09

The fan-induced flow was steady in nature and Figure 3-2 shows the time-averaged pitot tube velocities in the duct cross section. The measured velocities agree well with turbulent flow velocity profiles inside square ducts [51], represented by dotted curves in Figure 3-2. Pitot tube measurements were used to calculate the overall air exchange rates in the enclosure.

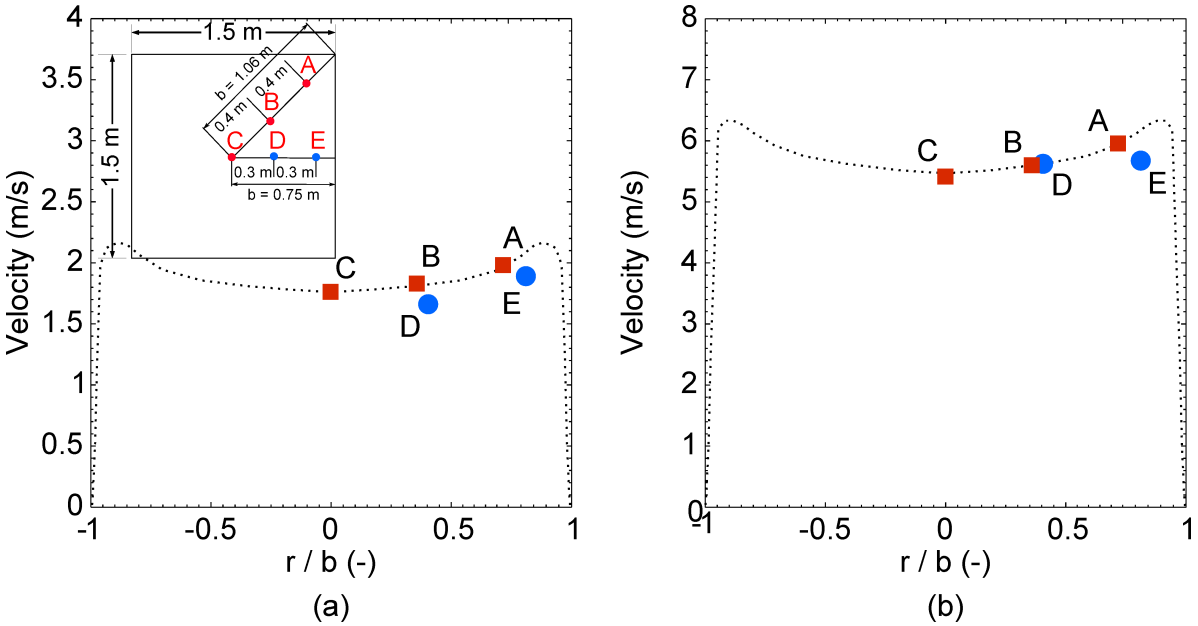

Figure 3-2: Pitot tube velocity measurements inside the fan duct downstream of the enclosure outlet. Flow normal velocity component as a function of distance from the center (location C) is shown at the air exchange rates of (a) 78 ACH, and (b) 265 ACH. The dotted curves are expected turbulent flow velocity profiles in square ducts.

3.1 SUBFLOOR MEASUREMENTS

Figure 3-3 shows three-component velocity measurements, obtained with the sonic anemometer, for locations in the subfloor. Three planes were selected located at different x distances from the south wall; all measurements were performed at an elevation of z = 0.76 m (2.5 ft). The velocities are plotted against distance in the y direction, with y = 0 m (0 ft) aligned with the inlet (east wall) and y = 7.3 m (24 ft) being the west wall. The coordinate system followed is shown in Figure 3-1. The velocities in the lateral (x), horizontal (y) and vertical (z) directions are presented as U, V and W, respectively. The air enters the subfloor from the inlet and flows towards the west wall. This can be observed in Figure 3-3 where V values start to decrease for

y > 2.1 m. It should be mentioned that the perforated cold aisle floor begins at y ≈ 2.0 m (6.6 ft). A corresponding increase in the vertical component of velocity, W, can be observed in Figure 3-3 for the x = 0.3 m (1 ft) plane. As the flow turns upwards through the perforated cold aisle floor, the V component reduces and the W component increases. At the y = 7.1 m (23.3 ft) location, the flow is completely oriented in the vertical direction, and the V component is not present. This increase in the W velocity is only observed at the x = 0.3 m (1 ft) plane as the flow turns upwards. At the x = 0.9 m (3.0 ft) and 2.1 m (6.9 ft) planes, the reduction in V velocity does not result in an increase of the W velocity, and the flow turns laterally towards the north and south directions (i.e., in the +x and –x directions). With increasing distance from the inlet, the U component of velocity grows, indicating the presence of recirculation near the west wall.

3.2 COLD AISLE MEASUREMENTS

The flow enters the cold aisle through the perforated floor and then turns towards the server cabinets. Sonic anemometer measurements in the middle of the cold aisle (i.e., at a location x = 0.38 m (1.25 ft) from the south wall) are presented in Figure 3-4. Measurements were taken for five y-distances, and at each y-distance four vertical locations from the cold aisle floor were selected. At z = 0.1 m (0.33 ft) above the cold aisle floor, the flow is generally in the vertical direction and, therefore, the W velocities show high values. The RMS components for W velocity are significant compared to their mean values for y = 2.1 m (6.9 ft) and 7.1 m (23.3 ft) locations where the wall affects the flow, creating recirculation regions. Similar higher RMS values for the U and V velocities are also observed for these locations. With increasing measurement height relative to the cold aisle floor, the vertical component of velocity decreases, and the flow increasingly turns towards the server cabinet entrance.

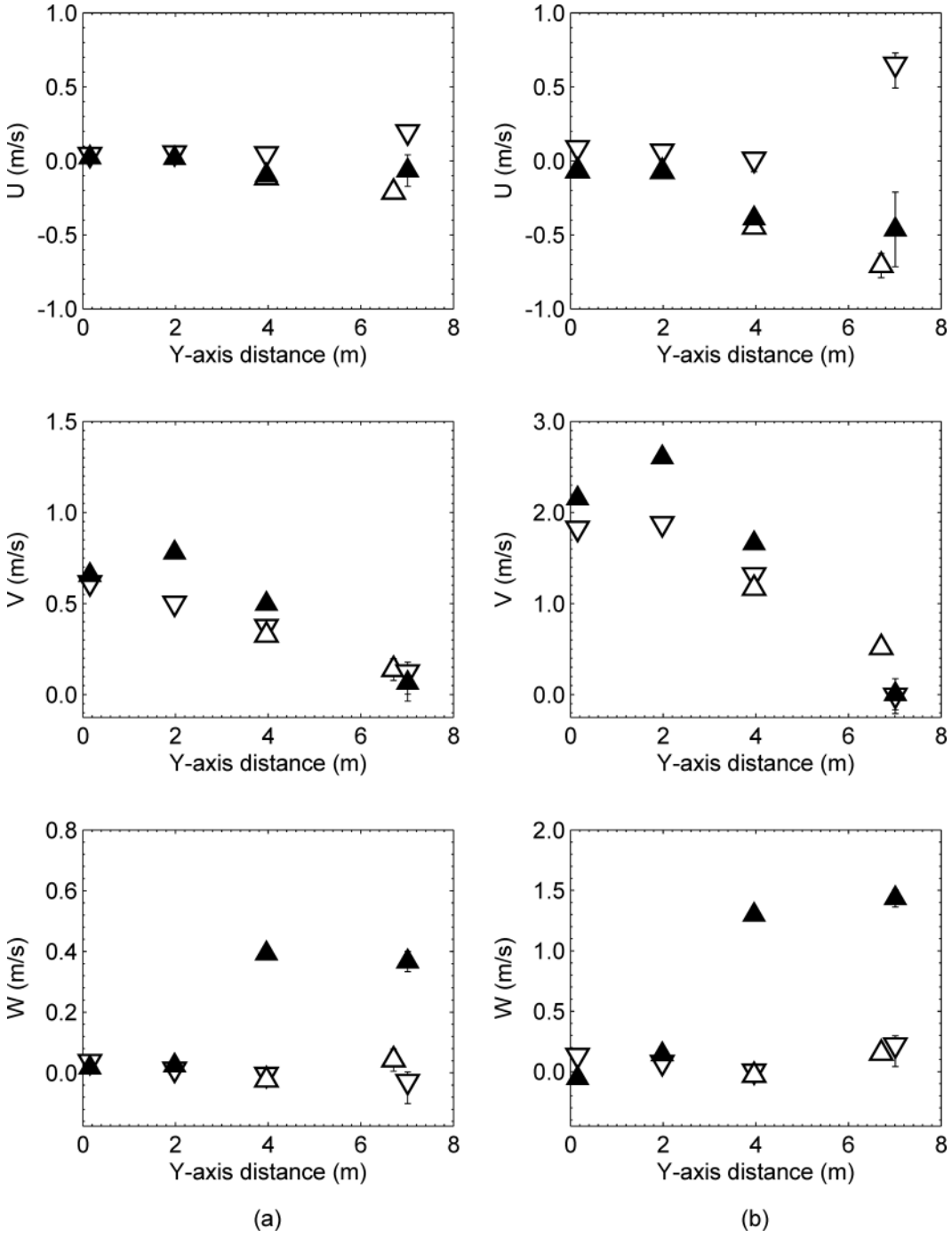

Figure 3-3: Sonic anemometer velocity measurements in the subfloor at a height of z = 0.76 m (2.5 ft) for the (a) 78 ACH, and (b) 265 ACH airflow rates. Symbols are mean values and error bars provide ±RMS variation from the mean. Measurements at x = 0.3 m (1 ft) ▲, 0.9 m (3.0 ft) △, and 2.1 m (6.9 ft) ▽.

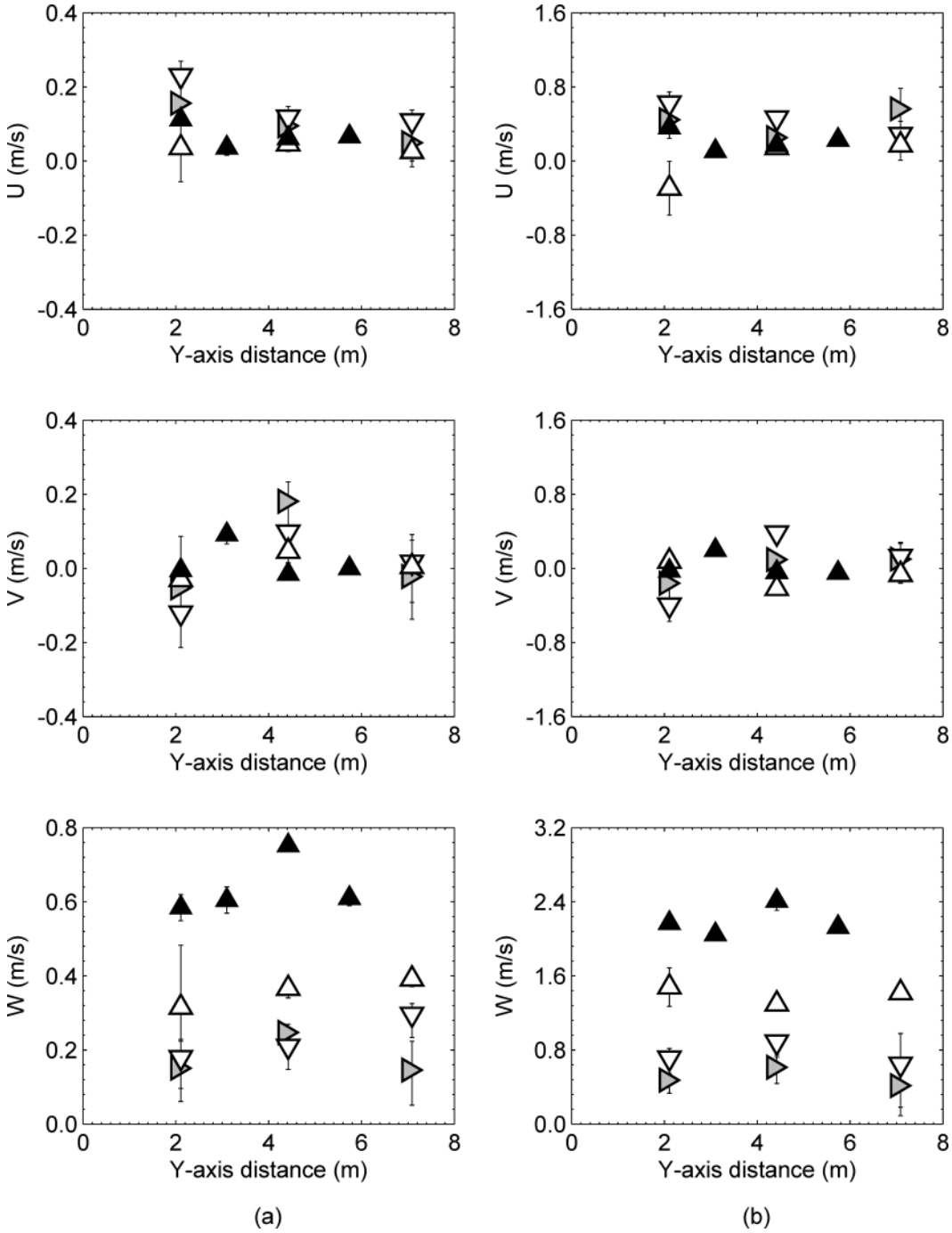

Figure 3-4: Velocity measurements upstream of the server cabinets in the cold aisle at a location x = 0.38 m (1.25 ft) for the (a) 78 ACH, and (b) 265 ACH airflow rates. Symbols are mean values and error bars provide ±RMS variation from the mean. Measurements at z = 0.1 m (0.33 ft) ▲, 0.6 m (2 ft) △, 1.2 m (3.9 ft) ▽, and 1.5 m (4.9 ft) ▷, above the server room floor.

3.3 HOT AISLE MEASUREMENTS

Velocity measurements in the hot aisle are presented for two planes: near the server cabinet ($x \approx 1.5$ m, 4.9 ft) and at the center of the server room ($x = 2.4$ m, 8 ft). The locations near the server cabinets provide valuable information regarding the flow across the servers, whereas the center plane measurements help identify larger-scale flow structures in the enclosure.

3.3.1 Next to Server Cabinets

Velocity measurements using the sonic anemometer downstream of the server cabinets are shown in Figure 3-5. Three vertical locations were selected $z = 0.6$, 1.2, and 1.8 m (2, 3.9, and 5.9 ft) above the server room floor. The flow exits the server cabinet primarily in the x-direction, which is observable in the U velocity measurements in Figure 3-5. At $z = 1.8$ m (5.9 ft) height above the server room floor, which coincides with the heights of the server cabinets, the U velocities are expectedly small. The RMS components of the velocities at $z = 1.8$ m (5.9 ft) are significant compared to their means, indicating the presence of unsteady, recirculating flow. For the 265 ACH air exchange rate, the V and W velocities are small compared to the U velocities, which is expected as the flow through the server cabinets, in most parts, is essentially one-dimensional in the x-direction. For the 78 ACH flow rate, as seen in Figure 3-5(a), the mean U velocities range between 0.1 m/s (20 ft/min.) and 0.3 m/s (59 ft/min.); however, their corresponding RMS values are considerable. The flow, therefore, is highly unsteady downstream of the server cabinets. Unlike the 265 ACH, the flow downstream of the server cabinets is three-dimensional for the 78 ACH flow rate case.

3.3.2 Center Plane in the Hot Aisle

Velocity measurements in the center of the hot aisle are presented in Figure 3-6. Three vertical locations were selected $z = 0.6$, 1.2, and 1.5 m (2.0, 3.9, and 4.9 ft) and $z = 0.6$, 1.2, and 1.8 m (2.0, 3.9, and 5.9 ft) above the server room floor for the 78 and 265 ACH cases, respectively. For the lower flow rate case of 78 ACH, at $y < 7.3$ m (24 ft) locations, the mean U velocity is in the range of ±0.05 m/s (10 ft/min.); these are low values compared to the RMS component, which is an indication that in the x-direction the mean flow was stationary and the unsteadiness in the flow was caused by turbulent fluctuations. Variations of U velocity at different measurement

heights from the server room floor are minor. This is not the case for the mean V velocity, which becomes increasingly negative with height. The W velocity values indicate that at locations closest to the east wall the flow is in the downward direction. The downward flow velocity, along with the negative V velocity, is probably due to the presence of the open area between the east wall and the server cabinets, which causes the flow to recirculate. With increasing y-distance, the W velocity magnitude decreases and at y = 7.1 m (23.3 ft) is negligible. The RMS components of the V and W velocities at locations closest to the east wall are also large. In addition, the reversal in the trend of the W velocities for the 265 ACH case is also indicative of the presence of the recirculation zone in the open space. For the higher flow rate case of 265 ACH, in Figure 3-6(b), it can be observed that the U velocities at every y-direction location vary in the range ±0.3 m/s (59 ft/min.) with high RMS components indicating fluctuating flow in the north-south directions.

3.3.3 Ceiling Plane in the Hot Aisle

In Figure 3-6 velocities measured at a plane 0.15 m (0.5 ft) below the ceiling are shown. Velocities for the low flow rate case, 78 ACH, are small (between ±0.3 m/s) for all components. No discernable trends are observed for the velocities. At y = 7.1 m, the U velocity shows greater scatter than the other two components. For the higher flow rate case, 265 ACH, the scatter in the data is pronounced and U and V velocities show positive and negative scatter, whereas, in general, the W velocity shows positive values. Since the flow near the ceiling is affected by the outlet vents and involves recirculation regions, it is difficult to characterize the flow in this plane.

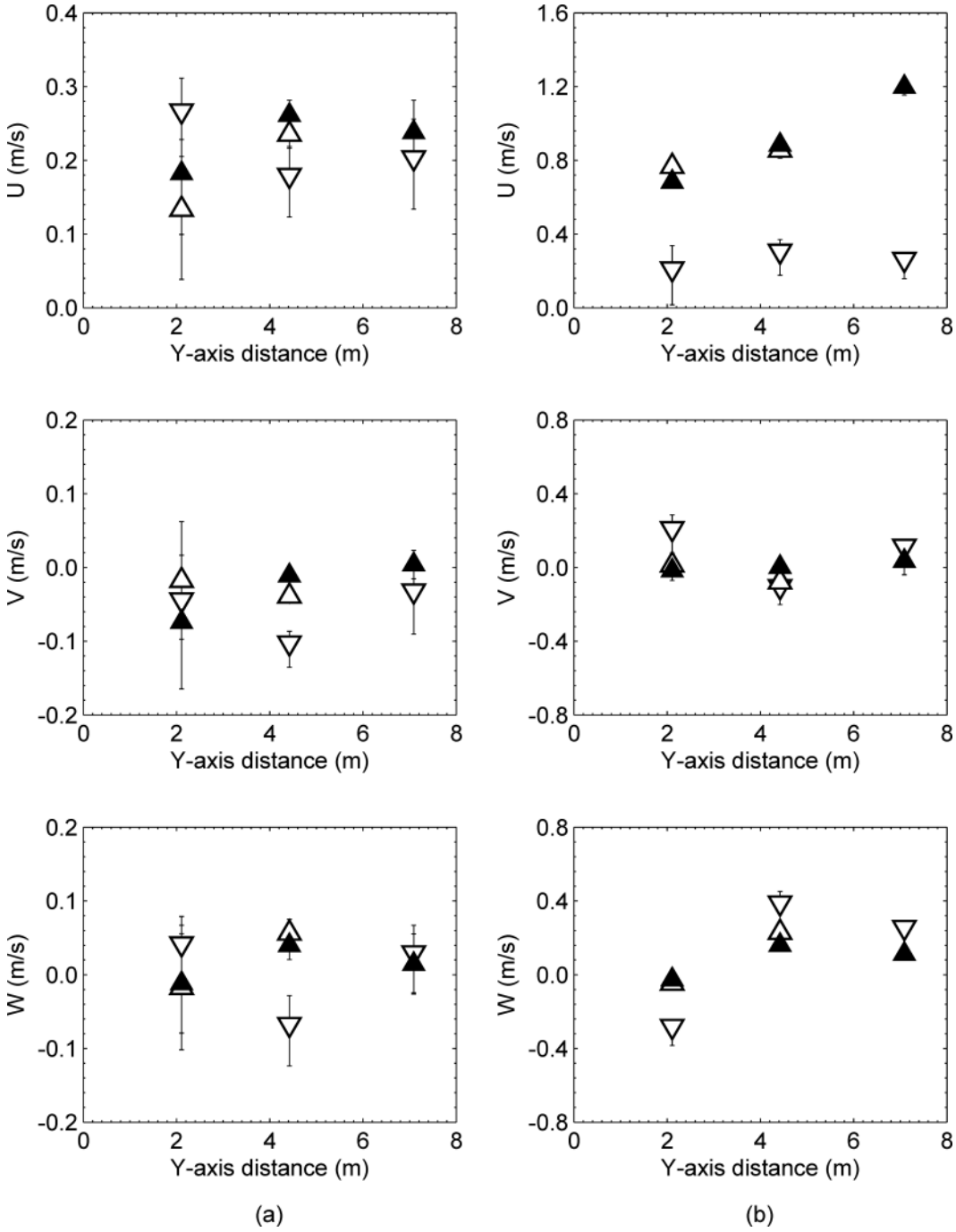

Figure 3-5: Velocity measurements downstream of the server cabinets (x ≈ 1.5 m, 4.9 ft) in the hot aisle for the (a) 78 ACH, and (b) 265 ACH airflow rates. Symbols are mean values and error bars provide ±RMS variation from the mean. Measurements at z = 0.6 m (2.0 ft) ▲, 1.2 m (3.9 ft) △, and 1.8 m (5.9 ft) ▽, above the server room floor.

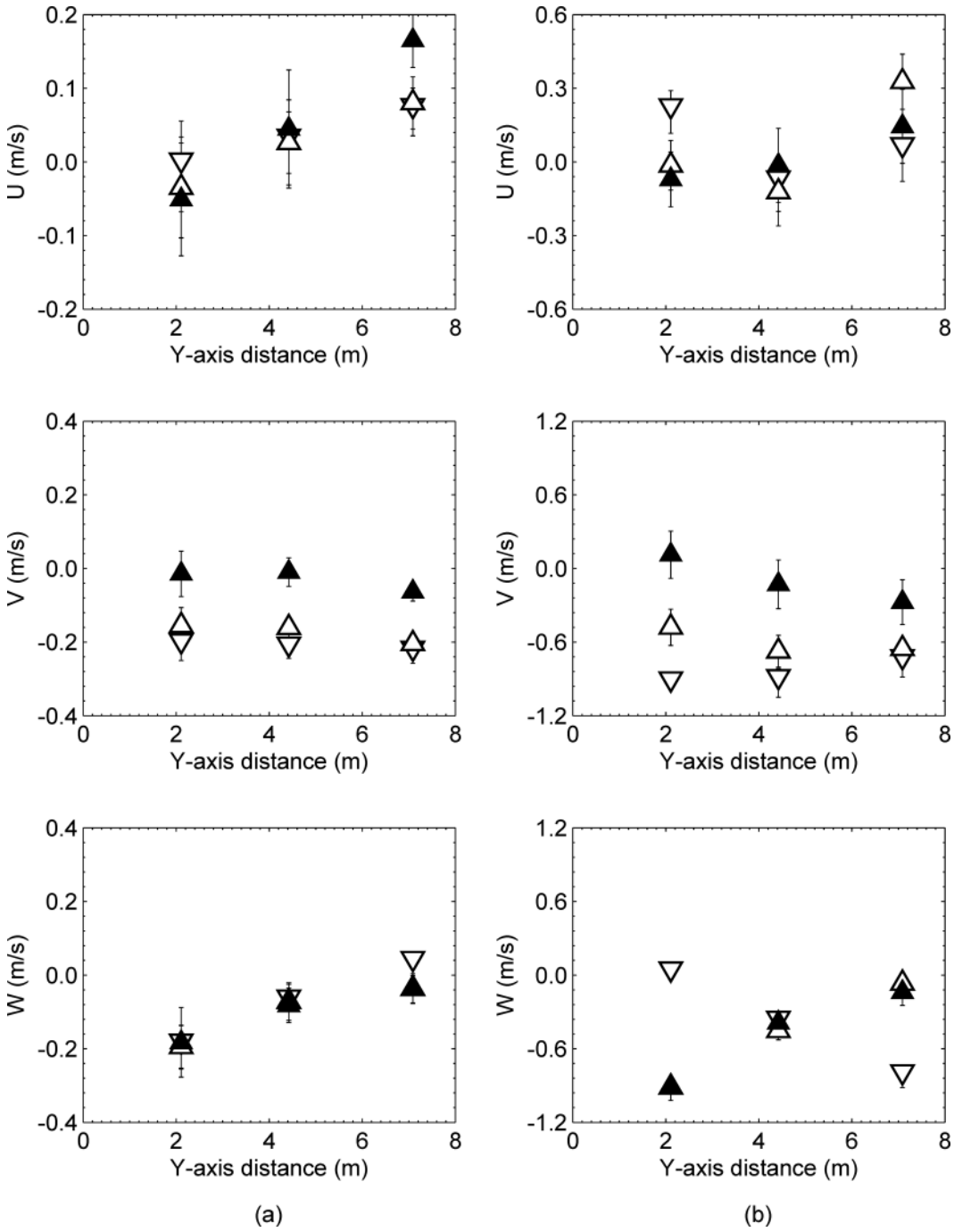

Figure 3-6: Velocity measurements on the vertical mid-plane (x = 2.4 m, 8 ft) of the hot aisle for the (a) 78 ACH, and (b) 265 ACH airflow rates. Symbols are mean values and error bars provide ±RMS variation from the mean. Measurements at z = 0.6 m (2.0 ft) ▲, 1.2 m (3.9 ft) △, and 1.5 m (4.9 ft) for 78 ACH or 1.8 m (5.9 ft) for 265 ACH ▽, above the server room floor.

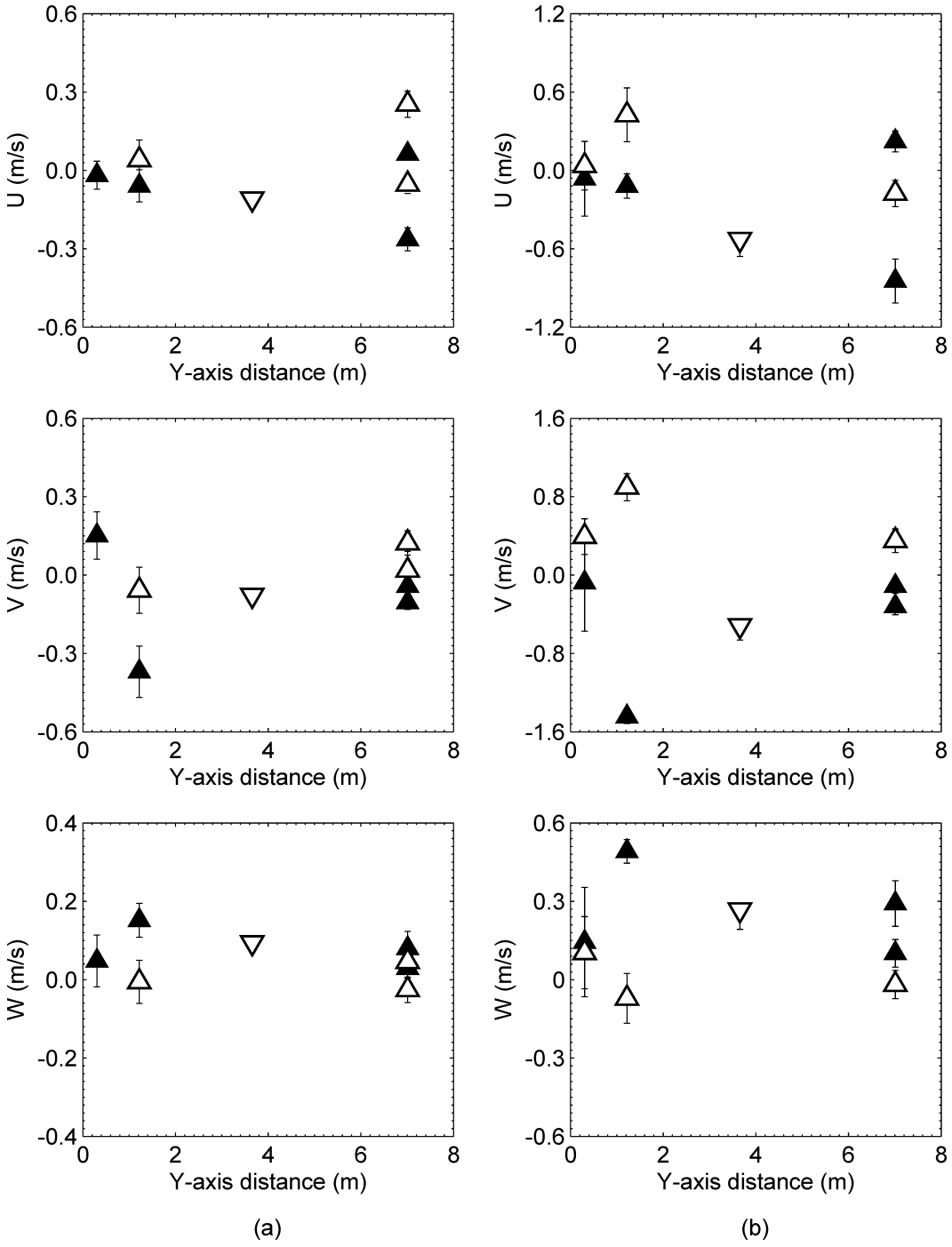

Figure 3-7: Sonic anemometer velocity measurements on a plane 0.15 m (0.5 ft) below the ceiling in the hot aisle for the (a) 78 ACH, and (b) 265 ACH airflow rates. Symbols are mean values and error bars provide ±RMS variation from the mean. Measurements at x = 0.9 m (3.0 ft) △, 2.1 m (6.9 ft) ▽, and 2.4 m (8 ft) ▲.

3.4 CEILING PLENUM MEASUREMENTS

The flow in the ceiling plenum is driven by the suction provided by the blower downstream of the plenum outlet and the resulting incoming air through the ceiling vents (see Figure 2-19 for vent locations on the ceiling). The flow enters vertically and then turns towards the plenum outlet (the negative y-direction). Sonic anemometer measurements were taken away from the ceiling vents; therefore, the vertical component of velocity was found to be smaller compared to the other two components. Measurements were taken at x = 0.9 m (3.0 ft) and close to the plenum centerline, x ≈ 2.4 m (7.9 ft). All measurements were performed at z = 0.76 m (2.5 ft) above the ceiling. At x = 0.9 m (3.0 ft) no vents are present, whereas measurements at the centerline were affected by the close proximity of the ceiling vents. Figure 3-8 shows the ceiling plenum velocity measurements for the two flow rate cases. A general trend in the V velocity can be observed for both the 78 ACH and 265 ACH cases – the V velocity becomes increasingly negative from the west wall, y = 7.3 m (24 ft), to the outlet plane, y = 0.0 m (0 ft). This is expected behavior due to the fan suction. The flow entering the plenum through the vents turns outwards in the north (+x) and south (-x) directions, resulting in higher U velocities at the outer regions (x = 0.9 m. 3.0 ft). The U velocity on the centerline remains small, and the flow is predominantly in the y-direction. The RMS components of the U velocity at x = 0.9 m (3.0 ft) are higher than on the centerline, indicating the presence of unsteady flow in the outer regions. The vertical component of velocity for both flow rates remains small – approximately ±0.2 m/s (39 ft/min.) for the 78 ACH case and ±0.5 m/s (98 ft/min.) for the 265 ACH flow rate. Higher W velocities are, however, expected at the inlet vent locations.

These tests establish the baseline velocity profile and conditions under which the smoke tests were conducted and serve as a good comparison for the computational models. In addition, the data from the bi-directional velocity probes (Appendix D) provide valuable information of velocity measurements in the vicinity of the smoke detectors. The velocity information from these tests can be used to first make comparisons with the airflow distribution in the model. Since the smoke transport is expected to be driven by this velocity distribution, the above set of data can then be used in the tests with the smoke sources as it is expected that the smoke sources have minimal effects on the airflow distribution.

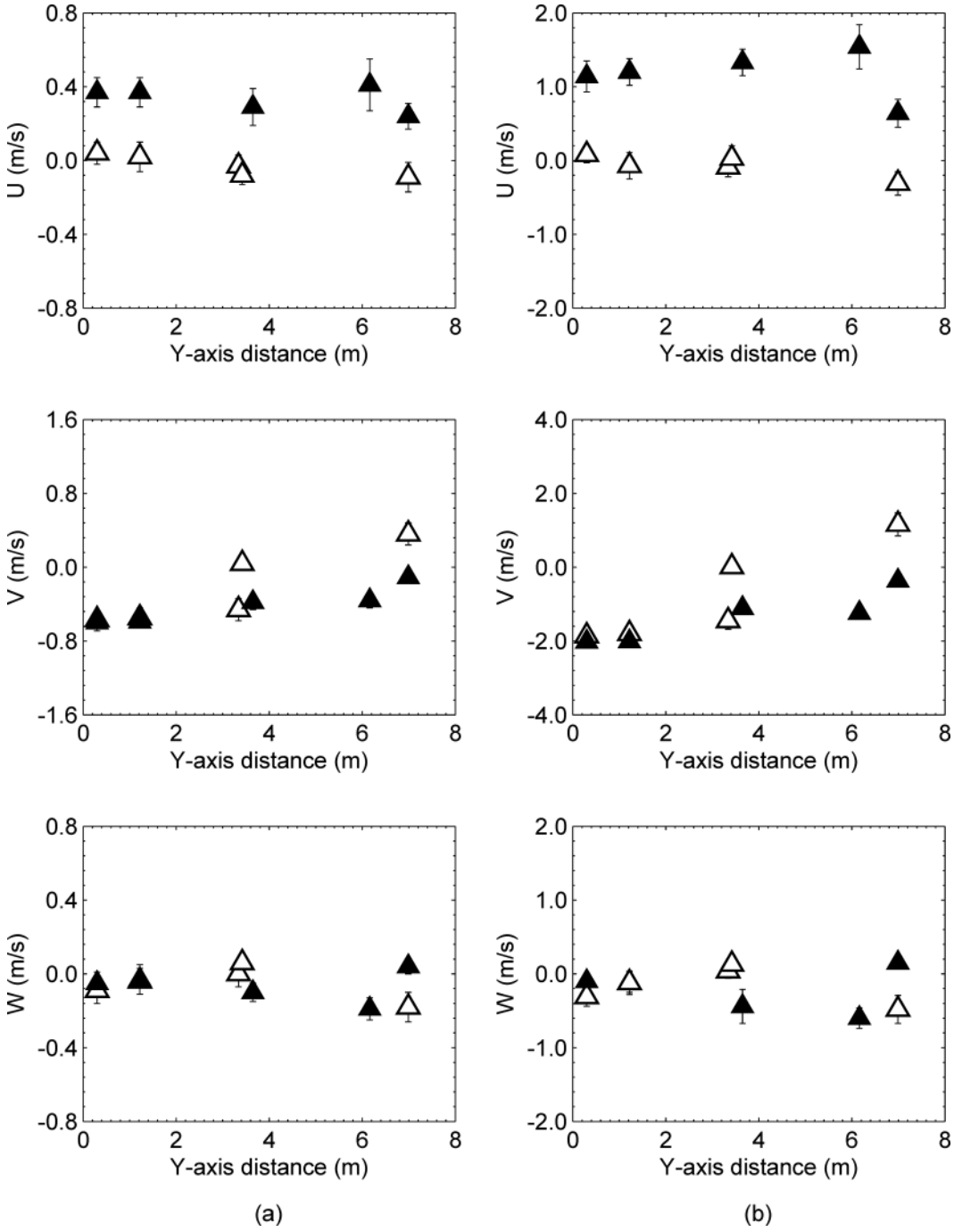

Figure 3-8: Velocity measurements in the ceiling plenum (at z = 0.76 m, 2.5 ft above the ceiling) for the (a) 78 ACH, and (b) 265 ACH airflow rates. Symbols are mean values and error bars provide ±RMS variation from the mean. Measurements at x = 0.9 m (3.0 ft) ▲, and 2.4 m (7.9 ft) △.

4 LARGE-SCALE SMOKE DISTRIBUTION TESTS

Ten large-scale smoke distribution tests were conducted to measure the smoke concentration dynamics and evaluate the detector response with smoke sources placed in various sections of the room. Tests were conducted at air exchange rates of 78 and 265 ACH. A summary of the test conditions, including the type of smoke source along with its location and air exchange rate, is shown in Table 4-1.

Primary measurement of the smoke concentration in the test enclosure was obtained with the smoke concentration meter (SCM). As described in Section 2.6.5, the SCM consists of the laser-based light extinction measurement (Aspirated Laser), which provides time-resolved smoke concentrations, and the smoke deposition measurement (Gravimetric Filter), which provides time averaged smoke mass. Measurements were independently sampled at three locations coinciding with the instrumentation clusters at *Subfloor West*, *Server Room Center* and *Ceiling Plenum East* locations.

The results of the smoke concentration meter are presented with two purposes. The Aspirated Laser measurements are provided (i) to characterize the dynamics of smoke concentration within the enclosure for model validation purposes and (ii) to provide data characterizing dynamic response of the smoke detectors to smoke concentration in their vicinity. Corresponding smoke mass measured by the Gravimetric Filter is provided to validate the results of the Aspirated Laser.

In addition to the smoke concentrations, the response of the 27 smoke detectors is also presented. As noted in Section 2.6, the detectors were clustered at nine locations with three clusters each in the subfloor, server room and ceiling plenum. Each cluster consisted of three detectors, referred to as Aspirated, Spot-S and Spot-T. The smoke concentration was independently measured at one cluster location in each section of the test enclosure using a separate smoke concentration meter. Schematics of the smoke concentration meter, detector and smoke source locations have been shown in Figure 2-18 through Figure 2-20.

Table 4-1: Description of test configurations.

Case #	Smoke Source			Air Exchange Rate (ACH)
	Type	**Location**	**Closest Smoke Detector Cluster**	
1a	Propylene	Subfloor	*Subfloor West*	78
	Propylene	Subfloor	*Subfloor West*	265
1b	Propylene	Hot Aisle	*Server Room West*	78
	Propylene	Hot Aisle	*Server Room West*	265
2	Foam	Cold Aisle	*Server Room Center*	78
	Foam	Cold Aisle	*Server Room Center*	265
3	Circuit Boards	Cabinet	*Server Room Center*	78
	Circuit Boards	Cabinet	*Server Room Center*	265
4	Cables	Subfloor	*Subfloor West*	78
	Cables	Subfloor	*Subfloor West*	265

Additional details on the location of the smoke sources can be found in Section 2.7.

4.1 PROPYLENE BURNER IN THE SUBFLOOR

Figure 4-1 shows photos of the flame from the propylene burner placed in the subfloor (close to the west enclosure wall), at air exchanges rates of 78 and 265 ACH. At the lower air exchange rate of 78 ACH (Figure 4-1a), the flames are nearly vertical and there is minimal leaning of the flames. At the higher air exchange rate of 265 ACH (Figure 4-1b) the flame exhibits considerable lean towards the west wall due to the momentum of the inlet airflow.

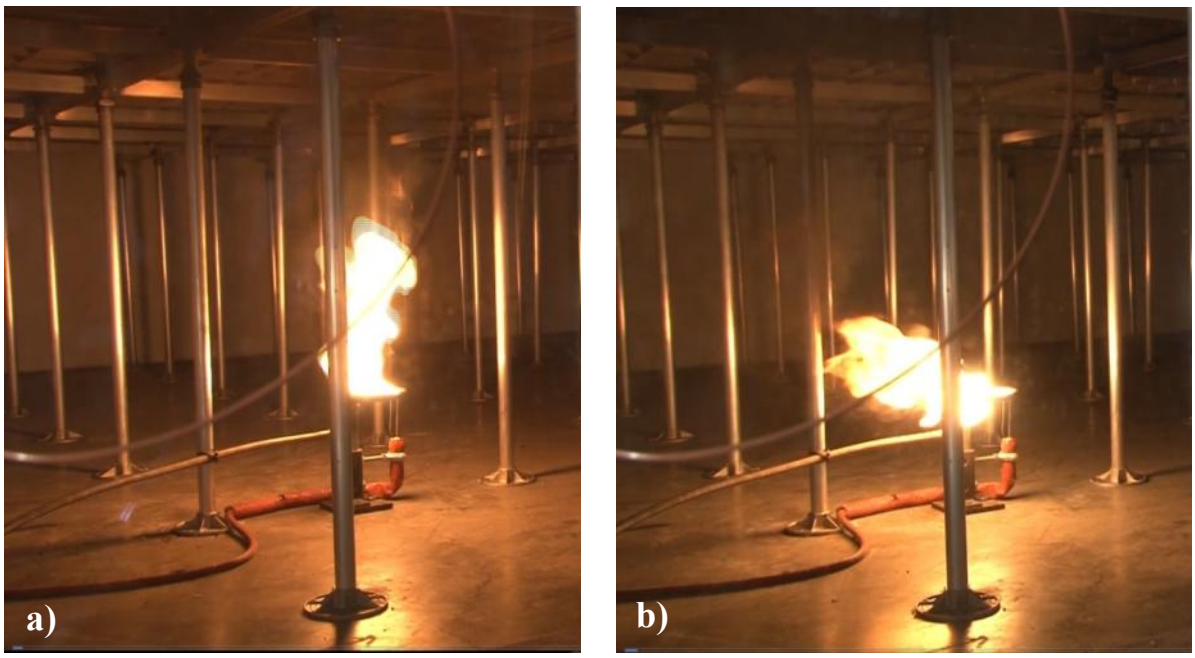

Figure 4-1: Photos of the flame from the propylene ring burner located at the subfloor at the air exchange rates of a) 78 ACH and b) 265 ACH.

4.1.1 Smoke Concentration Measurements

The time resolved smoke mass concentration for the sample case of the propylene burner in the subfloor is shown in Figure 4-2. As the propylene burner was located in close proximity to the Aspirated Laser located in the subfloor, the highest smoke level was correspondingly measured in the subfloor. This is due to the short transport distance from the smoke source to the Aspirated Laser (allowing for limited dilution to take place) and the fact that the measurement is taken downstream of the smoke source. The smoke then dilutes with ventilation air during transport through the enclosure. Smoke levels in the *Server Room Center* were below the detection limits of the Aspirated Laser suggesting that minimal smoke reached the center of the ceiling in the hot aisle. All ventilation air passed through the ceiling plenum before exiting the enclosure, resulting in the lower smoke level sampled in the *Ceiling Plenum East* location. The light extinction measurements from the laser system are presented in Appendix E.

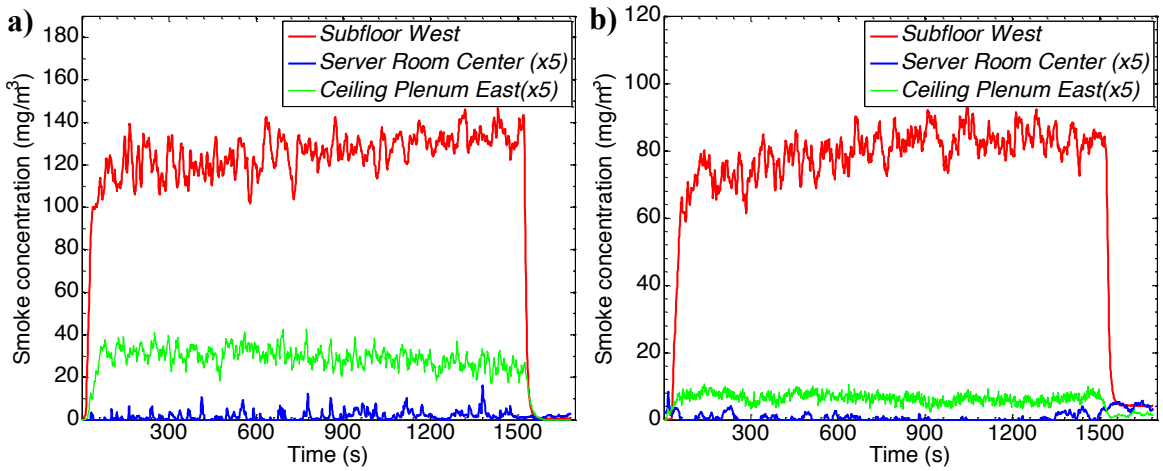

Figure 4-2: Smoke concentration for the Aspirated Laser to the propylene burner in the subfloor at an air exchange rate of (a) 78 ACH and (b) 265 ACH.

Table 4-2 contains the average smoke mass concentration during each test measured with the Aspirated Laser. Measurement locations where smoke was not present or where concentrations were below the detection limit are marked with a dash (-).

Table 4-2: Average smoke concentrations from the Aspirated Laser for the case of the propylene burner placed in the subfloor.

Smoke Source	Air exchange rate (ACH)	Measurement Location	Extinction (%/m)	Smoke concentration (mg/m^3)
Propylene (Subfloor)	78	Subfloor	71.8	126.3
		Server Room	0.4	0.36
		Ceiling Plenum	5.7	5.90
	265	Subfloor	55.3	80.1
		Server Room	-	-
		Ceiling Plenum	1.3	1.30

4.1.2 Smoke Detector Response

Figure 4-3 shows the obscuration levels from the smoke detectors at *Subfloor West* for air exchange rates of 78 and 265 ACH. As expected for the propylene burner, the data generally exhibited a short transient followed by a relatively steady-state behavior. From Figure 4-3a the

average (over 1,000 s) obscuration measurement from the Aspirated detector at an air exchange rate of 78 ACH was 4.8%/m (1.5 %/ft). From Figure 4-3b, increasing the air exchange rate to 265 ACH resulted in average obscuration measurements of 2.1 %/m (0.64 %/ft) for the Aspirated detector. At both air exchange rates, the Spot-T detector and Spot-S detectors recorded their respective saturation levels of ~ 6.6 %/m (2 %/ft) and ~ 13 %/m (4 %/ft). These high obscuration values are due to the fact that the detector cluster location is in the direction of the smoke transport and in close proximity to the burner.

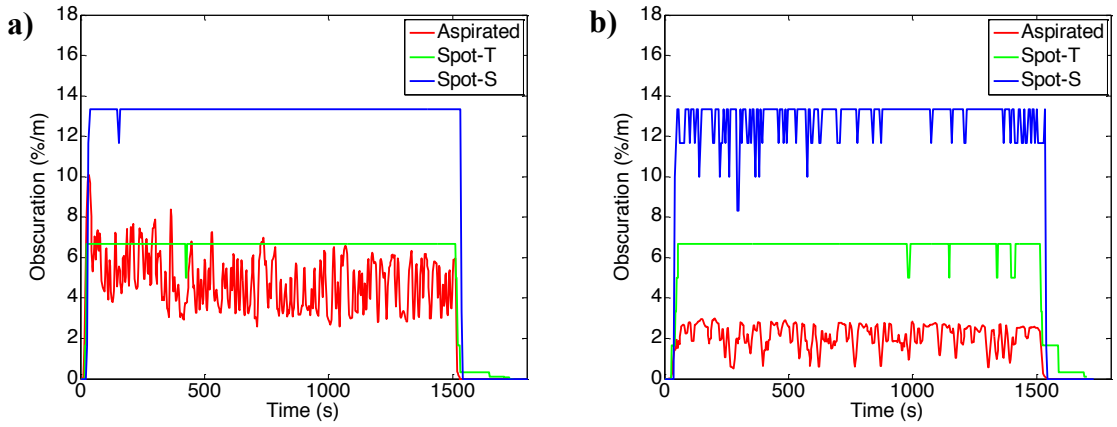

Figure 4-3: Sample response for the cluster of smoke detectors at *Subfloor West* to the propylene burner in the subfloor at air exchange rates of a) 78 ACH and b) 265 ACH.

The average response of the each smoke detector at air exchange rates of 78 and 265 ACH is shown in Table 4-3. Table 4-4 shows the initial response time of each smoke detector above its minimum obscuration threshold, listed in Section 2.6.1, at air exchanges rates of 78 and 265 ACH. For this evaluation, the Aspirated detector response threshold was set to 0.0067 %/m (0.0020 %/ft) to avoid signal noise that was observed at the minimum detection limit (i.e., 0.002 %/m (0.00061 %/ft).

The first response for each detector type occurred at *Subfloor West*, which was in close proximity to the burner and within the flow of smoke emitted from the flame. At this location, increasing the air exchange rate increased the initial response time, which can be attributed to the flame lean at 265 ACH, directing less smoke to the detector cluster (Figure 4-1). For the remainder of the detector clusters, increasing the air exchange rate decreased or had minimal impact on the

response time of the Aspirated detectors, while the response time increased for the Spot-T and Spot-S detectors.

Measurement conditions where the smoke detector did not respond are marked with a dash (-), and conditions where the detector was saturated are marked with a greater-than (>) symbol. Obscuration values below the manufacturer specified range, as detailed in Section 2.6.1, result from averaging of the discrete levels reported by the detector. Time-resolved obscuration plots for all tests can be found in Appendix F.

The reader is reminded that the detector response, i.e., obscuration measurement, does not directly relate to smoke concentration and should not be compared between detectors. As discussed in Section 1.1.3, even if the detectors receive the same amount of smoke, their outputs could be different. Furthermore, the obscuration measurements are a function of the type of smoke. For example, the smoke produced from a propylene burner and the smoke from the electric cables produce a different response. This is due to the fact that obscuration is based on light extinction which in turn depends on the type of smoke particles (see Section 1.1.3). In addition, for a given instrumentation cluster, each detector type was placed about 1 ft apart (see Figure 2-17). Hence, at the same cluster location, it is possible that each detector saw a different amount of smoke (based on the airflow). For the sake of this project, focus was placed on making comparisons across the different locations for the same type of detector, as a means of relating smoke transport to detector response, and not on comparing the performance between detectors.

The highest obscuration levels for each detector were recorded at *Subfloor West* due to the close proximity of the detector cluster to the smoke source. No response was recorded against the direction of airflow for any detector at *Subfloor East.* For the air exchange rate of 78 ACH, all detectors in the server room and ceiling plenum responded. At the increased air exchange rate of 265 ACH, only the Aspirated detectors consistently responded, while the Spot-T and Spot-S detectors did not respond at *Server Room Center* or *Server Room East.* The ceiling plenum was the most reliable measurement location, as all detector types consistently responded at both air exchange rates. These results highlight the importance of detector location and airflow currents

(i.e., smoke transport) in detecting a smoke source. In particular, the detector closest to the smoke source may not provide the most reliable response.

Table 4-3: Steady-state response of smoke detectors* (obscuration, %m (%/ft)) to propylene burner in the subfloor at air exchange rates of 78 and 265 ACH.

Detector Cluster		Aspirated Detector		Spot-T Detector		Spot-S Detector	
		78 ACH	265 ACH	78 ACH	265 ACH	78 ACH	265 ACH
Subfloor	East	-	-	-	-	-	-
	Center	0.11 (0.03)	-	-	-	1.13 (0.35)	-
	West	4.80 (1.5)	2.11 (0.64)	6.61 (2.02)	6.48 (1.98)	> 13.13 (> 4.0)	> 12.68 (> 3.87)
Server Room	East	0.16 (0.05)	0.02 (0.006)	0.32 (0.10)	-	0.84 (0.26)	-
	Center	0.04 (0.01)	0.01 (0.003)	0.01** (0.003)	-	0.92 (0.28)	-
	West	0.20 (0.06)	0.19 (0.06)	1.62 (0.49)	0.32 (0.10)	4.66 (1.42)	1.59 (0.49)
Ceiling Plenum	East	0.20 (0.06)	0.11 (0.03)	0.37 (0.11)	0.11 (0.03)	2.01 (0.06)	0.62** (0.19)
	Center	0.19 (0.06)	0.08 (0.02)	0.51 (0.16)	0.10 (0.03)	3.32 (1.0)	0.56** (0.17)
	West	0.21 (0.06)	0.10 (0.03)	1.09 (0.33)	0.49 (0.15)	2.96 (0.90)	1.68 (0.51)

* The reader is reminded that the detector response, i.e., obscuration measurement, does not directly relate to smoke concentration and should not be compared between detectors.

** Values below manufacturer minimum threshold value

Table 4-4: Time (s) of initial response of smoke detectors above minimum obscuration thresholds to propylene burner in the subfloor at air exchange rates of 78 and 265 ACH.

Detector Cluster		Aspirated Detector		Spot-T Detector		Spot-S Detector	
		78 ACH	265 ACH	78 ACH	265 ACH	78 ACH	265 ACH
Subfloor	East	-	-	-	-	-	-
	Center	256	-	-	-	501	-
	West	12	22	19	29	27	41
Server Room	East	35	38	91	-	132	-
	Center	25	25	418	-	253	-
	West	32	30	50	104	55	79
Ceiling Plenum	East	30	25	66	91	66	-
	Center	25	27	50	86	60	-
	West	38	30	42	68	71	123

4.2 PROPYLENE BURNER IN THE HOT AISLE

Figure 4-4 shows photos of the flame from the propylene burner placed in the hot aisle (close to the west enclosure wall), at air exchange rates of 78 and 265 ACH. In both cases, the flame extends to nearly 0.6 m (2 ft) above the floor, and the black smoke emitted from the flame reaches the ceiling nominally above the burner. As previously shown in Figure 2-19, this burner was located beneath the corner of a ceiling vent and was in close proximity to the detector cluster near the west wall of the enclosure (i.e., *Server Room West*).

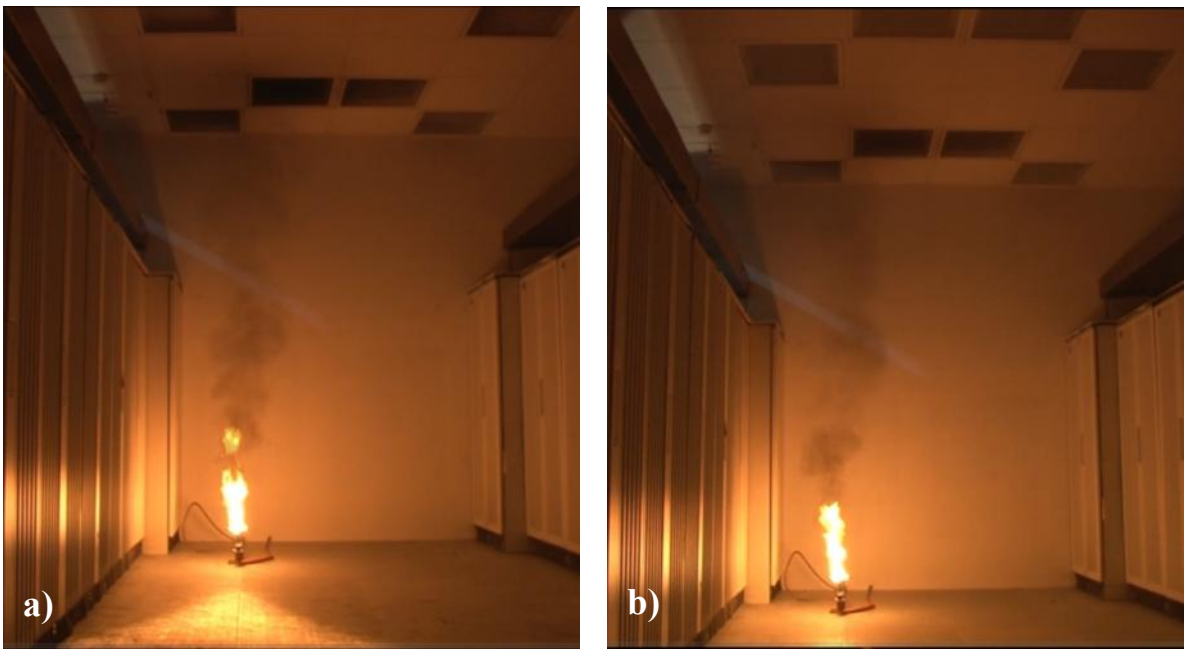

Figure 4-4: Photo of the flame from the propylene ring burner located in the hot aisle with an air exchange rate of a) 78 ACH and b) 265 ACH.

4.2.1 Smoke Concentrations Measurements

The time-resolved smoke mass concentration for the sample case of the propylene burner in the hot aisle is shown in Figure 4-5. At the lower air exchange rate of 78 ACH, it can be qualitatively seen that the *Ceiling Plenum East* location shows a steady smoke concentration of about 4 mg/m^3. At the higher air exchange rate of 265 ACH, due to the higher dilution, the smoke concentration at the *Ceiling Plenum East* location drops to about 1.7 mg/m^3. The light extinction measurements from the laser system are presented in Appendix E.

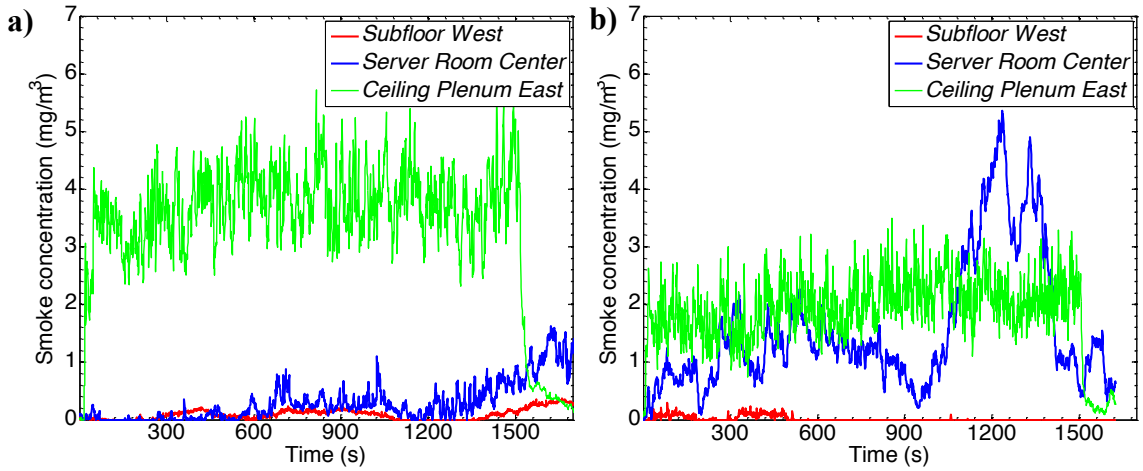

Figure 4-5: Smoke concentration from the Aspirated Laser for the propylene burner in the hot aisle of the server room at an air exchange rate of (a) 78 ACH and (b) 265 ACH.

Table 4-5 contains the average smoke mass concentration during each test measured with the Aspirated Laser. Measurement locations where smoke was not present or where concentrations were below the detection limit are marked with a dash (-). It can be noted that at the *Server Room Center* location, with an increase in the air exchange rate, the smoke concentration also increased, while at the Ceiling Plenum East location the smoke concentration decreased.

Table 4-5: Average smoke concentrations from the Aspirated Laser for the case of the propylene burner placed in the hot aisle.

Smoke Source	Air exchange rate (ACH)	Measurement Location	Extinction (%/m)	Smoke concentration (mg/m^3)
Propylene (Hot Aisle)	78	Subfloor	-	-
		Server Room	0.2	0.21
		Ceiling Plenum	3.8	3.90
	265	Subfloor	-	-
		Server Room	1.7	1.70
		Ceiling Plenum	2.0	2.01

4.2.2 Smoke Detector Response

Figure 4-6 shows the obscuration levels from the smoke detectors at *Server Room West* for air exchange rates of 78 and 265 ACH. As expected for the propylene burner, the data generally

exhibited a short transient followed by a relatively steady-state behavior.* From Figure 4-6a, the average obscuration measurements from each detector at an air exchange rate of 78 ACH were: 1.18 %/m (0.36 %/ft) for the Aspirated detector, 5.36 %/m (1.7 %/ft) for the Spot-T detector, and 10.1 %/m (3.2 %/ft) for the Spot-S detector. From Figure 4-6b, increasing the air exchange rate to 265 ACH resulted in obscuration measurements of: 0.13 %/m (0.04 %/ft) for the Aspirated detector, 0.01 %/m (0.003 %/ft) for the Spot-T detector, and 1.0 %/m (0.31 %/ft) for the Spot-S detector.

These data clearly indicate that increasing the air exhaust rate reduced the response of the smoke detectors. Obviously, the smoke concentration should decrease due to dilution as the exchange rate increases. The location of the detector relative to the ceiling vents also contributed to the lower response.

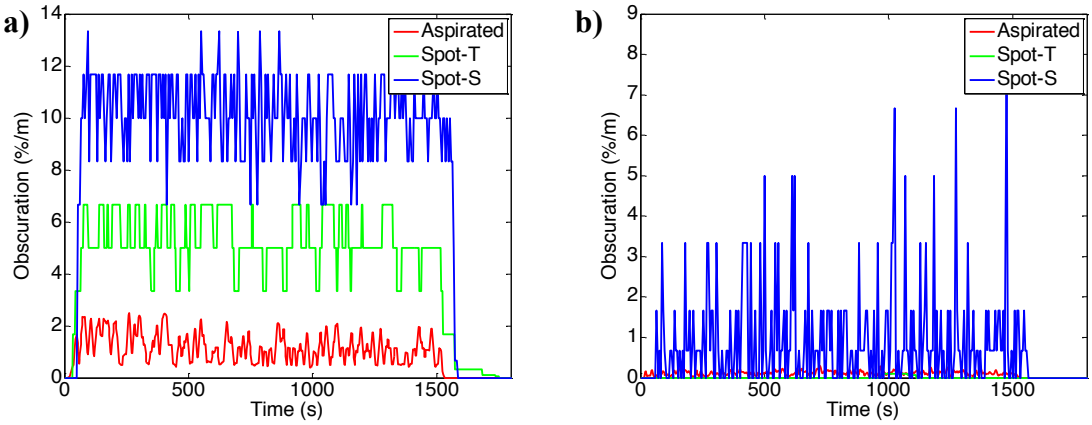

Figure 4-6: Sample response for the cluster of smoke detectors at *Server Room West* to the propylene burner in the hot aisle at air exchange rates of a) 78 ACH and b) 265 ACH.

Figure 4-7 shows the obscuration levels from the smoke detectors located just before the exhaust from the enclosure, i.e., *Ceiling Plenum East,* at air exchange rates of 78 and 265 ACH. From Figure 4-7a, the obscuration measurements (1,000 s average) at an air exchange rate of 78 ACH

* It should be noted that the Spot-S and Spot-T detectors respond in discrete steps based on the manufacturer's predefined threshold levels, while the Aspirated detector has a much greater sensitivity and hence the response appears smooth.

were: 0.22 %/m (0.07 %/ft) for the Aspirated detector, 0.35 %/m (0.11 %/ft) for the Spot-T detector, and 1.4 %/m (0.43 %/ft) for the Spot-S detector. Figure 4-7b shows similar data at the higher air exchange rate of 265 ACH and the resulting average obscurations were: 0.13 %/m (0.04 %/ft) for the Aspirated detector, 0.1 %/m (0.03 %/ft) for the Spot-T detector, and 0.7 %/m (0.21 %/ft) for the Spot-S detector.

Qualitatively, it can be seen that the increase in air exhaust rate decreases the response of the detectors in the ceiling plenum. The reduction in the detector response can be attributed to dilution of the local smoke concentration. However, while comparing this reduction in smoke concentration with those in the *Server Room West* location, it can be seen that the decrease in the ceiling plenum location is more pronounced. This is largely because all exhaust air travels past the detectors in the ceiling plenum and the effect of local air currents (significant in the server room) is minimal in the ceiling plenum.

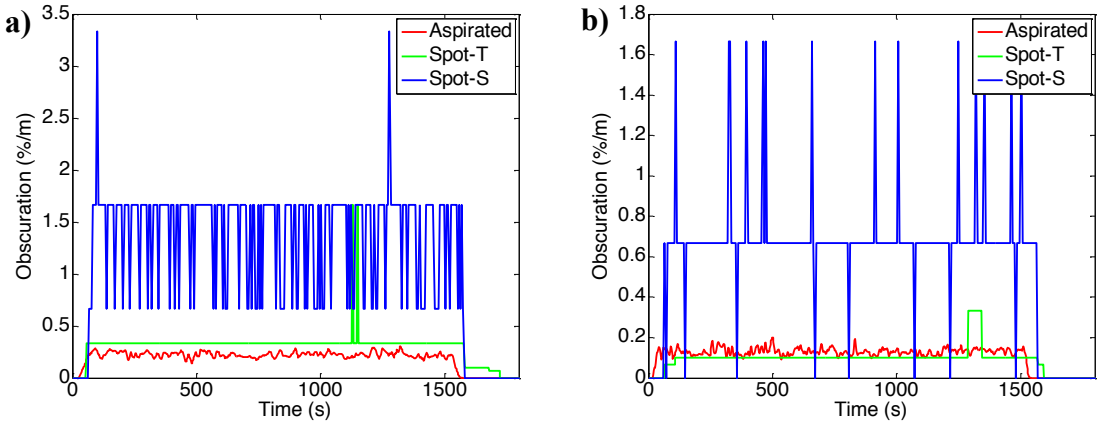

Figure 4-7: Sample response for the cluster of smoke detectors at *Ceiling Plenum East* to the propylene burner in the hot aisle at air exchange rates of a) 78 ACH and b) 265 ACH.

Table 4-6 presents the average response of each smoke detector at air exchange rates of 78 and 265 ACH. Measurement conditions where the smoke detector did not respond are marked with a dash (-). Obscuration values below the manufacturer specified range, as detailed in Section 2.6.1, result from averaging of the discrete levels reported by the detector (which can vary between

zero and the minimum reported threshold value). Time-resolved obscuration plots for all tests can be found in Appendix F.

Table 4-6: Steady-state response of smoke detectors* (obscuration, %m (%/ft)) to propylene burner in the hot aisle at air exchange rates of 78 and 265 ACH.

Detector Cluster		Aspirated Detector		Spot-T Detector		Spot-S Detector	
		78 ACH	265 ACH	78 ACH	265 ACH	78 ACH	265 ACH
Subfloor	East	-	-	-	-	-	-
	Center	-	-	-	-	-	-
	West	-	-	-	-	-	-
Server Room	East	0.03 (0.01)	0.02 (0.01)	-	-	-	-
	Center	-	-	-	-	-	-
	West	1.18 (0.37)	0.13 (0.04)	5.36 (1.7)	0.01** (0.003)	10.14 (3.1)	1.0 (0.30)
Ceiling Plenum	East	0.22 (0.07)	0.13 (0.04)	0.35 (0.11)	0.10 (0.03)	1.4 (0.43)	0.70 (0.21)
	Center	0.23 (0.07)	0.12 (0.04)	0.33 (0.10)	0.19 (0.06)	1.66 (0.52)	0.71 (0.22)
	West	1.25 (0.37)	0.06 (0.02)	2.88 (0.88)	0.30 (0.09)	7.57 (2.3)	0.31** (0.09)

* The reader is reminded that the detector response, i.e., obscuration measurement, does not directly relate to smoke concentration and should not be compared between detectors.

** Values below manufacturer's minimum threshold (obtained from averaging of the discrete values reported by the detector)

Comparison of the detector responses in the server room and ceiling plenum yield two key conclusions. First, increasing the air exchange rate reduced the obscuration level measured by the detectors. Second, the ceiling plenum was a more reliable measurement location to ensure smoke detection. For instance, the responses of Spot-T and Spot-S detectors were sporadic in the

server room, while the same detectors in the ceiling plenum always responded. In addition, no response is seen for any detectors in the subfloor, which is expected because the smoke does not flow against the direction of airflow.

Table 4-7 shows the initial response time of each smoke detector above its minimum obscuration threshold, listed in Section 2.6.1, at air exchanges rates of 78 and 265 ACH. For this evaluation, the Aspirated detector response threshold was set to 0.0067 %/m (0.002 %/ft) to avoid signal noise that was observed at the minimum detection limit (i.e., 0.002 %/m (0.00061 %/ft)). Measurement conditions where the smoke detector did not respond are marked with a dash (-).

These data provide a useful measure of the impact of smoke detector placement. For instance, for the 78 ACH conditions, the initial response of the Aspirated detector located at *Server Room West* occurred at 19 s, while that of the Aspirated detector at *Server Room East* did not occur until 60 s, and the detector at *Server Room Center* did not respond (above the minimum threshold value). The complex airflow within the server room likely contributed to the wide range of detector responses. The more uniform airflow in the ceiling plenum resulted in an initial response of all three Aspirated detectors within 24 – 30 s after ignition. Similar results are seen for the Spot-T and Spot-S detectors; however, a wider spread in the initial response times occurred due to the lower sensitivities of these detectors.

It is also observed that increasing the air exchange rate in the enclosure impacts the detector response to a given smoke source. The actual impact varies significantly by detector type and placement within the enclosure. For example at *Ceiling Plenum East*, the Aspirated detector initial response time decreased by 9 s, while the response of Spot-T and Spot-S detectors increased by 53 s and 43 s, respectively. These results suggest that understanding the impact of air exchange rate on both smoke concentration and transport time are critical to proper detector placement.[*]

[*] The detector response to the time rate of change in smoke concentration is also important for proper detector placement but was beyond the scope of this study.

Table 4-7: Time (s) of initial response of smoke detectors above minimum obscuration thresholds to propylene burner in the hot aisle at air exchange rates of 78 and 265 ACH.

Detector Cluster		Aspirated Detector		Spot-T Detector		Spot-S Detector	
		78 ACH	265 ACH	78 ACH	265 ACH	78 ACH	265 ACH
Subfloor	East	-	-	-	-	-	-
	Center	-	-	-	-	-	-
	West	-	-	-	-	-	-
Server Room	East	60	52	-	-	-	-
	Center	-	-	-	-	-	-
	West	19	18	34	972	55	65
Ceiling Plenum	East	30	21	55	108	66	109
	Center	24	16	50	82	61	126
	West	24	16	34	111	55	236

4.3 FOAM MATERIAL IN THE COLD AISLE

Figure 4-8 shows photos of the burning foam material at air exchange rates of 78 ACH and 265 ACH. This smoke source consisted of two blocks of polyethylene foam material separated by 0.3 m (1 ft) as detailed in Section 2.7.2. After ignition of the alcohol (within the holes drilled in each block), the surrounding hole diameter slowly increased as the foam material was consumed. There was no observed impact of air exchange rate on the combustion process. Minimal pooling of the foam was contained within the ignition holes, and the flames visually produced low amounts of smoke.

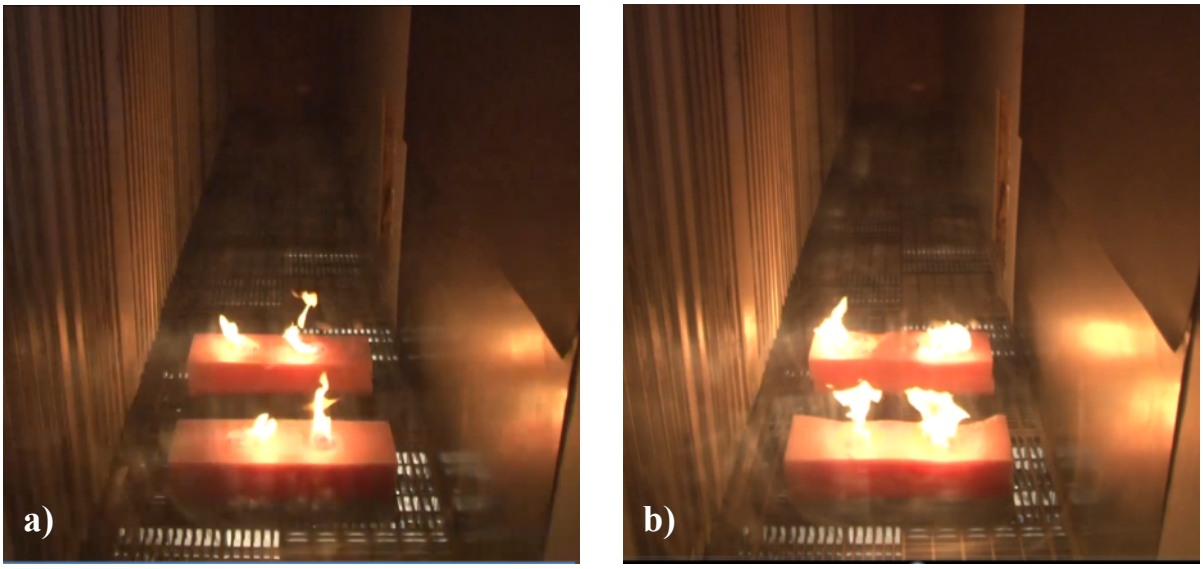

Figure 4-8: Photos of the flame from the foam material located in the cold aisle at air exchange rates of a) 78 ACH and b) 265 ACH.

4.3.1 Smoke Concentrations

The smoke concentration levels were very low in this case and did not reach the minimum threshold value as measured by the laser system. The gravimetric samples confirmed this result and did not show any measurable amounts of smoke collected.

4.3.2 Smoke Detector Response

Figure 4-9 show the obscuration levels from the smoke detectors at *Server Room West*. Unlike the steady-state propylene fires, the foam material represents a highly transient fire smoke source, which is reflected in the continually changing obscuration measurements from the detectors. From Figure 4-9a, at the air exchange rate of 78 ACH, the Spot-S detector measured four local peaks, with the first occurring at ~ 130 s after ignition with a magnitude of 0.7 %/m (0.24 %/ft). The Spot-T detector recorded three local peaks with the first occurring at approximately 320 s after ignition with a value of 1.6 %/m (0.49 %/ft). The Aspirated detector responded the earliest at 59 s (described in detail later). Similar results are seen in Figure 4-9b for the higher air exchange rate of 265 ACH, though the obscuration magnitudes are generally lower due to increased dilution of the smoke.

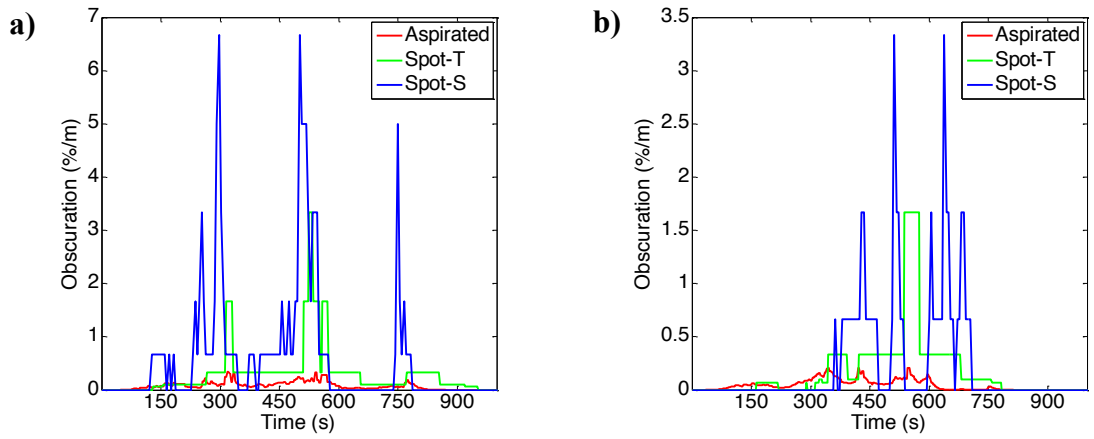

Figure 4-9: Sample response for the cluster of smoke detectors at *Server Room West* to the foam material in the cold aisle at air exchange rates of a) 78 ACH and b) 265 ACH.

Table 4-8 and Table 4-9 present the average and maximum response of each smoke detector at air exchange rates of 78 and 265 ACH, respectively. Measurement conditions where the smoke detector did not respond are marked with a dash (-) and conditions where the detector was saturated are marked with a greater-than (>) symbol. The average response of each detector was calculated as the integral of the obscuration measurements normalized by the duration of the foam fire (ignition to 730 s). Average obscuration values below the manufacturer specified range of the Spot-S and Spot-T detectors, as detailed in Section 2.6.1, result from time averaging of the discrete levels reported by the detector. Time-resolved obscuration plots for all tests can be found in Appendix F.

Similar detector response trends are seen at both air exchange rates. The detectors at *Server Room West* reported the highest obscuration levels (per detector type) in the enclosure, which suggests that the detector cluster is in the smoke transport path from the cold aisle into the ceiling plenum. Correspondingly, all three detectors directly above at *Ceiling Plenum West* also responded to the smoke source. All the remaining detectors in the server room and ceiling plenum recorded minimal or no response. In addition, no response was recorded from any detectors in the subfloor.

Table 4-8: Average and maximum response of detectors* (obscuration, %/m (%/ft)) to the foam material in the cold aisle at an air exchange rate of 78 ACH.

Detector Cluster		Aspirated Detector		Spot-T Detector		Spot-S Detector	
		Average	Maximum	Average	Maximum	Average	Maximum
Subfloor	East	-	-	-	-	-	-
	Center	-	-	-	-	-	-
	West	-	-	-	-	-	-
Server Room	East	~ 0.0	0.006 (0.002)	-	-	-	-
	Center	~ 0.0	0.004 (0.001)	-	-	-	-
	West	0.10 (0.03)	0.35 (0.11)	0.37 (0.11)	3.33 (1.02)	0.82 (0.25)	6.67 (2.08)
Ceiling Plenum	East	0.01 (0.003)	0.03 (0.01)	-	-	-	-
	Center	0.01 (0.003)	0.06 (0.02)	-	-	-	-
	West	0.04 (0.01)	0.13 (0.04)	0.12 (0.04)	0.33 (0.10)	0.25** (0.08)	3.33 (1.03)

* The reader is reminded that the detector response, i.e., obscuration measurement, does not directly relate to smoke concentration and should not be compared between detectors.

** Values below manufacturers minimum threshold value.

Table 4-9: Average and maximum response of detectors* (obscuration, %/m (%/ft)) to the foam material in the cold aisle at an air exchange rate of 265 ACH.

Detector Cluster		Aspirated Detector		Spot-T Detector		Spot-S Detector	
		Average	Maximum	Average	Maximum	Average	Maximum
Subfloor	East	-	-	-	-	-	-
	Center	-	-	-	-	-	-
	West	-	-	-	-	-	-
Server Room	East	-	-	-	-	-	-
	Center	-	0.01 (0.003)	-	-	-	-
	West	0.061 (0.019)	0.21 (0.064)	0.24 (0.07)	1.67 (0.51)	0.32** (0.099)	3.33 (1.02)
Ceiling Plenum	East	0.01 (0.003)	0.04 (0.012)	-	-	-	-
	Center	0.01 (0.004)	0.04 (0.01)	-	-	-	-
	West	0.03 (0.009)	0.08 (0.02)	0.05** (0.02)	0.33 (0.10)	0.15** (0.04)	1.67 (0.51)

* The reader is reminded that the detector response, i.e., obscuration measurement, does not directly relate to smoke concentration and should not be compared between detectors.

** Values below manufacturers minimum threshold value

Table 4-10 shows the initial response time of each smoke detector above its minimum obscuration threshold, listed in Section 2.6.1, at air exchanges rates of 78 and 265 ACH. For this evaluation, the Aspirated detector response threshold was set to 0.0067 %/m (0.002 %/ft) to avoid signal noise that was observed at the minimum detection limit (i.e., 0.002 %/m (0.00061 %/ft). Measurement conditions where the smoke detector did not respond are marked with a dash (-).

The first response for all the three detectors occurred at *Server Room West*, with the response times at this location increasing with air exchange rate. In the ceiling plenum, the detectors located at the *Ceiling Plenum West* locations responded the earliest and, while the Aspirated detector response time decreased with increasing air exchange rate, the opposite trend is seen to occur for the Spot-S and Spot-T detectors.

Table 4-10: Time (s) of initial response of smoke detectors above minimum obscuration thresholds to burning foam in the cold aisle at air exchange rates of 78 and 265 ACH.

Detector Cluster		Aspirated Detector		Spot-T Detector		Spot-S Detector	
		78 ACH	265 ACH	78 ACH	265 ACH	78 ACH	265 ACH
Subfloor	East	-	-	-	-	-	-
	Center	-	-	-	-	-	-
	West	-	-	-	-	-	-
Server Room	East	-	-	-	-	-	-
	Center	-	-	-	-	-	-
	West	59	69	156	322	126	363
Ceiling Plenum	East	210	110	-	-	-	-
	Center	171	105	-	-	-	-
	West	95	82	322	343	237	418

4.4 CIRCUIT BOARDS IN CABINETS

Figure 4-10 shows the placement of the circuit board within the server cabinet. The screen located inside the cabinet doors on the hot aisle side of the cabinet can also be seen. As detailed in Section 2.7.3, this smoke source consisted of two printed circuit boards sandwiched around a

heating element. Smoke from this assembly resulted from overheating of the combustible material, and no flaming combustion was observed at either air exchange rate of 78 or 265 ACH.

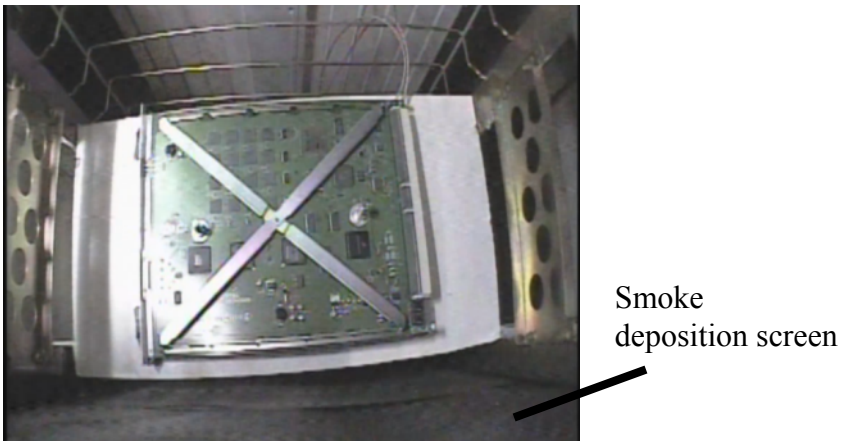

Figure 4-10: Circuit board placed inside a server cabinet.

4.4.1 Smoke Concentrations Measurements

The smoke concentration levels were very low in this case and did not reach the minimum threshold value as measured by the laser system. The gravimetric samples confirmed this result and did not show any measurable accumulation of smoke on the filters.

4.4.2 Smoke Detector Response

Figure 4-11 shows the obscuration levels from the detectors located at *Ceiling Plenum Center*. This location generally recorded the highest obscuration levels for each detector type. The trend in detector responses indicates that circuit boards produce smoke for a relatively short duration during this overheating condition. From Figure 4-11a, at the lower air exchange rate of 78 ACH the Spot-S detector recorded a peak response of 8 %/m (2.5 %/ft) and the Spot-T and Aspirated detectors recorded maximum obscuration levels of 1.5 %/m (0.46 %/ft) and 0.2 %/m (0.06 %/ft), respectively. From Figure 4-11b, at the higher air exchange rate of 265 ACH, the Spot-S detector showed the highest obscuration peak of 11 %/m (3.4 %/ft), followed by the Spot-T and Aspirated detectors which recorded maximum obscuration levels of 1.7 %/m (0.52 %/ft) and 0.4 %/m (0.12 %/ft) respectively.

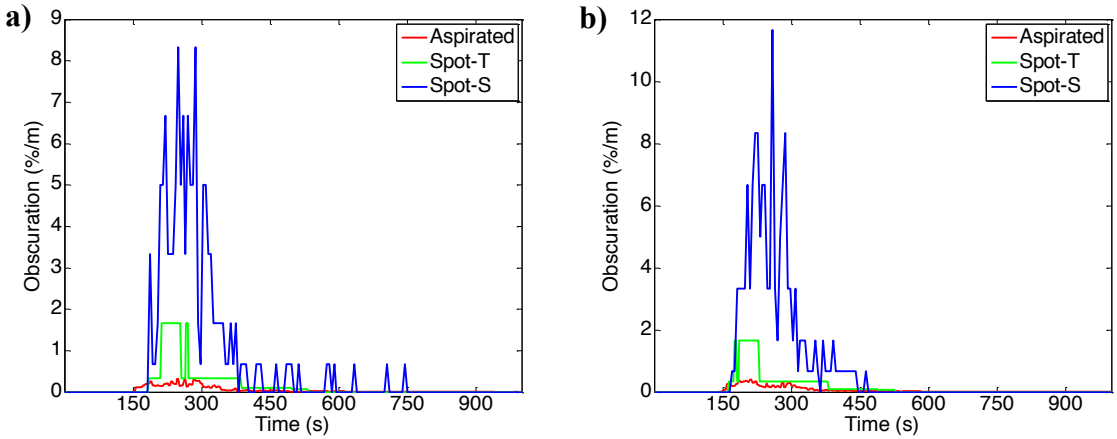

Figure 4-11: Sample response for the cluster of smoke detectors at *Ceiling Plenum Center* to overheated circuit boards inside a server cabinet at air exchange rates of a) 78 ACH and b) 265 ACH.

Table 4-11 and Table 4-12 present the average and maximum response of each smoke detector at air exchange rates of 78 and 265 ACH, respectively. Measurement conditions where the smoke detector did not respond are marked with a dash (-) and conditions where the detector was saturated are marked with a greater-than (>) symbol. The average response of each detector was calculated as the integral of the obscuration measurements divided by the heating time of the circuit boards (800 s). Average obscuration values below the manufacturer specified range of the Spot-S and Spot-T detectors, as detailed in Section 2.6.1, result from time averaging of the discrete levels reported by the detector. Time-resolved obscuration plots for all tests can be found in Appendix F.

At either air exchange rate, the highest response for each detector occurred at *Ceiling Plenum Center*, while the overheated circuit boards were located in a server cabinet (in the server room). The maximum detector responses throughout the enclosure generally reflect short duration peaks, as noted by the order of magnitude difference compared to the average response values. Similar to the other smoke sources, the ceiling plenum was generally the most reliable section to ensure detection.

Table 4-11: Average and maximum response of detectors* (obscuration, %/m (%/ft)) to overheated circuit boards in a server cabinet at an air exchange rate of 78 ACH.

Detector Cluster		Aspirated Detector		Spot-T Detector		Spot-S Detector	
		Average	Maximum	Average	Maximum	Average	Maximum
Subfloor	East	-	-	-	-	-	-
	Center	-	-	-	-	-	-
	West	-	-	-	-	-	-
Server Room	East	~ 0.0	0.003 (0.001)	-	-	-	-
	Center	~ 0.0	0.01 (0.003)	-	-	-	-
	West	0.01 (0.003)	0.07 (0.02)	-	-	0.02** (0.006)	0.67 (0.20)
Ceiling Plenum	East	0.02 (0.006)	0.13 (0.04)	0.04** (0.01)	0.33 (0.10)	0.12** (0.04)	1.67 (0.51)
	Center	0.05 (0.02)	0.32 (0.10)	0.18 (0.06)	1.67 (0.51)	0.90 (0.27)	8.33 (2.54)
	West	0.01 (0.003)	0.04 (0.01)	-	-	-	-

* The reader is reminded that the detector response, i.e., obscuration measurement, does not directly relate to smoke concentration and should not be compared between detectors.

** Values below manufacturers minimum threshold value.

Table 4-12: Average and maximum response of detectors* (obscuration, %/m (%/ft)) to overheated circuit boards in a server cabinet at an air exchange rate of 265 ACH.

Detector Cluster		Aspirated Detector		Spot-T Detector		Spot-S Detector	
		Average	Maximum	Average	Maximum	Average	Maximum
Subfloor	East	-	-	-	-	-	-
	Center	-	-	-	-	-	-
	West	-	-	-	-	-	-
Server Room	East	~ 0.0	0.01 (0.003)	-	-	-	-
	Center	0.02 (0.006)	0.23 (0.07)	-	-	0.18** (0.06)	6.67 (2.03)
	West	~ 0.0	0.02 (0.006)	-	-	-	-
Ceiling Plenum	East	0.03 (0.009)	0.27 (0.08)	0.07 (0.02)	0.33 (0.10)	0.20** (0.06)	3.33 (1.02)
	Center	0.07 (0.02)	0.40 (0.12)	0.19 (0.06)	1.67 (0.51)	0.99 (0.30)	11.67 (3.56)
	West	~ 0.0	0.01 (0.003)	-	-	-	-

* The reader is reminded that the detector response, i.e., obscuration measurement, does not directly relate to smoke concentration and should not be compared between detectors.

** Values below manufacturers minimum threshold value.

Table 4-13 shows the initial response time of each smoke detector above its minimum obscuration threshold, listed in Section 2.6.1, at air exchanges rates of 78 and 265 ACH. For this evaluation, the Aspirated detector response threshold was set to 0.0067 %/m (0.002 %/ft) to avoid signal noise that was observed at the minimum detection limit (i.e., 0.002 %/m (0.00061 %/ft)). Measurement conditions where the smoke detector did not respond are marked with a dash (-).

The first response for each detector type occurred at *Ceiling Plenum Center*, with the response times mostly decreasing as the air exchange rate increased. A similar trend was seen for the detector responses at the other locations throughout the enclosure. The only notable exception was the Spot-S detector at *Ceiling Plenum East*, which only responded at the 265 ACH air exchange rate.

Table 4-13: Time (s) of initial response of smoke detectors above minimum obscuration thresholds to the overheated circuit boards in a server cabinet at air exchange rates of 78 and 265 ACH.

Detector Cluster		Aspirated Detector		Spot-T Detector		Spot-S Detector	
		78 ACH	265 ACH	78 ACH	265 ACH	78 ACH	265 ACH
Subfloor	East	-	-	-	-	-	-
	Center	-	-	-	-	-	-
	West	-	-	-	-	-	-
Server Room	East	-	-	-	-	-	-
	Center	231	146	-	-	-	-
	West	203	184	-	-	-	-
Ceiling Plenum	East	164	153	205	176	-	198
	Center	151	146	184	163	188	182
	West	215	228	-	-	-	-

4.5 CABLES IN THE SUBFLOOR

Figure 4-12 shows a picture of the cable bundles located in the subfloor. As detailed in Section 2.7.4, this smoke source consisted of two bundles of five electrical cables wrapped around a heating cartridge. Smoke from this material resulted from overheating of the

combustible material, and no flaming combustion was observed at either air exchange rate of 78 or 265 ACH.

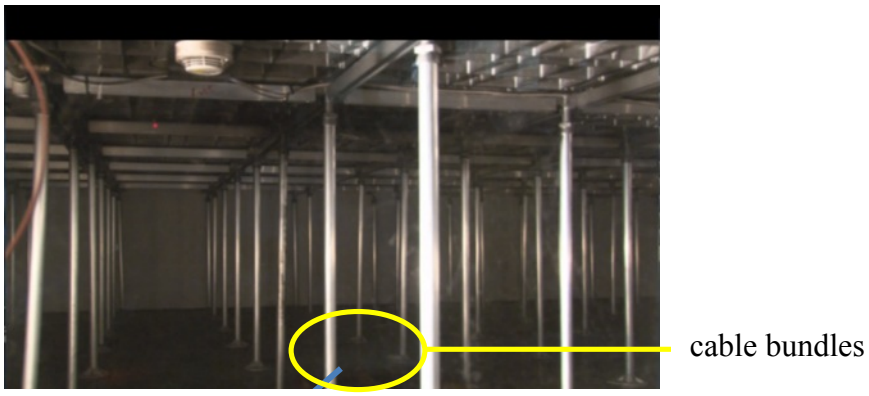

Figure 4-12: Cables placed in the subfloor.

4.5.1 Smoke Concentration from Aspirated Laser System

The time resolved smoke mass concentration for the case of the cables located in the subfloor at the lower air exchange rate of 78 ACH is shown in Figure 4-13. The smoke concentrations at the higher air exchange rate of 265 ACH were negligible, and this was confirmed by the gravimetric samples as well. For the overheated cables, the smoke, which is generated under non-flaming conditions, e.g., smoldering fires or pyrolysis, exhibits great differences in morphology compared to flame-generated smoke. Therefore, the light extinction properties for this "pyrolysis smoke" are considerably different from those of smoke from fires, as discussed in Section 1.1.3. Qualitatively, the smoke from the propylene fire was a deep black color, while the cables produced a white-gray smoke. For these reasons, the extinction coefficient employed in the interpretation of laser extinction data was set to σ_e^m = 4,670 m^2/kg, as described in Section 1.1.3.3. The measurement agreement between Aspirated Laser and Gravimetric filter for the overheated cables was found to be within 15% to 21%.

For this source location, the smoke source was in close proximity to the Aspirated Laser, and the highest smoke level was correspondingly measured in the subfloor. This is due to the short transport distance from the smoke source to the Aspirated Laser and the fact that the

measurement is taken downstream of the smoke source – similar to the case of the propylene burner in the subfloor. The smoke-laden flow is then diluted by ventilation air during transport through the enclosure. Smoke levels in the *Server Room Center* were below the detection limits of the Aspirated Laser, suggesting that minimal smoke reached the center of the ceiling in the hot aisle. All ventilation air passed through the ceiling plenum before exiting the enclosure, resulting in the low smoke levels sampled in the *Ceiling Plenum East* location.

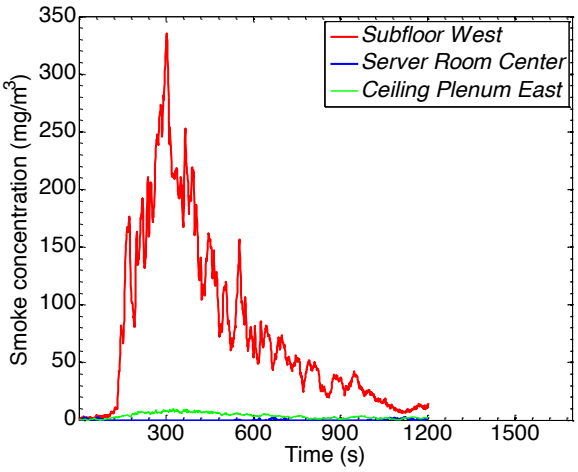

Figure 4-13: Smoke concentration from the Aspirated Laser for the case of the cables placed in the subfloor at the air exchange rate of 78 ACH.

Table 4-14 contains the average smoke mass concentration obtained during each test and measured with the Aspirated Laser. Measurement locations where smoke was not present or where concentrations were below the detection limit are marked with a dash (-). For tests using cables, the smoke concentrations were highly dependent on the air exchange rate in the room. In particular, at the 78 ACH air exchange rate, smoke from the overheated cables was transported to the sampling port in the subfloor, while at the 265 ACH air exchange rate negligible smoke was transported to this sampling port. Extinction and mass concentration plots for all tests cases can be found in Appendix E.

Table 4-14: Average smoke concentrations from the Aspirated Laser for the case of the cables placed in the subfloor

Smoke Source	Air exchange rate (ACH)	Measurement Location	Extinction (%/m)	Smoke concentration (mg/m^3)
Cables	78	Subfloor	30.4	77.6
		Server Room	-	-
		Ceiling Plenum	1.9	4.11
	265	Subfloor	-	-
		Server Room	-	-
		Ceiling Plenum	-	-

4.5.2 Smoke Detector Response

Figure 4-14 shows the obscuration levels from the smoke detectors at *Subfloor West* for air exchange rates of 78 and 265 ACH. This detector cluster is in close proximity to the smoke source and within the direction of airflow from the subfloor into the cold aisle (above).

From Figure 4-14a, at an air exchange rate of 78 ACH the Aspirated detector reported a maximum obscuration value of 22 %/m (6.7 %/ft) showing that it has saturated. The Spot-S detector shows a high response of 13 %/m (3.96 %/ft) and saturates at this value before decreasing. The Spot-T detector shows a maximum obscuration value of 6 %/m (1.8 %/ft), which also coincides with its saturation value. Figure 4-14b shows the obscuration levels at the higher exchange rate of 265 ACH. The Spot-S detector again shows a peak response of 13 %/m (3.96 %/ft), indicating saturation, while the Spot-T and the Aspirated detectors report obscurations of less than 0.5 %/m (0.15 %/ft). These figures show the highly unsteady response from the detectors, which is mainly due to the unsteady smoke output from the cables.

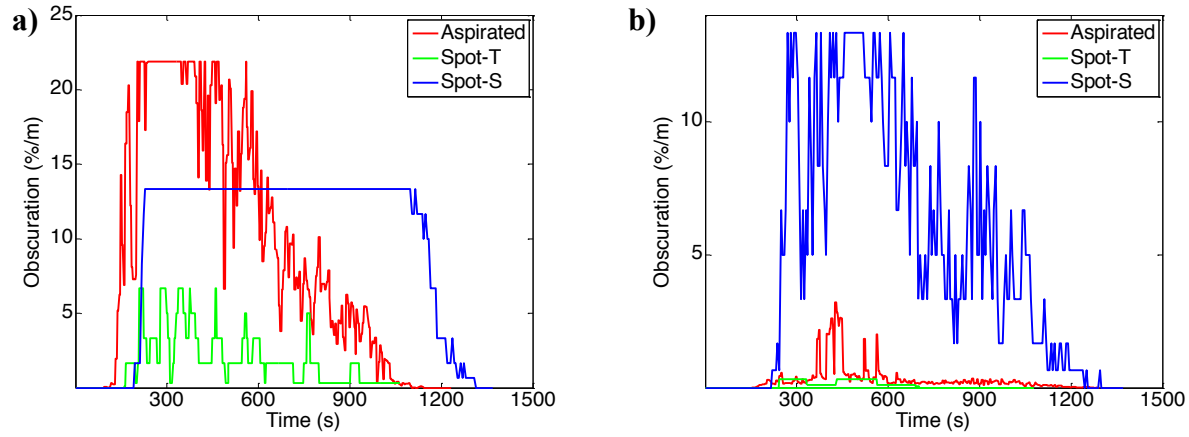

Figure 4-14: Sample response for the cluster of smoke detectors at *Subfloor West* to the overheated electric cables in the subfloor at air exchange rates of a) 78 ACH and b) 265 ACH.

Table 4-15 and Table 4-16 present the average and maximum response of the each smoke detector at air exchange rates of 78 and 265 ACH, respectively. Measurement conditions where the smoke detector did not respond are marked with a dash (-) and conditions where the detector was saturated are marked with a greater-than (>) symbol. The average response of each detector was calculated as the integral of the obscuration measurements divided by the time during which the cable bundles were heated (1,000 s). Average obscuration values below the manufacturer specified range of the Spot-S and Spot-T detectors, as detailed in Section 2.6.1, result from time averaging of the discrete levels reported by the detector. Time-resolved obscuration plots for all tests can be found in Appendix F.

Table 4-15: Average and maximum response of detectors* (obscuration, %/m (%/ft)) to overheated cables bundles in the subfloor at an air exchange rate of 78 ACH.

Detector Cluster		Aspirated Detector		Spot-T Detector		Spot-S Detector	
		Average	Maximum	Average	Maximum	Average	Maximum
Subfloor	East	-	-	-	-	-	-
	Center	-	-	-	-	-	-
	West	11.0 (3.5)	21.9 (7.26)	1.78 (0.55)	>6.67 (2.08)	10.6 (3.36)	>13.3 (4.26)
Server Room	East	0.18 (0.05)	0.45 (0.14)	0.60 (0.18)	3.33 (1.03)	3.03 (0.93)	11.7 (3.72)
	Center	n/a	n/a	0.14 (0.04)	1.67 (0.51)	0.18** (0.05)	1.67 (0.51)
	West	2.46 (0.76)	7.40 (2.32)	4.73 (1.47)	>6.67 (2.08)	10.04 (3.17)	>13.33 (4.26)
Ceiling Plenum	East	1.08 (0.33)	3.53 (1.09)	2.64 (0.81)	>6.67 (2.08)	6.29 (1.96)	>13.33 (4.26)
	Center	0.26 (0.08)	1.70 (0.52)	0.81 (0.25)	3.33 (1.03)	4.54 (1.41)	13.3† (4.26)
	West	2.67 (0.82)	6.60 (2.06)	4.69 (1.45)	6.67† (2.08)	9.70 (3.06)	13.33† (4.26)

* The reader is reminded that the detector response, i.e., obscuration measurement, does not directly relate to smoke concentration and should not be compared between detectors.

** Values below manufacturers minimum threshold value.

From Table 4-15 and Table 4-16, the maximum response is at the *Subfloor West* location as it is in close proximity to the cables. In the server room, the highest response is seen from the *Server Room West* location and, similarly, in the ceiling plenum, the *Ceiling Plenum West* location sees the highest response. It can also be observed that increasing the air exchange rate to 265 ACH causes additional dilution that makes the obscuration levels drop in magnitude (both average and maximum).

Table 4-16: Average and maximum response of detectors* (obscuration, %/m (%/ft)) to overheated cable bundles in the subfloor at an air exchange rate of 265 ACH.

Detector Cluster		Aspirated Detector		Spot-T Detector		Spot-S Detector	
		Average	Maximum	Average	Maximum	Average	Maximum
Subfloor	East	-	-	-	-	-	-
	Center	-	-	-	-	-	-
	West	0.37 (0.11)	3.20 (0.98)	0.10 (0.03)	0.33 (0.10)	6.27 (2.06)	>13.33 (4.06)
Server Room	East	0.03 (0.01)	0.08 (0.02)	0.04** (0.01)	0.10 (0.03)	0.19** (0.06)	0.67 (0.20)
	Center	n/a‡	n/a	0.03** (0.01)	0.10 (0.03)	0.19** (0.06)	1.67 (0.20)
	West	0.26 (0.08)	1.70 (0.52)	1.85 (0.56)	>6.67† (2.03)	6.50 (1.98)	>13.33 (4.06)
Ceiling Plenum	East	0.21 (0.06)	0.50 (0.15)	0.45 (0.14)	1.67 (0.51)	2.49 (0.76)	10.00 (3.05)
	Center	0.15 (0.05)	0.33 (0.10)	0.50 (0.15)	1.67 (0.51)	1.74 (0.53)	8.33 (2.54)
	West	0.71 (0.22)	2.20 (0.67)	3.10 (0.95)	6.67† (2.03)	6.85 (2.09)	>13.33 (4.06)

* The reader is reminded that the detector response, i.e., obscuration measurement, does not directly relate to smoke concentration and should not be compared between detectors.

** Values below manufacturers minimum threshold value‡Detector malfunction during test

Table 4-17 shows the initial response time of each smoke detector above its minimum obscuration threshold, listed in Section 2.6.1, at air exchanges rates of 78 and 265 ACH. For this evaluation, the Aspirated detector response threshold was set to 0.0067 %/m (0.002 %/ft) to avoid signal noise that was observed at the minimum detection limit (i.e., 0.002 %/m (0.00061 %/ft)). Measurement conditions where the smoke detector did not respond are marked with a dash (-) and detectors not operating properly were marked as not applicable (n/a).

Table 4-17: Time (s) of initial response of smoke detectors above minimum obscuration thresholds to the overheated cables in the subfloor at an air exchange rates of 78 and 265 ACH.

Detector Cluster		Aspirated Detector		Spot-T Detector		Spot-S Detector	
		78 ACH	265 ACH	78 ACH	265 ACH	78 ACH	265 ACH
Subfloor	East	-	-	-	-	-	-
	Center	-	-	-	-	-	-
	West	94	166	160	243	195	237
Server Room	East	155	215	196	-	283	-
	Center	n/a*	n/a	412	269	300	308
	West	109	166	140	199	228	242
Ceiling Plenum	East	125	171	160	222	256	264
	Center	122	169	165	217	250	259
	West	114	166	132	181	228	237

* Detector malfunction during test

4.6 SUMMARY OF SMOKE CONCENTRATION MEASUREMENTS ACROSS ALL TESTS

Smoke concentration measurements are important for model validation as they quantify smoke transport within the enclosure and at the detector locations. Before comparing the smoke concentration measurements across all the tests, it is important to address the reproducibility of the smoke flow conditions in the vicinity of the smoke detectors. Tests with the propylene burner in the server room and subfloor were each repeated once. As shown in Table 4-18, the smoke mass concentrations measured for each burner location agree well, with a difference between test repeats ranging from 3% to 24%. For reference, time-resolved smoke concentrations for the burner located in the server room and subfloor are shown in Figure 4-15. Note that smoke concentrations are only reported for locations where the minimum extinction threshold was exceeded. The highest measurement difference of 24% occurred in the subfloor when the burner

was also located in the subfloor. In this configuration, the burner was located in close proximity to the Aspirated Laser sampling port. The transport distance to this sampling port was short, causing large gradients in the local smoke concentrations. Conversely, the longer transport distance to the sampling port in the ceiling plenum improved the uniformity in the local smoke concentrations, which resulted in a decrease measurement difference of 8%. A similar result was seen for the burner in the server room, where the smoke concentrations measured in the ceiling plenum sampling port agreed within 3%.

Table 4-18: Reproducibility of smoke mass concentration for the propylene burner in the server room and subfloor.

Burner location	Measurement Location	Test 1	Test 2	Difference $\|(I_1-I_2)/I_1\|$
#	(-)	(mg/m^3)	(mg/m^3)	(%)
Server Room	Subfloor	-	-	-
	Hot aisle	0.21	0.18	14%
	Ceiling plenum	3.9	3.8	3%
Subfloor	Subfloor	82.3	62.9	24%
	Hot aisle	-	-	-
	Ceiling plenum	1.3	1.4	8%

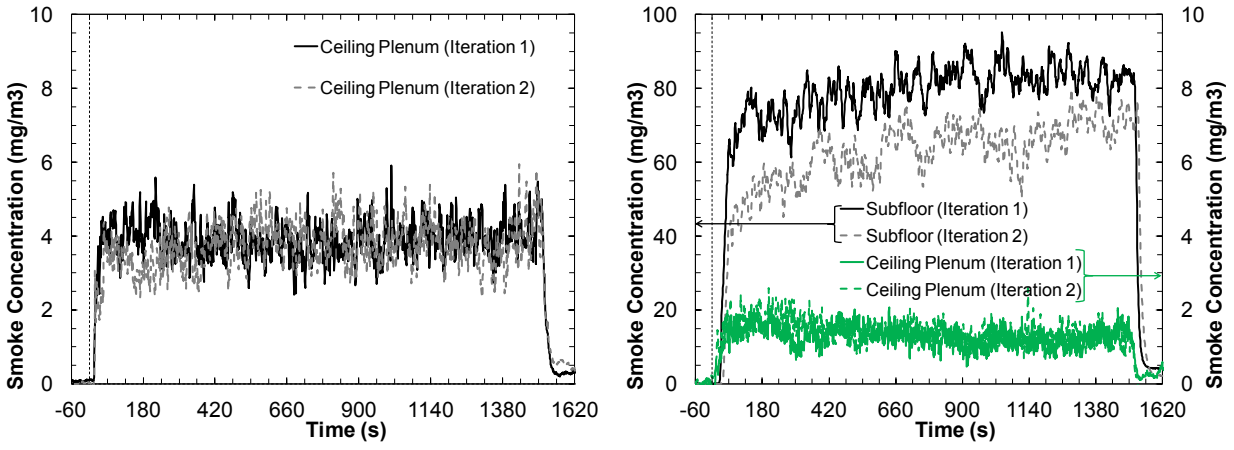

(a) **(b)**

Figure 4-15: Reproducibility of Aspirated Laser measurement for the propylene burner in (a) hot aisle of the server room and (b) subfloor.

4.6.1 Average Smoke Concentrations from Aspirated Laser System

Table 4-19 contains the average smoke mass concentration during each test measured with the Aspirated Laser. Measurement locations where smoke was not present or where concentrations were below the detection limit are marked with a dash (-). In general, the smoke concentrations were greater for the tests using a propylene smoke source. Low levels of smoke were detected for tests using foam and printed circuit boards. For tests using cables, the smoke concentrations were highly dependent on the air exchange rate in the room. In particular, at the 78 ACH air exchange rate, smoke from the overheated cables was transported to the sampling port in the subfloor; while at the 265 ACH air exchange rate, negligible smoke was transported to the sampling port. Extinction and mass concentration plots for all tests cases can be found in Appendices E and F, respectively.

Table 4-19: Summary of average response of Aspirated Laser for test condition.

Smoke Source	Air exchange rate (ACH)	Measurement Location	Extinction (%/m)	Smoke concentration (mg/m^3)
Propylene (Subfloor)	78	Subfloor	71.8	126.3
		Server Room	0.4	0.35
		Ceiling Plenum	5.7	5.90
	265	Subfloor	55.3	80.1
		Server Room	-	-
		Ceiling Plenum	1.3	1.30
Propylene (Server Room)	78	Subfloor	-	-
		Server Room	0.2	0.21
		Ceiling Plenum	3.8	3.90
	265	Subfloor	-	-
		Server Room	1.7	1.70
		Ceiling Plenum	2.0	2.01
Cables	78	Subfloor	30.4	77.6
		Server Room	-	-
		Ceiling Plenum	1.9	4.11
	265	Subfloor	-	-
		Server Room	-	-
		Ceiling Plenum	-	-

4.6.2 Comparison of Total Smoke Mass from the Aspirated Laser and Gravimetric Filter

Smoke was collected on a gravimetric filter after passing through the Aspirated Laser and sample images for the four smoke sources are shown in Figure 4-16.

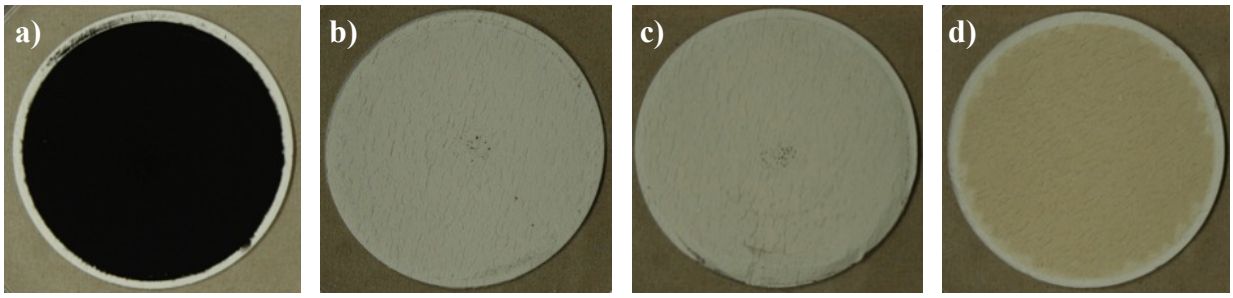

Figure 4-16: Sample Images of Gravimetric Filters from: a) propylene, b) foam, c) circuit boards, and d) cables (all data at 78 ACH).

Table 4-20 contains the total smoke mass measured with the Aspirated Laser and Gravimetric Filters for each test case. For the Aspirated Laser, the smoke mass was calculated, from Equation 6, by integrating the temporal smoke concentrations (Appendix E) over the entire test duration and multiplying the result by the volumetric sampling rate of the Smoke Concentration Meter. Tabulated sampling rates for each measurement location can be found in Appendix G. The smoke mass from the Gravimetric Filter was simply the difference of the filter weight before and after the test. Measurement locations where smoke levels were below the minimum threshold values (Appendix B) are marked with a dash (-).

The benefit of the light extinction technique can be easily observed in Table 4-20 by comparing the sampling locations where the minimum detection limit was not exceeded. The Aspirated Laser detection limit is related to the instantaneous smoke concentration, while the Gravimetric Filter detection limit is related to the overall smoke deposited on the filter throughout the entire test. As a result, the Aspirated Laser can measure low smoke levels or short transient spikes in the smoke concentration that do not accumulate enough total mass to exceed the detection limit

of the Gravimetric Filter. Smoke mass was not measured above the Gravimetric Filter minimum detection limit at any sampling location for the foam and circuit board smoke sources, or for the cable smoke source at the high air exchange rate.

At sampling locations where the smoke mass exceeded the minimum detection limit for both Aspirated Laser and Gravimetric Filter, the smoke mass generally agreed within 30%, e.g., tests using propylene as a smoke source (regardless of air exchange rate). The lone exception was the ceiling plenum for the propylene burner in the subfloor at the 265 ACH air exchange rate, where the difference was 42%.

Table 4-20: Comparison of total smoke mass measured by the Aspirated Laser and Gravimetric Filter.

Smoke Source	Air Exchange Rate	Measurement Location	Aspirated Laser (A_L)*	Gravimetric Filter (G_F)**	Difference $\lvert(A_L - G_F)/A_L\rvert$
	(ACH)		(mg)	(mg)	(%)
Propylene (Subfloor)	78	Subfloor	26.1	28.73	10%
		Hot aisle	0.44	-	-
		Ceiling plenum	2.56	2.95	15%
	265	Subfloor	16.6	18.16	10%
		Hot aisle	-	-	-
		Ceiling plenum	1.87	2.66	42%
Propylene (Server Room)	78	Subfloor	-	-	-
		Hot aisle	0.06	-	-
		Ceiling plenum	1.65	2.13	29%
	265	Subfloor	-	-	-
		Hot aisle	0.93	-	-
		Ceiling plenum	2.48	2.98	20%
Cables	78	Subfloor	14.97	12.79	15%
		Hot aisle	-	-	-
		Ceiling plenum	1.20 ‡	0.95	21%
	265	Subfloor	-	-	-
		Hot aisle	-	-	-
		Ceiling plenum	-	-	-

* Includes measurement uncertainty from Aspirated Laser and mass flow meter.
** Includes measurement uncertainty from analytical balance.

Figure 4-17 presents a graphical comparison of the smoke mass measurements for the propylene burner and the cables shown in Table 4-20 where the minimum detection limit was exceeded by

both the Aspirated Laser and Gravimetric Filter. Data from tests using propylene as a smoke source are shown with diamonds and cable data are shown with circles.

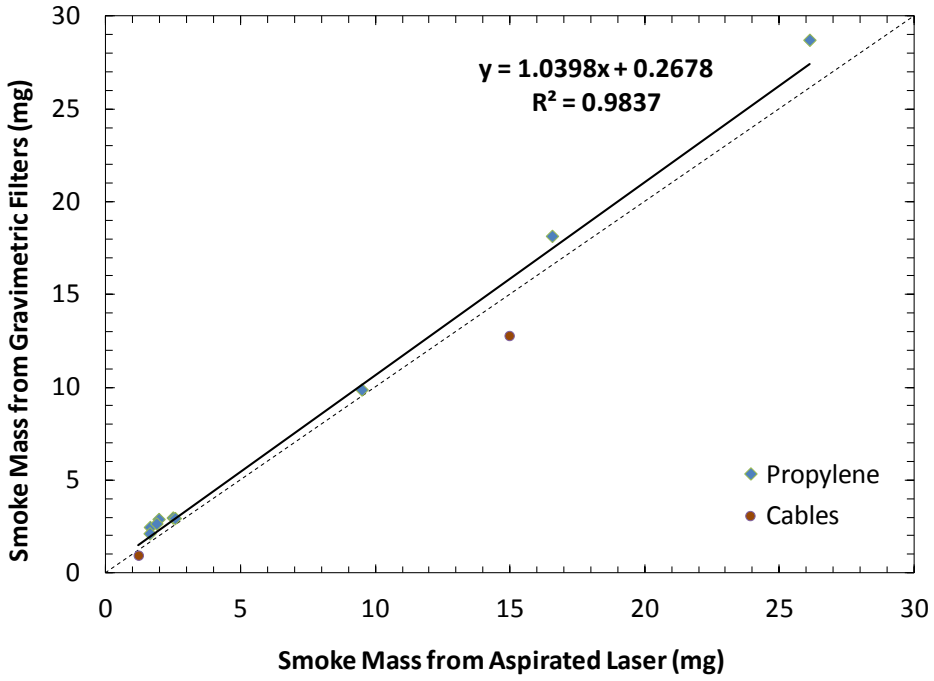

Figure 4-17: Comparison of the overall smoke mass (for cases exceeding the minimum detection limits) from the Aspirated Laser and the Gravimetric Filter.

5 SUMMARY AND CONCLUSIONS

A large-scale experimental study was conducted to provide data on the smoke transport in data centers involving high airflow rates and the corresponding response of multiple types of smoke detectors. The primary objective of this study was to provide an experimental dataset for validation of CFD models. This report describes testing conducted in a representative data center involving a characteristic confined cold aisle design. The experiments included a) characterization of airflow with detailed velocity measurements and b) smoke concentration measurements and response of smoke detectors to various smoke sources. All testing was conducted at the FM Global Research Campus in West Glocester, Rhode Island, USA.

A 7.3 m long x 4.9 m wide x 4.9 m tall (24 ft x 16 ft x 16 ft) mockup of a data center was constructed in the Small Burn Laboratory at the FM Global Research Campus. The facility consisted of three main sections: a subfloor from which the inlet air was drawn, the server room which comprised of the server cabinets separating the hot and cold aisle, and the ceiling plenum through which the exhaust air and smoke were drawn through a fan. The rationale behind choosing this facility design was to provide experimental data under a challenging scenario for model validation. Donated server cabinets were uniformly refurbished and installed to accurately represent the airflow conditions in a real data center.

The data center was instrumented to measure the temperature and velocity of air movement, as well as the static pressure in each section of the enclosure. Measuring low levels of local smoke concentrations was a considerable challenge and for this purpose three aspirated smoke concentration meters were developed at FM Global. These smoke concentration meters used laser light extinction and gravimetric filtering methods at one location each in the subfloor, server room and the ceiling plenum.

Nine clusters of smoke detectors were placed at three locations each in the subfloor, server room and ceiling plenum. Each cluster consisted of one aspirated detector and two spot detectors, for an overall number of twenty-seven detectors. The placement of the detectors was chosen with the objective of providing benchmark data for model validation.

Testing was divided into two series. First the airflow inside each section of the test enclosure was characterized at air exchange rates of 78 and 265 air changes per hour (ACH). Over 200 airflow characterization tests were conducted with the application of an advanced three-component velocity measurement technique (sonic anemometer) at over 100 locations within the test enclosure. Pressure measurements within the enclosure were acquired to aid CFD model validation. The acquired dataset is important for establishing the baseline airflow pattern and, therefore, the smoke transport in the test setup.

The second test series involved measurements of smoke concentrations and smoke detector responses at various locations. Ten tests, involving the following four smoke sources were conducted:

- 10 kW propylene flame (located in the hot aisle and subfloor)
- Polyethylene foam packaging material (located in the cold aisle)
- Printed circuit boards (located inside the cabinets)
- Cables (located in the subfloor)

The test results are summarized as follows:

1. Airflow measurements
    - Detailed quasi-steady airflow measurements were provided as baseline flow conditions for the validation of CFD airflow modeling.

2. Smoke concentration measurements
    - Time-dependent local smoke concentration measurements, with a well characterized propylene burner as the smoke source, were collected for validation of CFD models.
    - A novel aspirated smoke concentration meter, developed as part of this project, was shown to be effective as a point source measurement of smoke concentration with a minimum light extinction measurement limit of 2 %/m (0.61 %/ft) corresponding to a concentration of 2 mg/m^3, characteristic of smoke production in flaming combustion.
    - Good quantitative agreement was obtained between the overall smoke concentration measured by the aspirated laser system and the gravimetric samples.

- It was confirmed that different values of extinction coefficient should be used in the interpretation of light extinction data depending on the nature of the smoke being measured (i.e., smoke generated from flaming combustion versus pyrolysis).
- On a comparative basis, the propylene burner produced the highest amount of smoke followed by the cables, foam material and circuit boards. The smoke concentrations produced by the foam material and circuit boards were below the measurement threshold of the laser system.

3. Smoke detector response
    - The responses from the three types of smoke detectors at the same location showed similar trends.
    - The smoke detectors closest to the smoke source and in the direction of the exhaust flow showed the fastest response and the highest concentration. This reemphasizes the principal role of airflow in determining smoke detector response.
    - In general, a detector response does not provide information on the location of the fire source.
    - The exhaust (ceiling plenum) of the setup was the most reliable location in detecting the smoke. The detectors in the exhaust (ceiling plenum) of the test setup always showed a response irrespective of the location of the smoke source. However, they activated later than the detectors in the other sections of the setup.
    - In all cases, the increase of the air exchange rate reduces the overall magnitude of smoke obscuration. This is mainly due to the higher mixing and dilution of the smoke from the sources at the higher air exchange rates.

In conclusion, the airflow distribution, smoke concentration and detector obscuration measurements were quantified to provide a benchmark dataset for validation of computational models designed for evaluating smoke transport and detector response in data centers.

6 REFERENCES

[1] News report "Fire Destroys Wisconsin Data Center" on fire in Wisconsin Data Center (March 2008) at Camera Corner/Connecting Point (Green Bay, WI) http://www.datacenterknowledge.com/archives/2008/03/31/fire-destroys-wisconsin-data-center/

[2] News report " Data Center Fire Disrupts Key Services in Calgary" on fire in Calgary Data Center (July 2012) at Shaw Communications, http://www.datacenterknowledge.com/archives/2012/07/16/data-center-fire-disrupts-calgary/

[3] News report "Michigan County Offline After Data Center Fire" on fire in Michigan Data Center (April 2013) http://www.datacenterknowledge.com/archives/2013/04/19/michigan-county-offline-after-data-center-fire/

[4] US Environmental Protection Agency, "Report to Congress on Server and Data Center Energy Efficiency Public Law 109-431" http://www.energystar.gov/ia/partners/prod_development/downloads/EPA_Datacenter_Report_Congress Final1.pdf

[5] Fire and Extinguishing Tests on Computer Equipment, ANSUL Incorporated, Marinette, WI, White Paper 1009, (2001)

[6] Grant, C.C., Report of a workshop on fire protection challenges in telecommunications and information technology centers, Fire Protection Research Foundation, Workshop held in conjunction with SUPDET 2011, Orlando, FL, March 23, 2011.

[7] "The NIST Definition of Cloud Computing." National Institute of Science and Technology. http://csrc.nist.gov/publications/nistpubs/800-145/SP800-145.pdf

[8] "Telecommunications Infrastructure Standard for Data Centers, Telecommunications Industry Association" ANSI/TIA-942-2005 standard: (April 2005).

[9] Emerson Network Power, "Cost of Data Center Outages" Technical Report (2013)

[10] “Standard for the Fire Protection of Information Technology Equipment,” National Fire Protection Association Standard 75, 2013, Quincy MA

[11] “Standard for the Fire Protection of Information Technology Equipment” NFPA 75 Operating standards (2013), Quincy, MA

[12] “Data Centers and Related Facilities,” FM Global Property Loss Prevention Data Sheet 5-32, (July, 2012), Norwood, MA.

[13] “Automatic Fire Detection,” FM Global Property Loss Prevention Data Sheets 5-48, (Jan 2011), Norwood, MA

[14] Elliott, B., “Introduction to Data Centre Design – Fire Detection, Alarm and Suppression,” Capitoline: *Data Centre Design and Training*, UK, 2009.

[15] Saurabh, S., Sammakia, B., Schmidt, R., and Iyengar, M., “Comparative Analysis of Different Data Center Airflow Management Configurations.” *Proceedings of the ASME Pacific Rim Technical Conference and Exhibition on Integration and Packaging of MEMS, NEMS, and Electronic Systems,* San Francisco, CA, July 17-22, 2005, pp. 329-336.

[16] Rambo, J. and Joshi, Y., “Modeling of Data Center Airflow and Heat Transfer: State of the Art and Future Trends,” *Distributed and Parallel Databases* 21 (2007) 193-225.

[17] Rambo, J. and Joshi, Y., “Physical Models in Data Center Airflow Simulations,” *Proceedings of the ASME International Mechanical Engineering Congress and R&D Exposition, Washington D.C.,* November 15-21, 2003, pp. 153-159.

[18] VanGilder, J.W. and Schmidt, R.R. “Airflow Uniformity through Perforated Tiles in a Raised-Floor Data Center,” *Proceedings of the ASME Pacific Rim Technical Conference and Exhibition on Integration and Packaging of MEMS, NEMS, and Electronic Systems,* San Francisco, CA, July 17-22, 2005, pp. 493-501.

[19] Schmidt, R.R., Cruz, E.E., and Iyengar, M., “Challenges of Data Center Thermal Management." *IBM Journal of Research and Development* 49 (2005) 709-723.

[20] Patel, C.D., Bash, C.E., Belady, C., Stahl, L., and Sullivan, D., “Computational Fluid Dynamics Modeling of High Compute Density Data Centers to Assure System Inlet Air

Specifications," Proceedings of t*he Pacific Rim/ASME International Electronic Packaging Technical Conference and Exhibition,* Kauai, HI, July 8–13, 2001, pp. 8-13.

[21] Bhopte, S., Agonafer, D., Schmidt, R., and Sammakia, B., "Optimization of Data Center Room Layout to Minimize Rack Inlet Air Temperature," *Journal of Electronic Packaging* 128 (2006) 380-387.

[22] Aggarwal S. and Motevalli V., "Investigation of an Approach to Fuel Identification for Non-flaming Sources Using Light-scattering and Ionization Smoke Detector Response", *Fire Safety Journal* 29 (1997) 99-112.

[23] Milke J.A, Mowrer F.W., and Gandhi P., "Validation of a Smoke Detection Performance Prediction Methodology, Volume 3: Evaluation of Smoke Detector Performance", Technical Report issued by *Fire Protection Research Foundation* (2008).

[24] Miller J.H.T, "Analyzing Photo-Electric Smoke Detector Response Based on Aspirated Smoke Detector Obscuration," Masters Thesis, *University of Maryland* (2010)

[25] Newman, J.S. and Steciak, J., "Characterization of Particulates from Diffusion Flames" *Combustion and Flame* 67 (1987), 55-64.

[26] Dalzell, W.H. and Sarofim, A.F., "Optical Constants of Soot and Their Application to Heat-Flux Calculations," *Journal of Heat Transfer* 91 (1969) 100-104.

[27] Megaridis, C.M. and Dobbins, R.A., "Soot Aerosol Dynamics in a Laminar Ethylene Diffusion Flame," *Proceedings of the Combustion Institute* 22 (1988) 353-362.

[28] Smyth, K.C. and Shaddix, C.R., "The Elusive History of $\tilde{m}$ = 1.57-0.56i for the Refractive Index of Soot," *Combustion and Flame* 107 (1996) 314-320.

[29] Dobbins, R.A., Mulholland, G.W., and Bryner, N.P., "Comparison of a Fractal Smoke Optics Model With Light Extinction Measurements," Atmospheric Environment 28 (1994) 889-897.

[30] Choi, M.Y., Mulholland, G.W., Hamins, A., and Kashiwagi, T., "Comparisons of the Soot Volume Fraction Using Gravimetric and Light Extinction Techniques," *Combustion and Flame* 102 (1995) 161-169.

[31] Mulholland, G.W. and Croarkin, C., "Specific Extinction Coefficient of Flame Generated Smoke," *Fire and Materials* 24 (2000) 227-230.

[32] Mulholland, G.W. and Mountain, R.D., "Coupled Dipole Calculation of Extinction Coefficient and Polarization Ratio for Smoke Agglomerates," *Combustion and Flame* 119 (1999) 56-68.

[33] Köylü, Ü.Ö. and Faeth, G.M., "Optical Properties of Overfire Soot in Buoyant Turbulent Diffusion Flames at Long Residence Times," *Journal of Heat Transfer* 116 (1994) 152-159.

[34] Bond, T.C. and Bergstrom, R.W., "Light Absorption by Carbonaceous Particles: An Investigative Review," *Aerosol Science and Technology* 40 (2006) 27-67.

[35] Janzen J., "Extinction of Light by Highly Nonspherical Strongly Absorbing Colloidal Particles: Spectrophotometric Determination of Volume Distributions for Carbon Blacks," *Applied Optics* 19 (1980) 2977-2985.

[36] Mulholland, G.W. and Ohlemiller, T.J., "Aerosol Characterization of a Smoldering Source," *Aerosol Science and Technology* 1 (1981) 59-71.

[37] Weinert, D.W., Cleary, T.G., Mulholland, G.W., and Beever, P.F., "Light Scattering Characteristics and Size Distribution of Smoke and Nuisance Aerosols," *Fire Safety Science* 7 (2003) 209-220. doi:10.3801/IAFSS.FSS.7-209

[38] Seader, J.D. and Einhorn, I.N., "Some Physical, Chemical, Toxicological, and Physiological Aspects of Fire Smokes," *Proceedings of the Combustion Institute* 16 (1977) 1423-1445.

[39] Perera, I.E. and Litton, C.D., "Quantification of Optical and Physical Properties of Combustion-Generated Carbonaceous Aerosols ($<PM_{2.5}$) Using Analytical and Microscopic Techniques," *Fire Technology*, published online December 22, 2013. doi:10.1007/s10694-013-0376-z

[40] ANSI/UL 217, "Single and Multiple Station Smoke Alarms," Underwriters Laboratories, Northbrook, IL, 2006.

[41] ANSI/UL 268, "Smoke Detectors for Fire Alarm Systems," Underwriters Laboratories, Northbrook, IL, 2009.

[42] Mulholland, G.W., "How Well Are We Measuring Smoke?" *Fire and Materials* 6 (1982) 65-67.

[43] Clark, F.R.S., "Assessment of Smoke Density with a Helium-Neon Laser," *Fire and Materials* 9 (1985) 30-35.

[44] Chow, W.K. and Lai, K.F., "Optical Measurement of Smoke," *Fire and Materials* 16 (1992) 135-139.

[45] International Standards Organization (ISO/IEC) 17025:2005, General Requirements for the Competence of Testing and Calibration Laboratories, International Standards Organization, Geneva, Switzerland, 2005.

[46] McCaffrey, B.J. and Heskestad, G., "A Robust Bidirectional Low-Velocity Probe for Flame and Fire Application," *Combustion and Flame* 26 (1976) 125-127.

[47] Ingason, H., "Plume Flow in High Rack Storages," *Fire Safety Journal* 36 (2001) 437-457.

[48] https://s.campbellsci.com/documents/us/manuals/csat3.pdf

[49] Ditch B., Chaos M., Silva M., Thumuluru S.K., "Smoke Concentration Measurement System and Related Methods" Patent Application # 14230398, 03-31-2014

[50] Sivathanu Y.R. and Faeth G.M., "Soot Volume Fractions in the Overfire Region of Turbulent Diffusion Flames,", *Combustion and Flame* 81 (1990) 133-149.

[51] Melling, A. and Whitelaw, J. H., "Turbulent Flow in a Rectangular Duct," *Journal of Fluid Mechanics* 78 (1976) 289-315.

APPENDIX A. DETAILS OF SMOKE DETECTORS

A.1 ASPIRATED DETECTOR: NOTIFIER FSA-8000 (FAAST)

The *Aspirated Detector* is shown in Figure A-1. The unit is a Notifier Fire Alarm Aspiration Sensing Technology (FAAST) aspirating smoke detector (ASD). The detector was installed on the *north* and *south* walls of the test enclosure. Sampling ports 2.54 cm (1 in) in diameter were run from the interior locations to the *Aspirated Detector* and for simplicity the outputs were left open to the atmosphere. The sampling air pipes were designed and installed in accordance with manufacturer (System Sensor) instructions. The detector reported an operating fan speed of 5012 RPM and was listed for air velocities up to 4000 ft/min. (20.3 m/s) and sampled air temperatures from -4°F (-20°C) to 140°F (60°C) as well as operating temperatures from 32°F (0°C) to 100°F (38°C). The detector obscuration output was monitored on five digital channels, each scaled to represent smoke thresholds corresponding to levels labeled as Alert, Action 1, Action 2, Fire 1, and Fire 2.

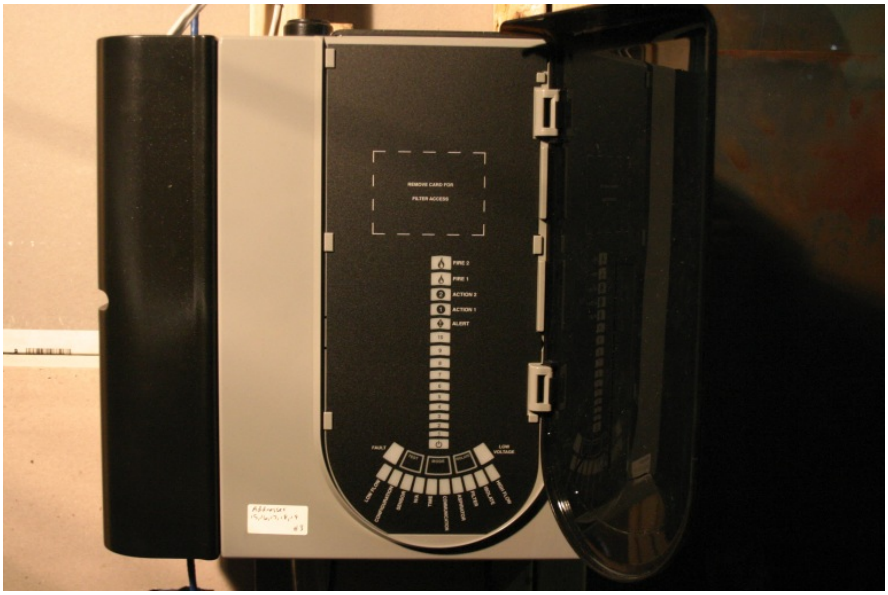

Figure A-1: Notifier FSA-8000 FAAST smoke detector (i.e., Aspirated Detector).

The Aspirated detector has a manufacturer specified obscuration range of 0.0015 to 21.7 %/m (0.00046 to 6.6 %/ft). The five user-selectable alarm thresholds were set to 0.039, 0.16, 0.33, 3.28, and 9.84 %/m (0.012, 0.05, 0.1, 1.0, and 3.0 %/ft). For each user-selected threshold, the

detector provided a continuous analog measurement with a resolution equivalent to 1% of the thresholds. The transport time (~ 6 s) across all the Aspirated Detectors used in the current test setup was maintained constant by using the same pipe length.

Alarm thresholds and detector status were controlled and monitored using PipeIQ version 1.4.10. The Flashscan SLC output of the detector was monitored by an Advanced Protocol Endcal and continuously recorded using the New Endcal GUI Beta 15 software provided by the manufacturer. The Endcal GUI was also used for normalization of the detector flow rate.

A.2 SPOT-S: SIMPLEX 4098-9754 TRUEALARM

A Simplex 4098-9754 TrueAlarm analog addressable photoelectric and heat multi-sensor detector was installed at nine locations. The manufacturer specified range was 0.66 – 14.11 %/m (0.2 – 4.3 %/ft) with nine preset discrete levels of 0.66, 1.65, 3.28, 4.92, 6.56, 8.20, 9.84, 11.48 and 13.12 %/m (0.20, 0.50, 1.00, 1.50, 2.00, 2.50, 3.00, 3.50 and 4.00 %/ft). No additional resolution beyond these seven discrete levels was available. The TrueAlarm detector is listed to operate in the range 32°F to 120°F (0°C to 49°C) and 10 to 95% humidity. The detector response levels were continuously recorded during exposure using proprietary software supplied by Simplex. This interface unit and program recorded the sensor outputs from the photoelectric smoke, temperature, and CO sensors during exposure every 5.5 seconds. The detectors tested were calibrated by the manufacturer using the UL smoke box and the output values were correlated. In this study no research was performed into the calibrations and smoke obscurations were calculated from the sensor output using this correlation provided by the manufacturer. A baseline sensor output (denoted by the manufacturers as “Photo”) was measured prior to each smoke exposure, and the increase in signal (denoted as “PhotoDelta”) due to smoke was measured and converted into obscuration using the data provided in Table A-1. The TrueAlarm detector mounted in the air duct is shown in Figure A-2.

Table A-1: Correlation between smoke obscuration (%/m) and PhotoDelta.

Smoke Obscuration		
[%/*ft*]	[%/*m*]	PhotoDelta
0.20	0.67	4
0.50	1.67	10
1.00	3.33	21
1.50	5.00	34
2.00	6.67	48
2.50	8.33	64
3.00	10.00	82
3.50	11.67	100
4.00	13.33	128

Figure A-2: SIMPLEX spot detector.

A.3 SPOT-T: NOTIFIER LPX-751L (VIEW)

A Notifier LPX-751L View photoelectric laser smoke detector was mounted on the top face of the ceilings of the subfloor, ceiling of the server room and the ceiling plenum. The manufacturer

specified range was from 0.066 to 6.56 %/m (0.02 to 2 %/ft) at seven preset discrete alarm thresholds, of 0.066, 0.098, 0.328, 1.64, 3.28, 4.92 and 6.56 %/m (0.02, 0.03, 0.1, 0.5, 1.0, 1.5 and 2.0 %/ft). No additional resolution beyond these seven levels was available. The data from the detector was recorded using the New Endcal GUI Beta 15 software and laptop provided by the manufacturer. The View detector was listed to operate between 32°F and 120°F (0°C and 49°C) and 10 to 93% humidity. The View detector mounted in the duct is shown in Figure A-3. In this study no research was performed into the calibrations, and smoke obscurations were calculated from the correlations provided by the manufacturer.

Figure A-3: VIEW spot detector.

APPENDIX B. ASPIRATED LASER DESIGN AND ERROR ANALYSIS

The major components of the smoke concentration meter are a 1.2 mW stabilized Helium-Neon (HeNe) laser, operating at a wavelength of 6.328×10^{-7} m, two silicon photodiode detectors (compensation and main), and a custom beam extension chamber. With exception of the beam extension chamber, the system components were obtained from commercial sources. An overall schematic of the smoke concentration meter is shown in Figure B-1. Light exiting the laser was split, using a beam splitter, and sent to the compensation and main photodiode detectors. The compensation diode is used as a reference measurement of the light intensity exiting the laser. The laser light sent to the main diode enters the beam extension chamber through optical windows and is reflected by mirrors located on opposing sides to extend the optical path length. An adjustable mirror controls the entrance angle of the laser beam into the chamber, which determines the number of passes (i.e., mirror reflections) and, therefore, the overall path length. The optical path length, L, is obtained by the number of reflection points on each chamber mirror, N, and the mirror separation, S, as $L = (2N+1)S$. A 2-μm quartz filter is positioned downstream of the beam extension chamber to collect smoke samples. The filters were weighed with an analytical electronic balance (Ohaus Corporation AP250D) which has an accuracy of ±0.02 mg for measurements up to 52 g.

The beam extension chamber was constructed of a stainless steel tube that was machined to have a 44 mm (1.75 in.) outer diameter pipe and a 25.4 mm (1 in.) inner diameter. Opposing sides of the tube were machined flat to provide a mounting surface for optical mirrors and windows, with a separation distance of $S = 34.5$ mm (1.36 in.). Slots were machined on each flat surface, with dimensions of 130 mm long x 10 mm wide (5 in. x 0.4 in.) to allow transmission of the laser beam between the mirrors. The mirrors and windows were held firmly against the chamber with copper mounting brackets using a machine bolt near each corner. With this arrangement the number of reflections per mirror could be typically set to $N = 21$, see Figure B-2, for an overall optical path length of $L = 1.48$ m.

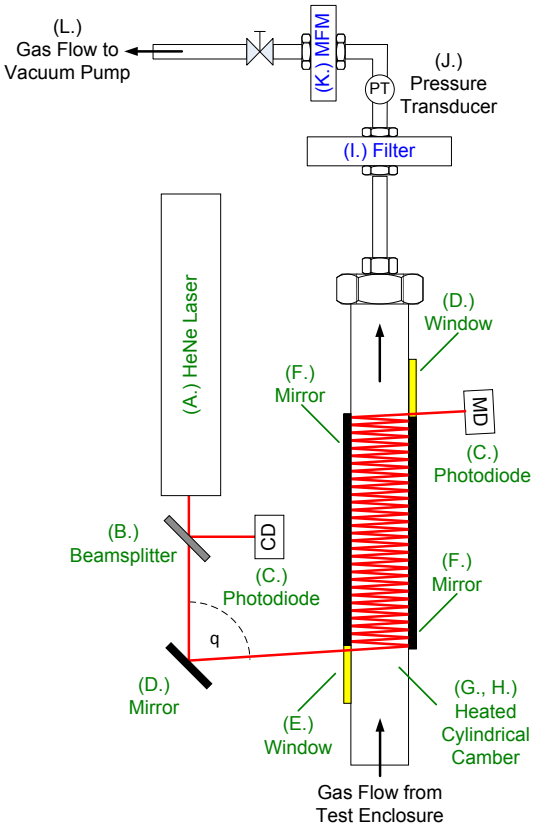

Figure B-1: Overview schematic of Aspirated Laser.

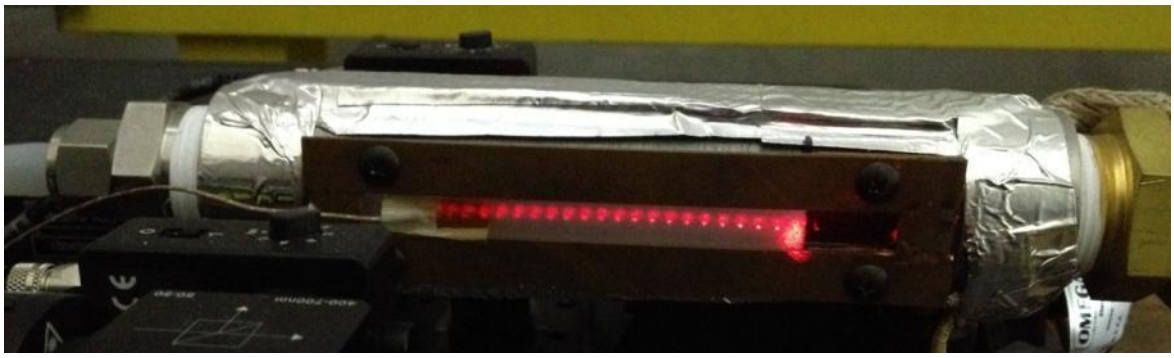

Figure B-2: Picture of beam extension tube showing laser reflection points.

To reduce thermophoretic smoke deposition on optical surfaces, the chamber was maintained at 43°C (110°F), approximately 20°C higher than typical sample gas temperatures, with heat tape (Omega SRT051-020) secured to the chamber with aluminum tape. The set temperature was maintained with a controller (Fuji, PXR-4).

Aspirated gas samples were obtained using a vacuum pump (Gast, 1023). Flow was controlled with a 6.3 mm (0.25 in.) diameter ¼-turn ball valve and monitored with a mass flow meter (Omega FMA-1828 for flow rates ≤ 50 L/min. and FMA-1841 for flow rates > 50 L/min.). The gas pressure entering the mass flow meter was monitored with a pressure transducer (Invensys, IAP20), though this transducer was not used in the tests described here as pressure of the gas flowing through the flow meter was near atmospheric pressure.

B.1 ERROR ANALYSIS DUE TO LASER VOLTAGE VARIATION

The minimum detection limit of the laser-based smoke measurements is directly related to the signal-to-noise ratio stemming from the combination of light source and detector systems. Figure B-3 shows compensation diode measurements for the *Aspirated Laser* taken over a 600 s period. For ease of review, the baseline signal for the photodiode (averaged over the entire test period) has been subtracted from the diode measurement and the data have been normalized by the baseline voltage to correct for the gain setting of the photodiode. The resulting normalized signal variation for the *Aspirated Laser* is ±0.001.

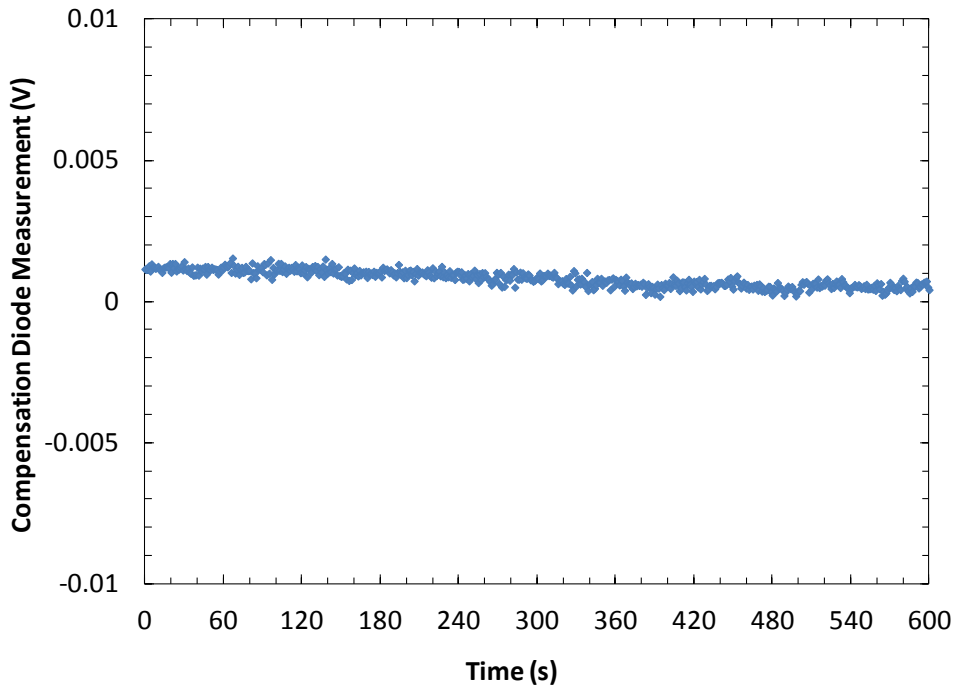

Figure B-3: Compensation photodiode measurement for the *Aspirated Laser* system.

The effect of the voltage variation on the calculation of smoke mass flow rate is not linear due to the logarithmic function shown in Equation 6. The error in the laser extinction measurement resulting from voltage variation can be calculated as

$$Relative\ error = {f_{v,true}}/{f_{v,measured}} \tag{B.1}$$

Where,

$$f_{v,true} = ln\left({I_o}/{I}\right),\ I_o = (I_{max} + I_{min})/2 \tag{B.2}$$

$$f_{v,measured} = ln\left({I_o^*}/{I}\right),\ I_o^* = I_{max} \tag{B.3}$$

$$I = I_o \cdot (1 - extinction) \tag{B.4}$$

Figure B-4 presents the relative error due to laser voltage variation for the *Aspirated Laser*. The relative error is inversely proportional to the level of light extinction, e.g., low extinction levels have higher relative errors than high extinction levels. For example, the relative error calculated with Equation B.1 decreases from 64% to 0.06% over a range of extinction levels from 0.1% to 95%, respectively.

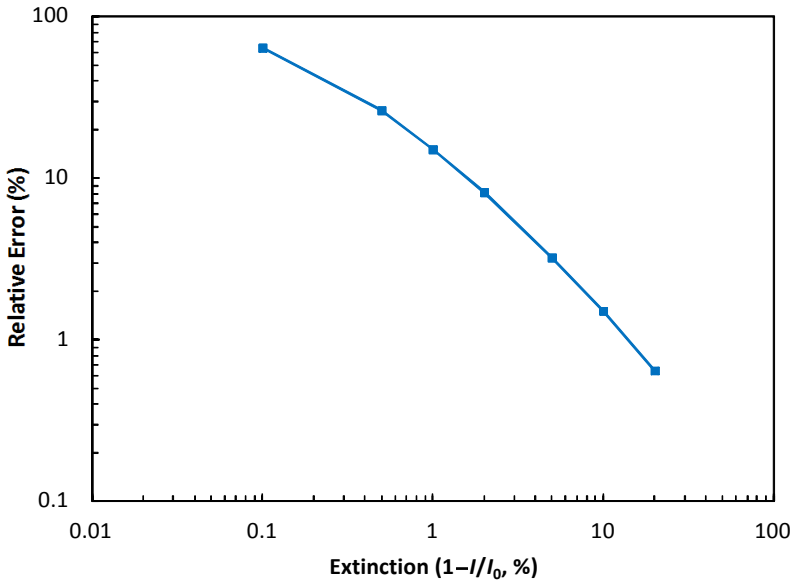

Figure B-4: Effect of laser voltage drift on smoke obscuration measurements for *Aspirated Laser* and FPA Laser systems.

The data shown in Figure B-4 can also be used to estimate the measurement error of the *Aspirated Laser* system in regards to smoke concentration and obscuration. Using Equations 5 and B.1 along with the relative error values of Figure B-4, the relative errors for smoke concentration and obscuration measurements, respectively, can be computed; these are shown in Figure B-5. As shown, an extinction level of 0.5% corresponds to a smoke concentration of 3.4 mg/m^3 and an obscuration level of 0.34 %/m with a relative error of approximately 30% for both measurements. The reader is, once again, reminded that smoke obscuration is presented here for reference and represents a monochromatic obscuration and, thus, the values shown may not be comparable to smoke detector sensitivities for the reasons provided in Section 1.1.3.4.

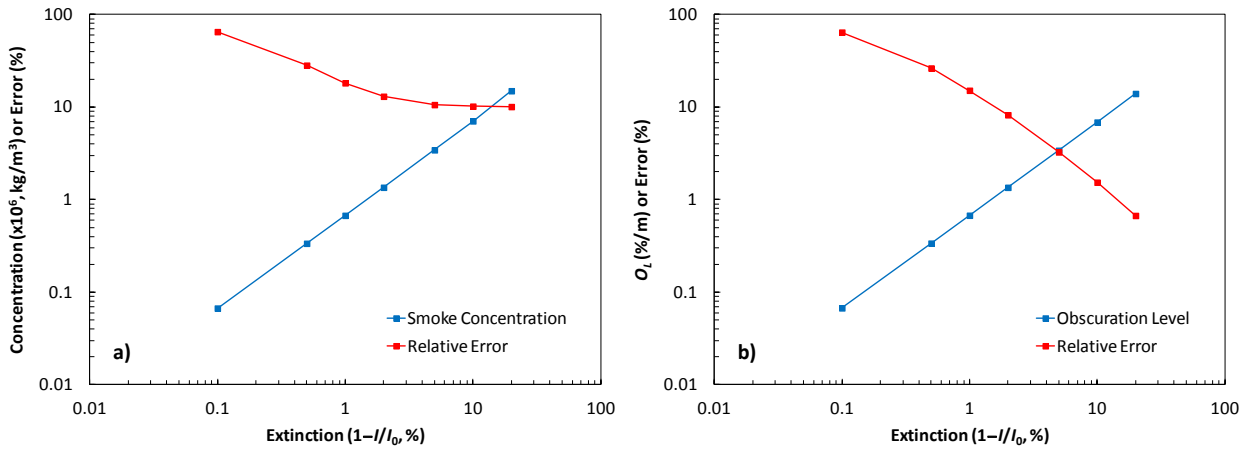

Figure B-5: Smoke concentration (a) and obscuration (b) measurement error for the *Aspirated Laser*.

Using Equation 6 to calculate smoke mass flow rate from the light extinction measurements introduces the uncertainty of the mass flow meter, which monitors the gas flow through the *Aspirated Laser*. The Omega FMA-1828 has a range of 0 – 50 L/min. and an accuracy of ± 1.5% FS (i.e., ± 0.75 L/min.). The Omega FMA-1841 has a range of 0 – 80 L/min. and an accuracy ± 3% FS (± 2.4 L/min.) for flow range of 0 – 20% FS, or ± 1.5% FS (± 1.2 L/min.) for a flow range of 20 – 100% FS. These measurement uncertainties are added to the uncertainty from the *Aspirated Laser* shown in Figure B-5.

B.2 MINIMUM THRESHOLD VALUES

The minimum threshold value for light extinction measurements with the *Aspirated Laser* is 0.3 %/m (0.1 %/ft) to achieve an uncertainty of approximately 30% or less, as shown in Figure B-5. The corresponding minimum threshold value for smoke mass concentration is dependent on the sampling rate of the *Aspirated Laser* and can be calculated individually for each test and measurement location. It should be noted the *Aspirated Laser* provides a dynamic measurement of smoke mass concentration and has a different minimum threshold value than the static measurement provided by the Gravimetric Filter.

The minimum threshold value for Gravimetric Filter weight has been set at 0.64 mg and is related to the inherent moisture content of the filters. On a dry basis, the moisture content of the filters was 3.75 mg. This was determined by placing three weighed filters in a 105^{o}C oven for 4 days. The filters were then removed from the oven, placed in a dessicator to cool for at least 0.5 hour, and reweighed. When located in the smoke concentration meter, the filter moisture content can increase or decrease depending on the temperature and moisture content of the gas flow. Comparison of the smoke mass collected with the Aspirated Laser and the Gravimetric Filter, during the tests described in Section 3.1, have shown that a deposition on the filters of greater than 0.64 mg was necessary for agreement within 60%. In many cases a negative mass change was measured, which reasonably corresponds to loss of filter moisture content during the experimental exposure phase. These mass changes were considered to be zero, i.e., negligible smoke was deposited on the filters.

APPENDIX C. MEASUREMENT UNCERTAINITY IN AIRFLOW CHARACTERIZATION

This section details the uncertainty in the airflow measurements. The uncertainty in the smoke concentration measurements using the laser is discussed in Chapter 4 (Section 4.6).

C.1 SONIC ANEMOMETER

The sonic anemometer provided 3-D velocity measurements and the results across all the measurement locations have been presented in Chapter 3. The overall uncertainty in the velocity measurements is the sum of systematic (bias) and random components.

$$Overall\ uncertainty = Systematic\ (bias)\ +\ Random\ uncertainty \quad \text{(C.1)}$$

The systematic component is the accuracy of the instrument. The random component is due to the uncertainty in the fan flow speed (pitot tube) and the placement/orientation of the anemometer. These two contributions are addressed separately below.

C.1.1 Systematic (bias) uncertainty

The anemometer has a systematic error associated with its measurements and this accuracy is provided by the manufacturer for the operating range of -30^o to 40^o C, wind speed < 30 m/s (5900 fpm); azimuth angles between ±170^o) as:

Table C-1: Offset and gain errors of the 3-D sonic anemometer

Maximum Offset Error	± 0.08 m/s (16 fpm)
Maximum Gain Error	± 6% of reading

C.1.2 Random uncertainty (fan flow and instrument placement)

The random uncertainty is estimated by repeating velocity measurements across several locations in the hot aisle. The random uncertainty in the measurements at each location is assumed to be the same as the uncertainty of the measurements at all other locations. This uncertainty is characterized by the deviations of the measurement points from the 45 degree line in plots of all the repeat velocity components against each other at 15 locations in the hot aisle. The uncertainties in both, the fan flow speeds and the anemometer placement are reflected in this estimate of random uncertainty. The standard deviation (σ) of this data set is estimated to be

0.106 m/s (20.8 fpm). It can be seen that most measurements fall within these uncertainty bounds. The few points that lie outside these bounds correspond to locations at the ceiling of the hot aisle. These measurements demonstrate high velocity fluctuations due to the fact they are close to the East and West walls.

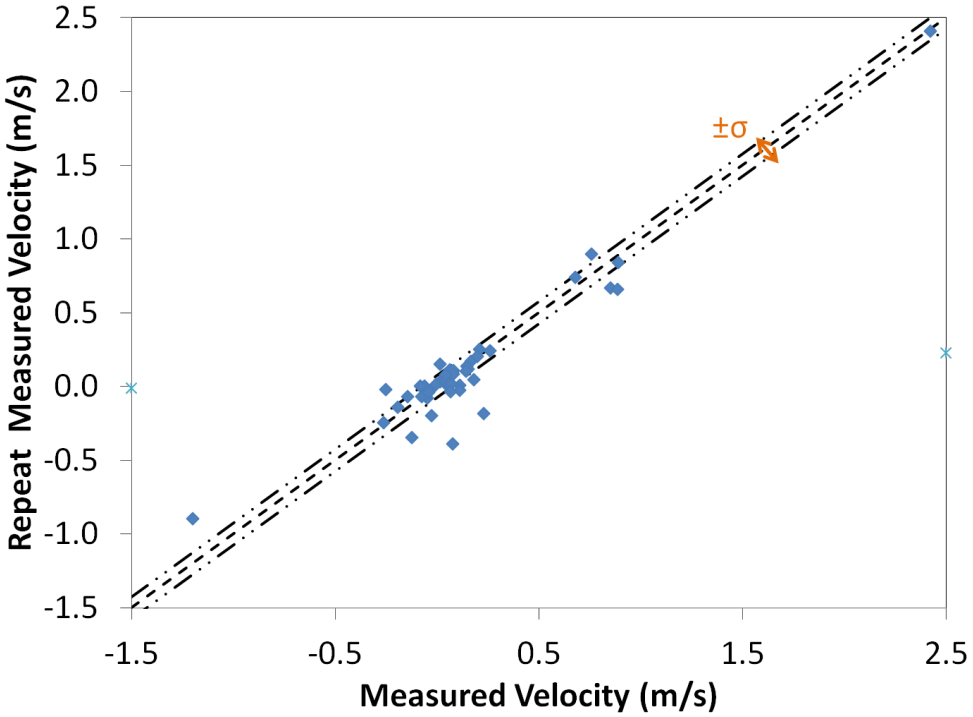

Figure C-1: All components of velocity plotted against the corresponding repeat measurements.

C.1.3 Overall uncertainty

The overall uncertainty[a] is the square root of the sum of the systematic and random components and is estimated to be:

$$\text{Overall uncertainty (m/s)} = \pm\sqrt{0.106^2 + 0.08^2 + (6\%\ of\ reading)^2}$$

$$\text{Overall uncertainty (m/s)} = \pm\sqrt{0.0176 + (6\%\ of\ reading)^2} \qquad \text{(C.2)}$$

For the median range of measured velocities of 1m/s, this works to

$$\text{Overall uncertainty (m/s)} = \pm\sqrt{0.106^2 + 0.08^2 + 0.06^2} = \pm 0.146$$

[a] Castrup H., "Estimating and Combining Uncertainties", *8th Annual ITEA Instrumentation Workshop* (2004).

C.2 PITOT TUBES

Five pitot tubes were used in the exhaust section to measure the volumetric flow rate. The results are discussed in Section 3.1.

C.2.1 Systematic uncertainty (accuracy)

The manual from the manufacturer (Dwyer Instruments) reports a maximum systematic error of 5%.

C.2.2 Random (measurement) uncertainty

The locations of the pitot tube are as shown in Figure 2-13. The repeatability in the pitot tube measurements across all the smoke tests is shown in Table C-2 and it can be seen that the maximum uncertainty across all the measurement locations and smoke tests is 5.5%.

C.2.3 Effect of pitot tube uncertainty on air velocity measurements

Due to the fact that the volumetric air flow rate was set for each specific test, the random uncertainty in the flow rate was one of the contributors to the random uncertainty of the flow velocity measurements evaluated in section C.1.2. However, no additional correction to the air velocity measurement uncertainty is required to reflect the uncertainty of the volumetric flow rate setting. The accuracy of the pitot tube as per section C2.1 does not affect the uncertainty of the flow velocity measurements. It can only be treated as the uncertainty in the volumetric flow rate setting, but should not be added to the uncertainty of the flow velocity measurements.

Table C-2: Deviations from the mean values of the pitot tube measurements across all the smoke source tests

Pitot Tube Location	Mean Values (cfm)		Deviations from Mean	
	78 ACH	265 ACH	78 ACH	265 ACH
A	8083	26426	3.31%	1.56%
B	8354	26056	3.60%	1.54%
C	8192	25958	5.42%	1.99%
D	8684	27038	5.29%	1.69%
E	8751	26321	1.16%	1.45%

APPENDIX D. VELOCITY MEASUREMENTS

D.1 BI-DIRECTIONAL VELOCITY PROBE MEASUREMENTS

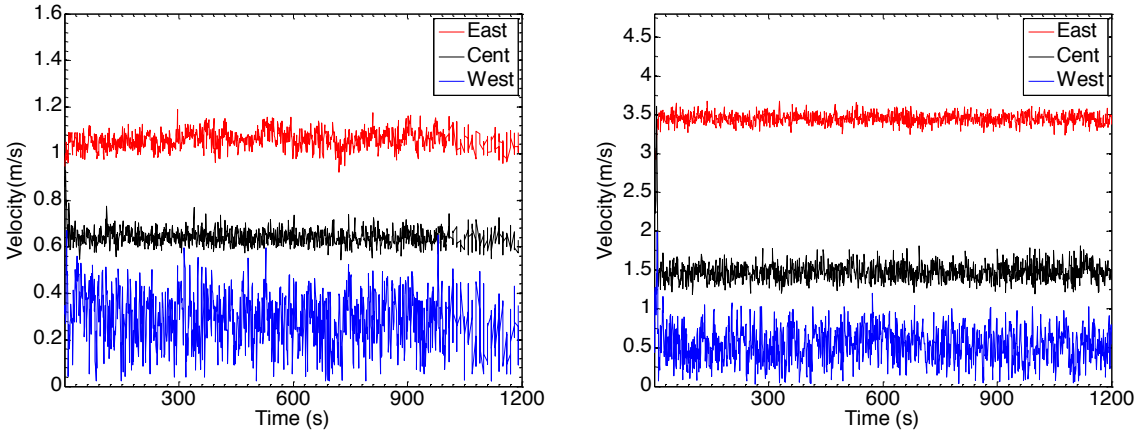

Figure D-1: Velocities from bi-directional velocity probes in the horizontal (y) direction at the subfloor smoke detector locations and at air exchange rates of (a) 78 ACH and (b) 265 ACH.

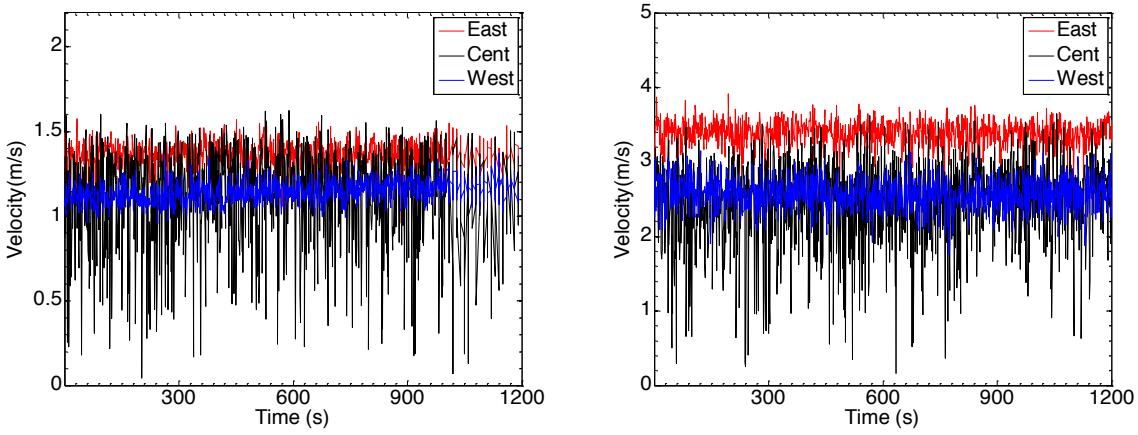

Figure D-2: Velocities from bi-directional velocity probes in the horizontal (y) direction at the ceiling plenum smoke detector locations and at air exchange rates of (a) 78 ACH and (b) 265 ACH.

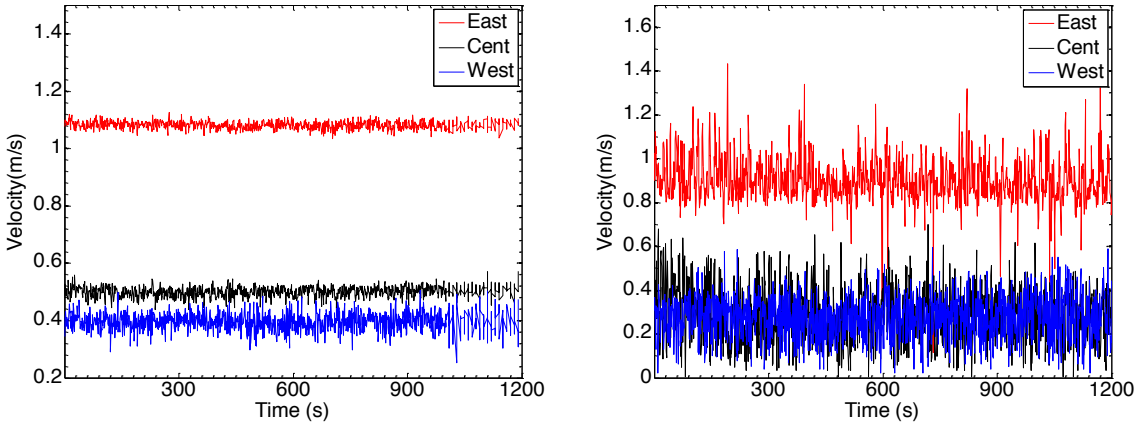

(a) **(b)**

Figure D-3: Velocities from bi-directional velocity probes at the smoke detector locations in the server room and placed in the lateral (x) direction and at air exchange rates of (a) 78 ACH and (b) 265 ACH.

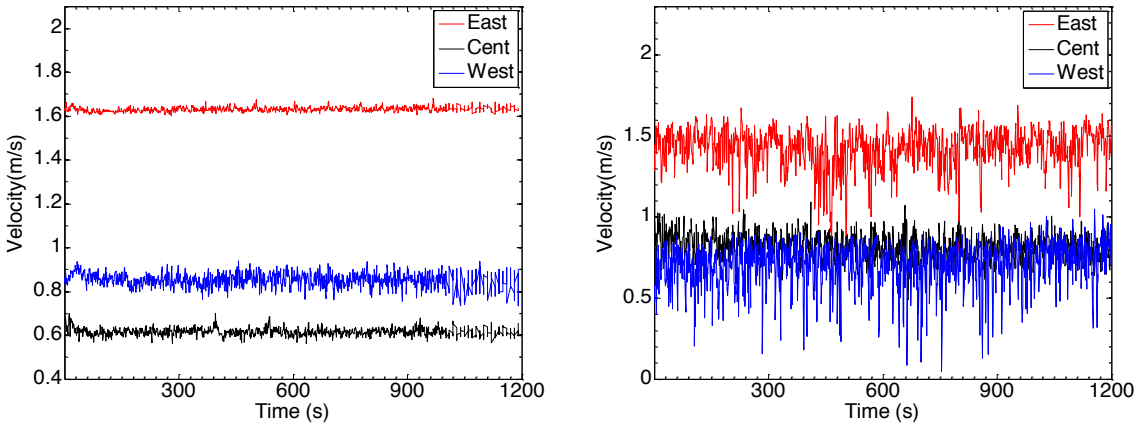

(a) **(b)**

Figure D-4: Velocities from bi-directional velocity probes at the smoke detector locations in the server room and placed in the horizontal (y) direction and at air exchange rates of (a) 78 ACH and (b) 265 ACH.

D.2 SONIC ANEMOMETER MEASUREMENTS

Table D-1: Airflow velocities at 78 ACH; (x,y,z) values are referenced to coordinates shown in Figure 2-5 and Figure 2-6.

x(m)	y(m)	z(m)	U (m/s)	V (m/s)	W (m/s)	U rms (m/s)	V rms (m/s)	W rms (m/s)
Subfloor								
0.30	7.01	0.76	-0.07	0.06	0.37	0.11	0.10	0.03
0.91	6.71	0.76	-0.21	0.14	0.04	0.04	0.06	0.04
2.44	7.01	0.76	0.15	0.09	-0.05	0.04	0.09	0.05
2.13	3.96	0.76	0.01	0.34	-0.02	0.03	0.05	0.02
0.91	3.96	0.76	-0.12	0.33	-0.03	0.03	0.03	0.01
0.30	3.96	0.76	-0.10	0.50	0.39	0.01	0.02	0.01
0.30	1.98	0.76	0.01	0.78	0.02	0.01	0.02	0.02
2.13	1.98	0.76	0.02	0.47	-0.01	0.02	0.03	0.01
2.13	0.15	0.76	0.00	0.58	0.02	0.01	0.01	0.01
0.30	0.15	0.76	0.02	0.66	0.02	0.01	0.01	0.01
Hot Aisle								
2.44	2.11	0.61	-0.05	-0.01	-0.18	0.08	0.06	0.09
2.44	4.42	0.61	0.04	-0.01	-0.08	0.08	0.04	0.05
2.44	7.09	0.61	0.17	-0.06	-0.04	0.04	0.03	0.04
2.44	7.09	1.22	0.08	-0.20	-0.04	0.04	0.02	0.04
2.44	4.42	1.22	0.03	-0.16	-0.08	0.06	0.03	0.05
2.44	2.11	1.22	-0.03	-0.15	-0.20	0.07	0.05	0.06
2.44	2.11	1.55	-0.01	-0.21	-0.19	0.06	0.04	0.06
2.44	4.42	1.55	0.03	-0.22	-0.07	0.04	0.02	0.05
2.44	7.09	1.55	0.07	-0.23	0.03	0.03	0.02	0.03
Hot Aisle next to Servers								
1.45	2.11	1.22	0.13	-0.02	-0.02	0.09	0.08	0.08
1.45	4.42	1.22	0.24	-0.04	0.06	0.02	0.01	0.02
1.60	7.09	0.61	0.24	0.00	0.01	0.04	0.02	0.04
1.45	4.42	0.61	0.26	-0.01	0.04	0.02	0.01	0.02
1.45	2.11	0.61	0.18	-0.07	-0.01	0.08	0.09	0.07
1.45	2.11	1.83	0.26	-0.05	0.03	0.05	0.03	0.05
1.45	4.42	1.83	0.17	-0.11	-0.08	0.05	0.02	0.05
1.60	7.09	1.83	0.19	-0.04	0.02	0.06	0.05	0.05

Cold Aisle								
0.38	7.09	0.61	0.03	0.01	0.39	0.03	0.01	0.02
0.38	4.42	0.61	0.05	0.05	0.37	0.02	0.03	0.03
0.38	2.11	0.61	0.04	-0.03	0.32	0.09	0.12	0.17
0.38	2.11	1.22	0.21	-0.14	0.16	0.06	0.08	0.07
0.38	4.42	1.22	0.10	0.08	0.19	0.05	0.03	0.05
0.38	7.09	1.22	0.09	0.00	0.28	0.05	0.09	0.05
0.38	7.09	1.55	0.04	-0.03	0.14	0.06	0.11	0.09
0.38	4.42	1.55	0.09	0.17	0.24	0.03	0.06	0.03
0.38	2.11	1.55	0.15	-0.06	0.14	0.05	0.08	0.08
0.38	2.11	0.10	0.11	-0.01	0.58	0.01	0.02	0.04
0.38	4.42	0.10	0.06	-0.02	0.75	0.01	0.01	0.02
0.38	5.74	0.10	0.07	0.00	0.61	0.01	0.01	0.02
0.38	3.10	0.10	0.04	0.09	0.60	0.02	0.03	0.04
Ceiling								
0.91	7.01	2.95	-0.05	0.12	-0.03	0.03	0.05	0.03
2.44	7.01	2.95	-0.26	-0.10	0.03	0.04	0.03	0.03
4.27	6.40	2.95	-0.23	0.07	-0.01	0.05	0.04	0.04
2.06	3.66	2.95	-0.13	-0.10	0.08	0.03	0.03	0.03
3.66	6.40	2.95	-0.06	-0.14	0.02	0.08	0.04	0.04
2.44	7.01	2.95	0.06	-0.04	0.08	0.03	0.02	0.04
2.44	1.22	2.95	-0.06	-0.37	0.15	0.06	0.10	0.04
0.91	1.22	2.95	0.04	-0.06	-0.01	0.08	0.09	0.06
0.91	7.01	2.95	0.25	0.02	0.05	0.05	0.07	0.05
2.44	0.30	2.95	-0.02	0.15	0.05	0.05	0.09	0.07
Ceiling Plenum								
3.34	0.91	0.76	0.02	-0.69	0.16	0.05	0.11	0.08
2.36	1.22	0.76	-0.02	-0.55	-0.04	0.08	0.11	0.07
2.43	0.30	0.76	-0.04	-0.57	-0.09	0.06	0.07	0.07
0.91	0.30	0.76	-0.37	-0.60	-0.05	0.08	0.09	0.06
0.91	1.22	0.76	-0.37	-0.59	-0.03	0.08	0.07	0.08
0.91	3.65	0.76	-0.29	-0.38	-0.10	0.10	0.08	0.05
2.28	3.34	0.76	0.03	-0.46	0.00	0.06	0.12	0.07
2.43	6.99	0.76	0.09	0.36	-0.18	0.08	0.12	0.08
0.91	6.99	0.76	-0.24	-0.11	0.04	0.07	0.07	0.04
1.22	6.16	0.76	-0.41	-0.36	-0.19	0.14	0.08	0.06

Table D-2: Airflow velocities at 265 ACH; (x,y,z) values are referenced to coordinates shown in Figure 2-5 and Figure 2-6.

x(m)	y(m)	z(m)	U (m/s)	V (m/s)	W (m/s)	U rms (m/s)	V rms (m/s)	W rms (m/s)
Subfloor								
0.30	7.01	0.76	-0.46	0.00	1.43	0.25	0.17	0.07
0.91	6.71	0.76	-0.71	0.52	0.15	0.08	0.07	0.06
2.44	7.01	0.76	0.61	-0.08	0.17	0.12	0.13	0.13
2.13	3.96	0.76	-0.03	1.25	-0.03	0.04	0.10	0.03
0.91	3.96	0.76	-0.45	1.17	-0.05	0.05	0.07	0.03
0.30	3.96	0.76	-0.39	1.66	1.30	0.02	0.03	0.03
0.30	1.98	0.76	-0.07	2.60	0.14	0.03	0.04	0.03
2.13	1.98	0.76	0.02	1.81	0.02	0.02	0.03	0.02
2.13	0.15	0.76	0.05	1.76	0.08	0.02	0.01	0.02
0.30	0.15	0.76	-0.07	2.15	-0.05	0.02	0.01	0.02
Hot Aisle								
2.44	2.11	0.61	-0.07	0.11	-0.92	0.11	0.19	0.10
2.44	4.42	0.61	-0.01	-0.13	-0.39	0.15	0.20	0.09
2.44	7.09	0.61	0.14	-0.27	-0.14	0.15	0.18	0.11
2.44	7.09	1.22	0.33	-0.65	-0.07	0.11	0.07	0.05
2.44	4.42	1.22	-0.12	-0.67	-0.45	0.14	0.13	0.07
2.44	2.11	1.22	-0.01	-0.48	-0.91	0.10	0.15	0.06
2.44	2.11	1.83	0.20	-0.95	0.00	0.09	0.06	0.05
2.44	4.42	1.83	-0.09	-0.93	-0.40	0.11	0.12	0.07
2.44	7.09	1.83	0.04	-0.77	-0.84	0.12	0.11	0.08
Hot Aisle next to Servers								
1.45	2.11	1.22	0.77	0.01	-0.05	0.04	0.06	0.03
1.45	4.42	1.22	0.85	-0.08	0.23	0.04	0.04	0.03
1.60	7.09	1.22	0.69	-0.12	0.04	0.09	0.09	0.05
1.60	7.09	0.61	1.20	0.03	0.11	0.04	0.07	0.03
1.60	7.09	0.61	0.90	0.03	-0.02	0.06	0.12	0.05
1.45	4.42	0.61	0.88	0.00	0.16	0.04	0.04	0.02
1.45	2.11	0.61	0.68	-0.02	-0.03	0.03	0.05	0.04
1.45	2.11	1.83	0.18	0.18	-0.31	0.16	0.11	0.07
1.45	4.42	1.83	0.27	-0.14	0.36	0.10	0.06	0.10

Cold Aisle								
0.38	7.09	0.61	0.17	-0.07	1.42	0.06	0.07	0.07
0.38	4.42	0.30	0.14	-0.22	1.30	0.07	0.03	0.04
0.38	2.11	0.30	-0.29	0.08	1.48	0.29	0.14	0.21
0.38	2.11	1.22	0.56	-0.46	0.65	0.19	0.11	0.17
0.38	4.42	1.22	0.40	0.32	0.82	0.08	0.06	0.07
0.38	7.09	1.22	0.22	0.06	0.58	0.21	0.22	0.40
0.38	7.09	1.55	0.53	0.07	0.38	0.25	0.20	0.29
0.38	4.42	1.55	0.22	0.06	0.58	0.07	0.06	0.14
0.38	2.11	1.55	0.41	-0.19	0.44	0.17	0.20	0.11
0.38	2.11	0.10	0.36	-0.03	2.17	0.03	0.03	0.03
0.38	4.42	0.10	0.17	-0.04	2.42	0.02	0.02	0.02
2.44	4.42	0.10	0.17	-0.04	2.41	0.02	0.02	0.10
0.38	5.74	0.10	0.23	-0.05	2.13	0.02	0.02	0.04
0.38	3.10	0.10	0.11	0.20	2.05	0.04	0.06	0.04

Ceiling								
0.91	7.01	2.95	-0.18	0.35	-0.02	0.10	0.12	0.05
2.44	7.01	2.95	-0.85	-0.32	0.10	0.17	0.09	0.05
4.27	6.40	2.95	-0.77	0.21	-0.02	0.14	0.10	0.07
2.06	3.66	2.95	-0.58	-0.58	0.24	0.08	0.08	0.05
3.66	6.40	2.95	0.00	-0.02	0.03	0.24	0.17	0.20
2.44	7.01	2.95	0.22	-0.11	0.29	0.08	0.07	0.09
2.44	1.22	2.95	-0.12	-1.44	0.49	0.09	0.07	0.05
0.91	1.22	2.95	0.43	0.90	-0.07	0.21	0.14	0.10
0.91	0.30	2.95	0.04	0.39	0.10	0.19	0.18	0.14
2.44	0.30	2.95	-0.06	-0.08	0.14	0.29	0.50	0.21

Ceiling Plenum								
3.34	0.91	0.76	0.12	-2.18	0.53	0.12	0.21	0.13
2.36	1.22	0.76	0.07	-1.80	-0.12	0.18	0.17	0.16
2.43	0.30	0.76	-0.08	-2.02	-0.31	0.11	0.12	0.13
0.91	0.30	0.76	-1.14	-1.86	-0.10	0.21	0.20	0.11
0.91	1.22	0.76	-1.20	-2.01	-0.11	0.18	0.12	0.14
0.91	3.65	0.76	-1.33	-1.11	-0.44	0.18	0.18	0.23
2.28	3.34	0.76	0.09	-1.45	0.04	0.13	0.23	0.10
2.43	6.99	0.76	0.31	1.16	-0.48	0.16	0.31	0.19
0.91	6.99	0.76	-0.64	-0.37	0.15	0.19	0.14	0.09
1.22	6.16	0.76	-1.54	-1.24	-0.60	0.30	0.16	0.14

APPENDIX E. ASPIRATED LASER MEASUREMENTS

E.1 PROPYLENE BURNER IN THE SUBFLOOR

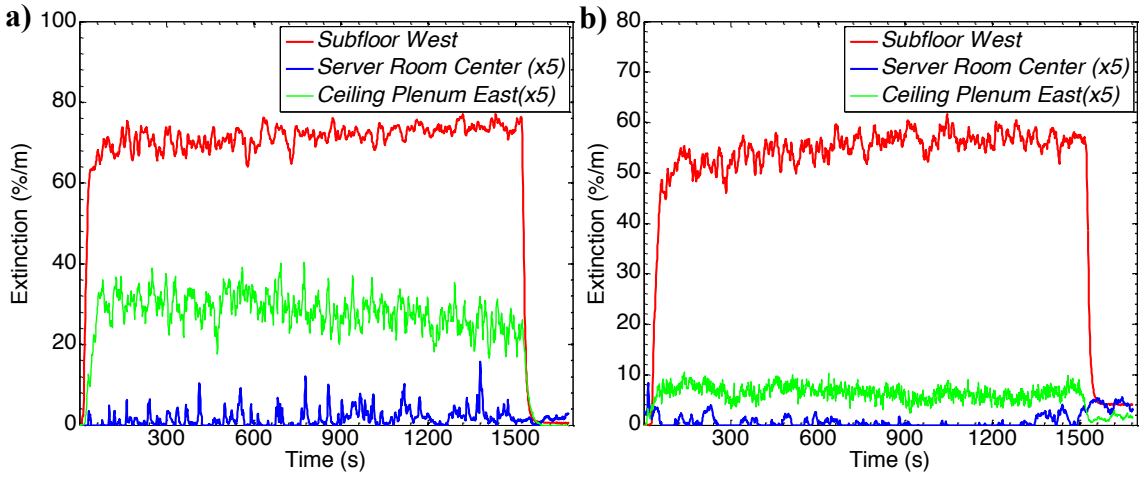

Figure E-1: Light extinction measurements from the *Aspirated Laser* for the propylene burner placed in the subfloor at (a) 78 ACH and (b) 265 ACH.

E.2 PROPYLENE BURNER IN THE HOT-AISLE

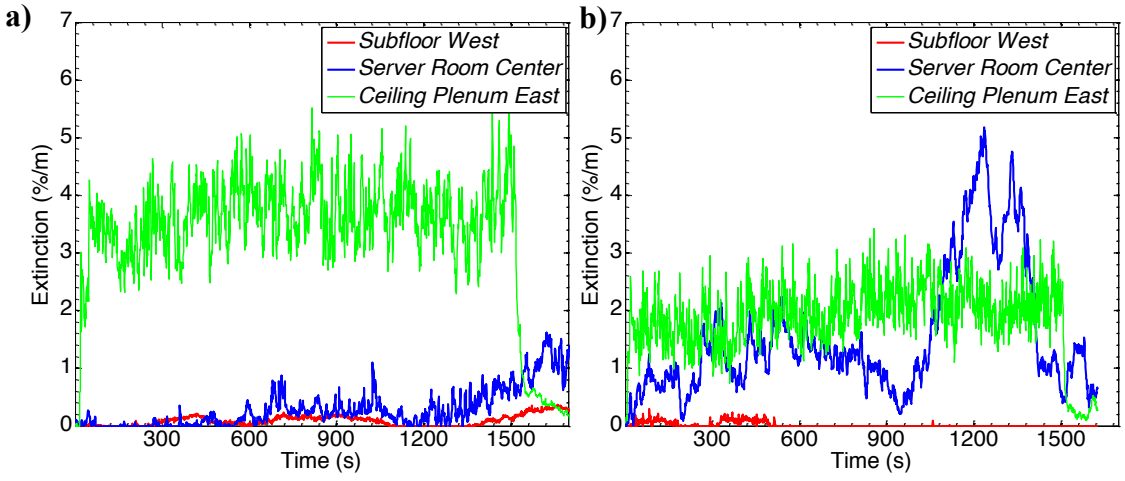

Figure E-2: Light extinction measurements from the *Aspirated Laser* for the propylene burner in the server room at (a) 78 ACH and (b) 265 ACH.

E.3 CABLES IN THE SUBFLOOR

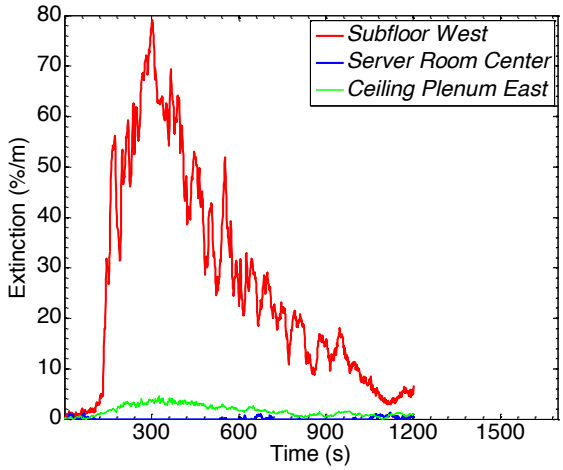

Figure E-3: Light extinction measurements from the *Aspirated Laser* for the cables placed in the subfloor at 78 ACH.

APPENDIX F. SMOKE DETECTOR OBSCURATION MEASUREMENTS

F.1 PROPYLENE BURNER IN THE SUBFLOOR

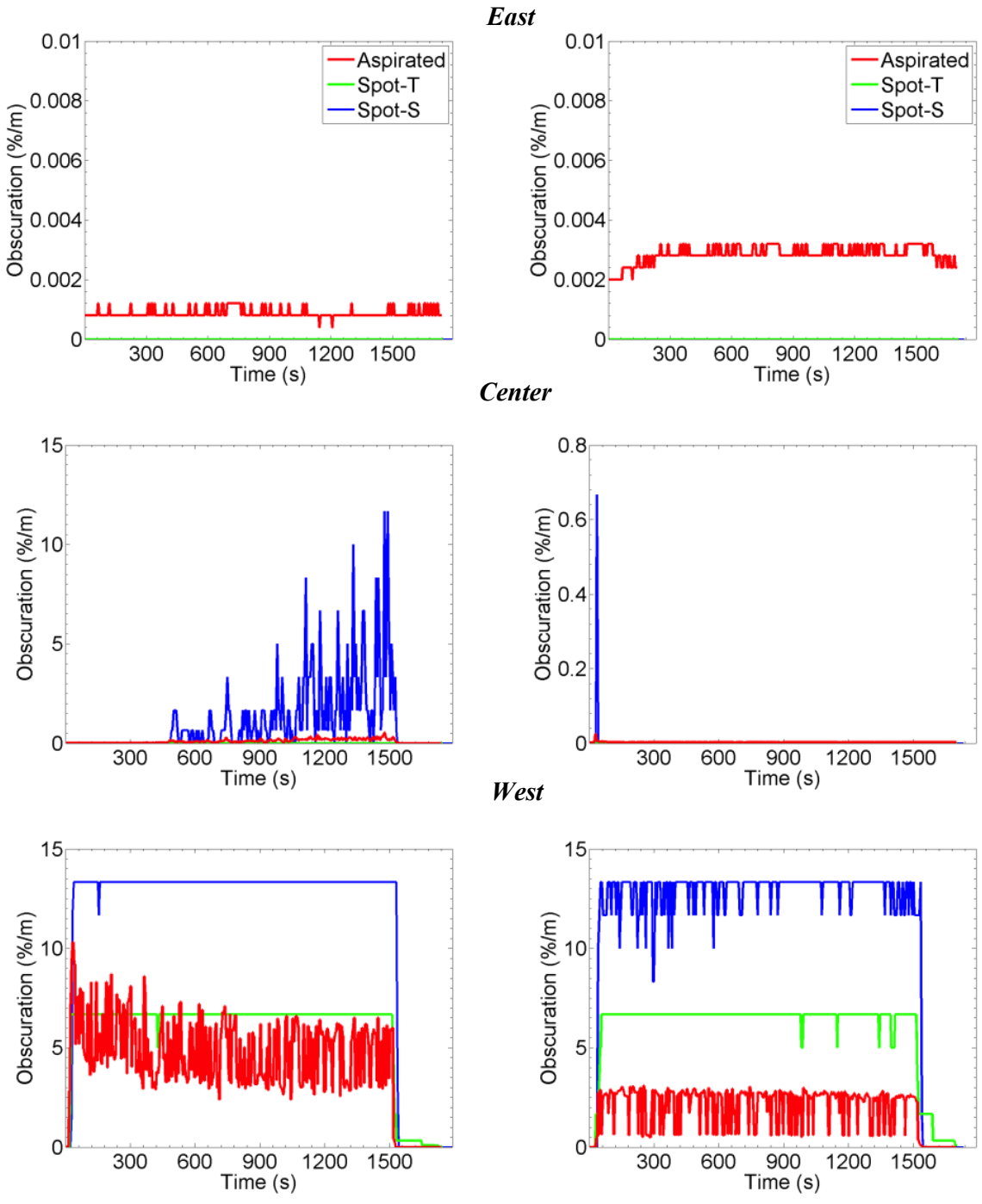

Figure F-1: Detector response in the *Subfloor* for the propylene smoke source placed in the hot aisle and at air exchange rates of (a) 78 ACH and (b) 265 ACH.

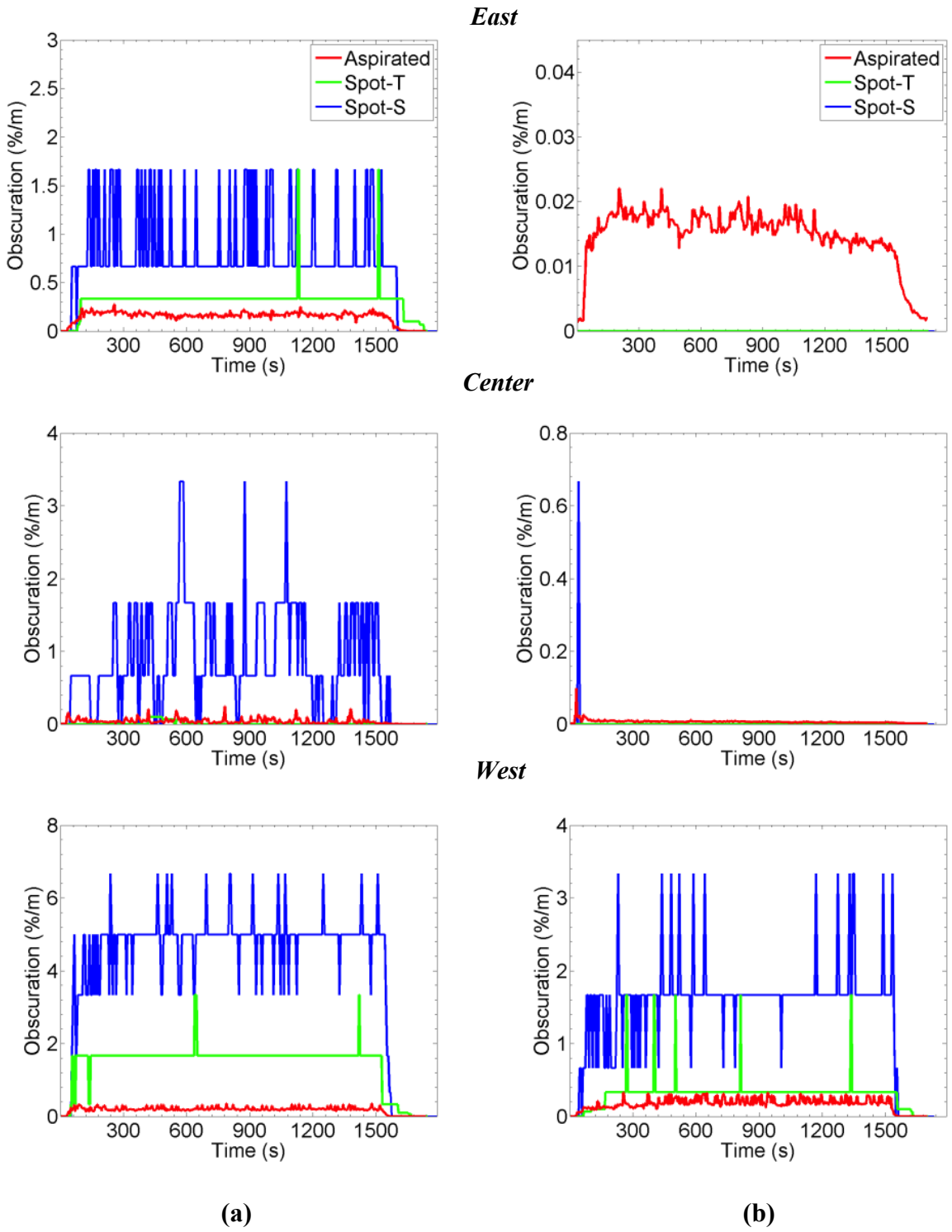

Figure F-2: Detector response in the *Server Room* for the propylene smoke source placed in the hot aisle and at air exchange rates of (a) 78 ACH and (b) 265 ACH.

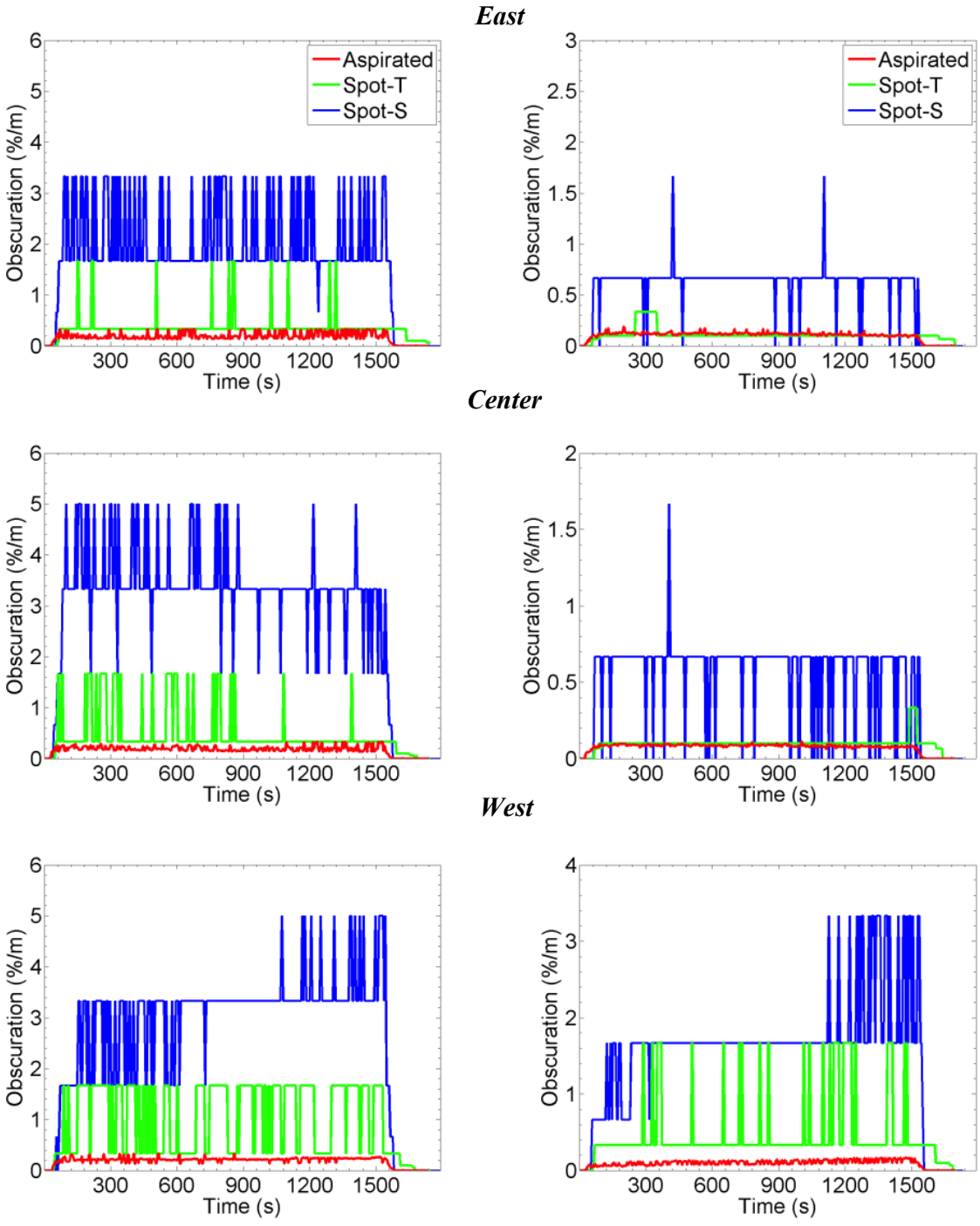

Figure F-3: Detector response in the *Ceiling Plenum* for the propylene smoke source placed in the hot aisle and at air exchange rates of (a) 78 ACH and (b) 265 ACH.

F.2 CASE 2: PROPYLENE BURNER IN THE HOT AISLE

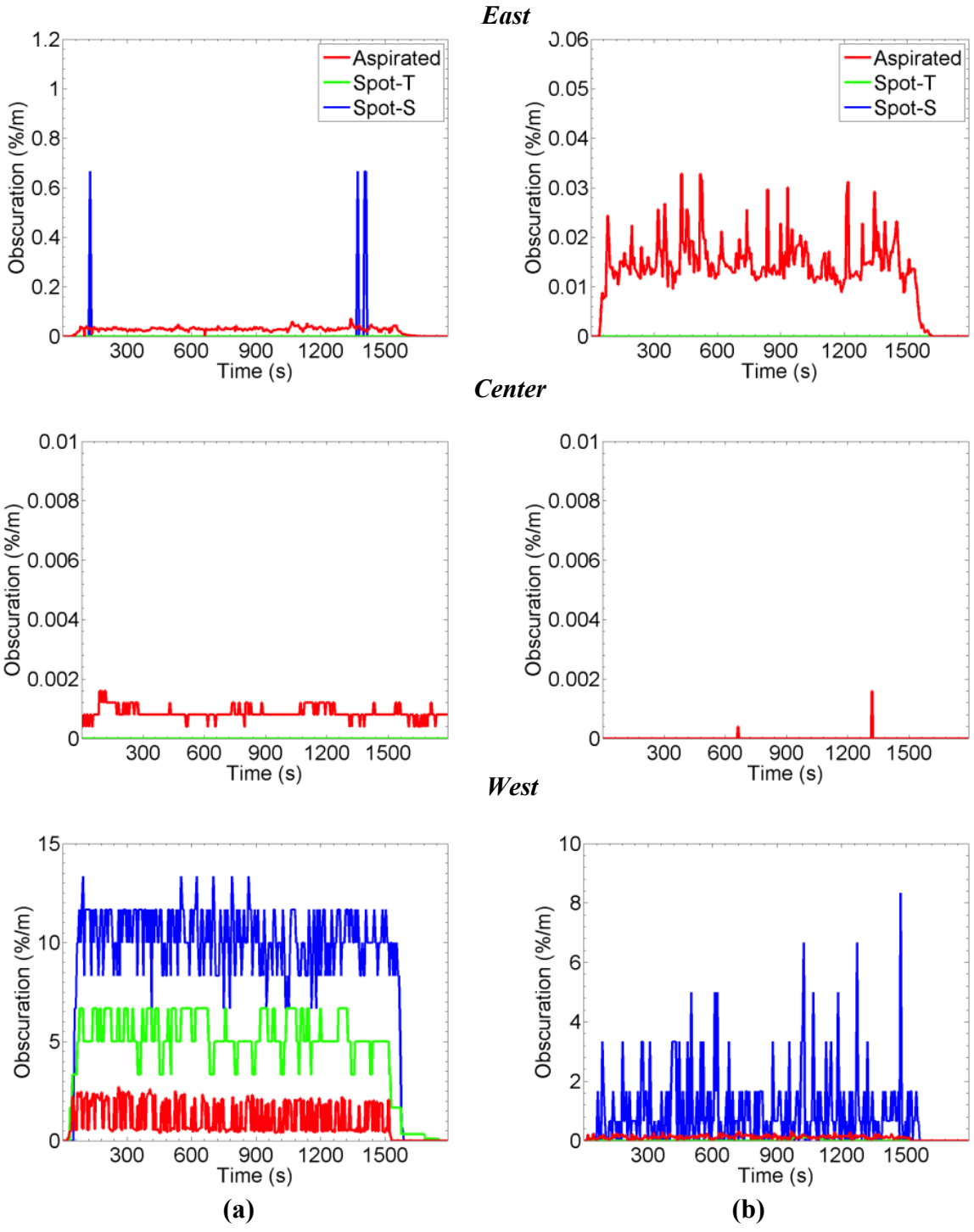

Figure F-4: Detector response in the *Subfloor* for the propylene smoke source placed in the hot aisle of the server room at air exchange rates of (a) 78 ACH and (b) 265 ACH.

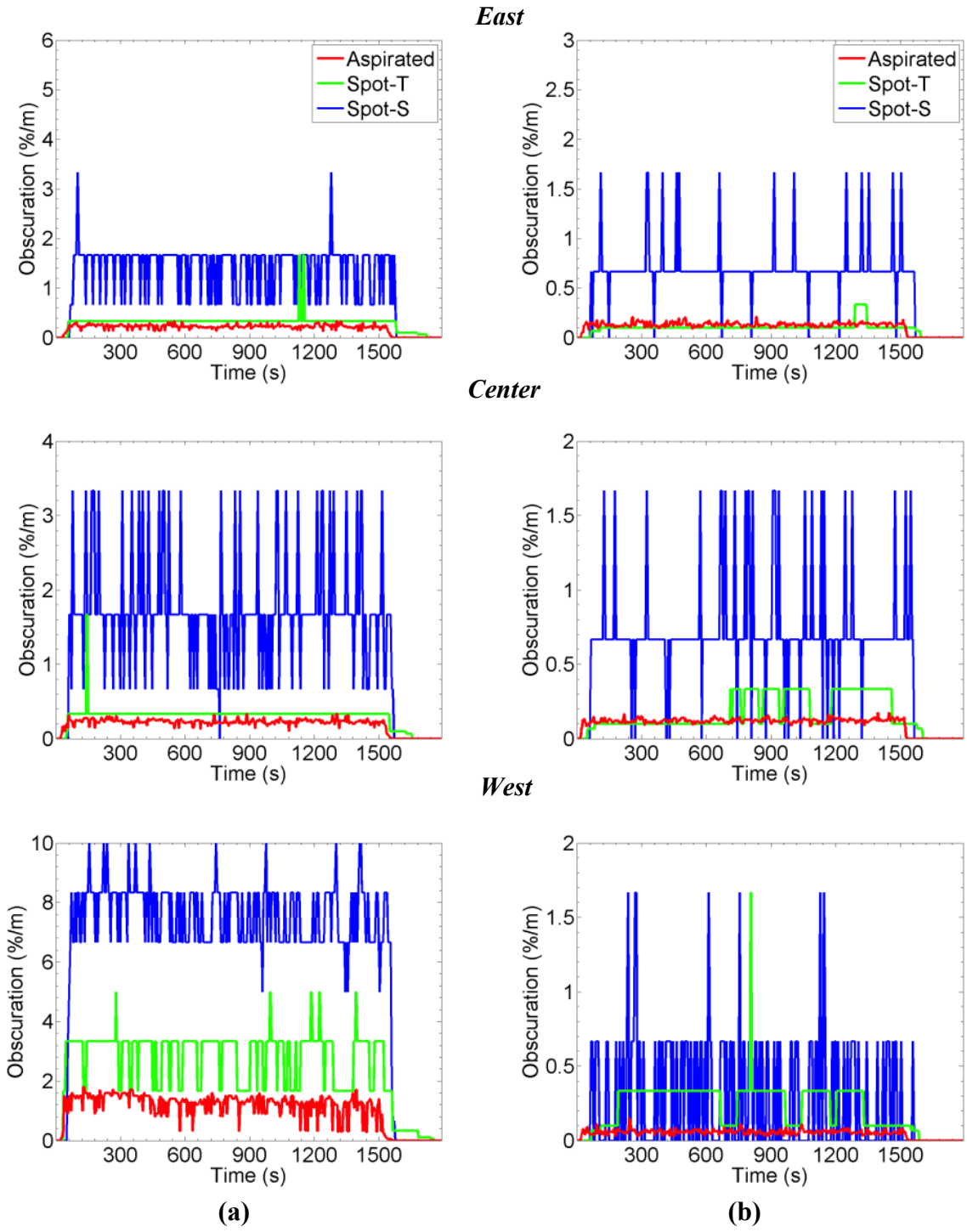

Figure F-5: Detector response in the *Server Room* for the propylene smoke source placed in the hot aisle of the server room at air exchange rates of (a) 78 ACH and (b) 265 ACH.

F.3 FOAM MATERIAL IN THE COLD AISLE

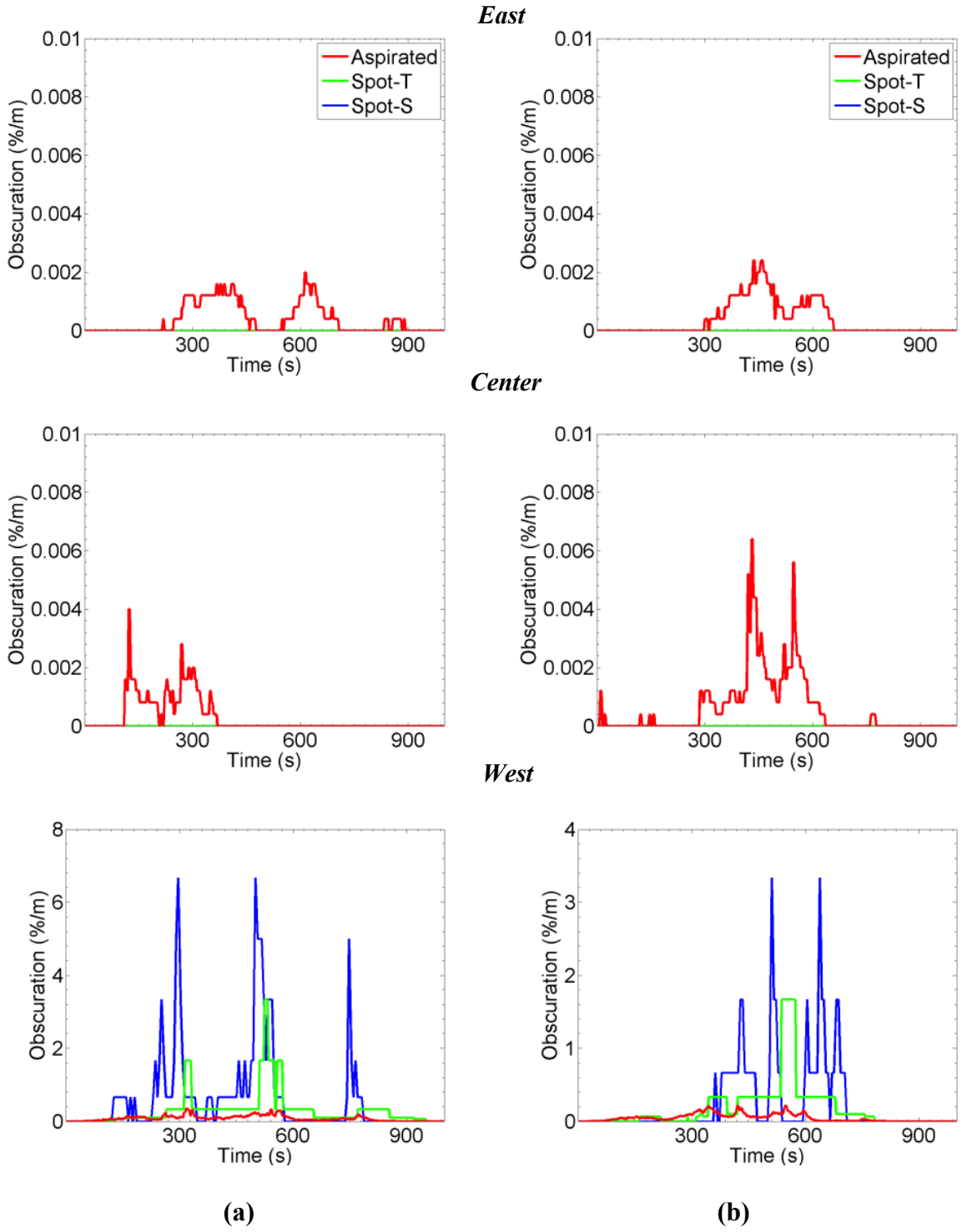

Figure F-6: Detector response in the *Server Room* for the foam smoke source placed in the cold aisle at air exchange rates of (a) 78 ACH and (b) 265 ACH.

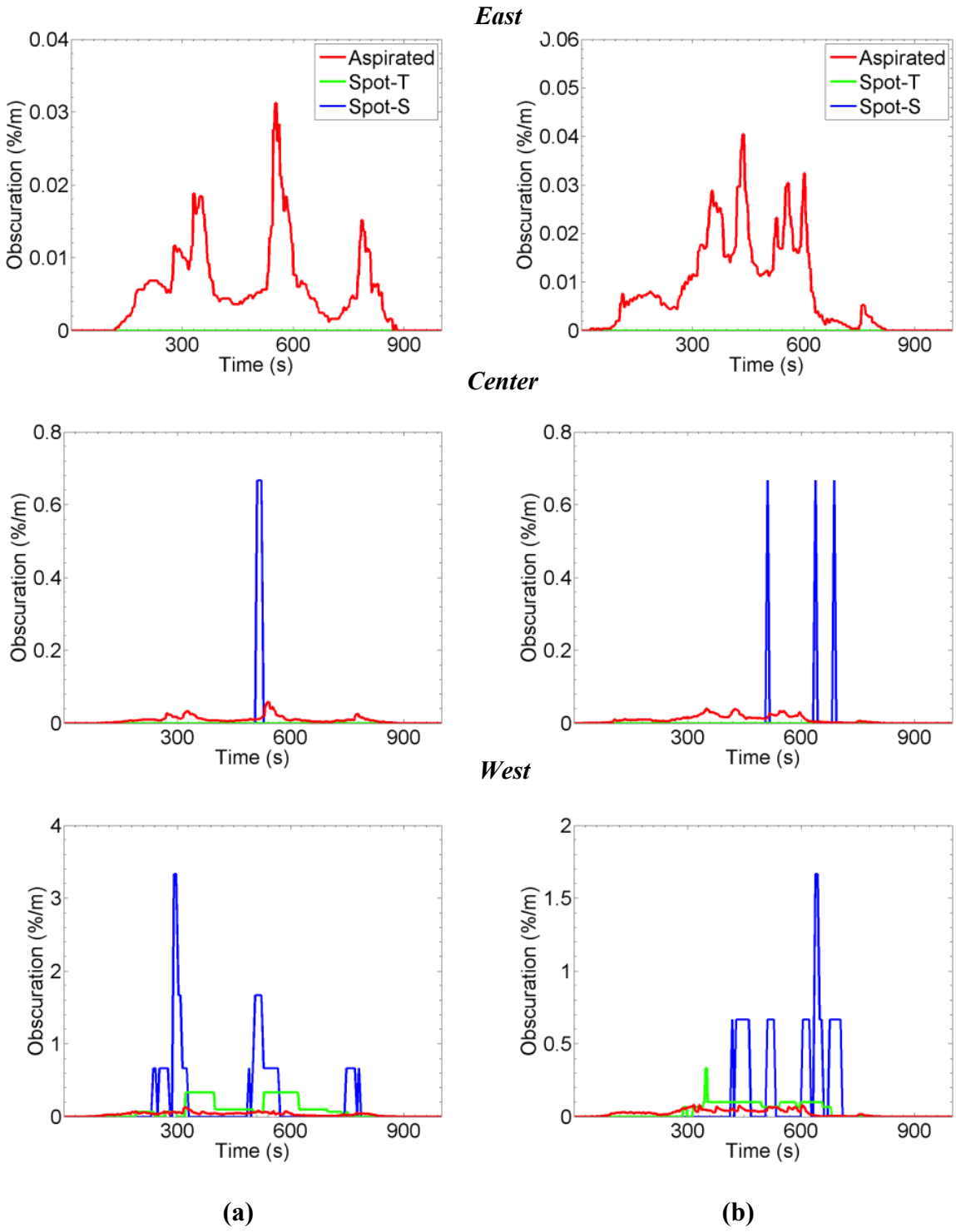

Figure F-7: Detector response in the *Ceiling Plenum* for the foam material smoke source placed in the cold aisle at air exchange rates of (a) 78 ACH and (b) 265 ACH.

F.4 CIRCUIT BOARDS IN THE CABINETS

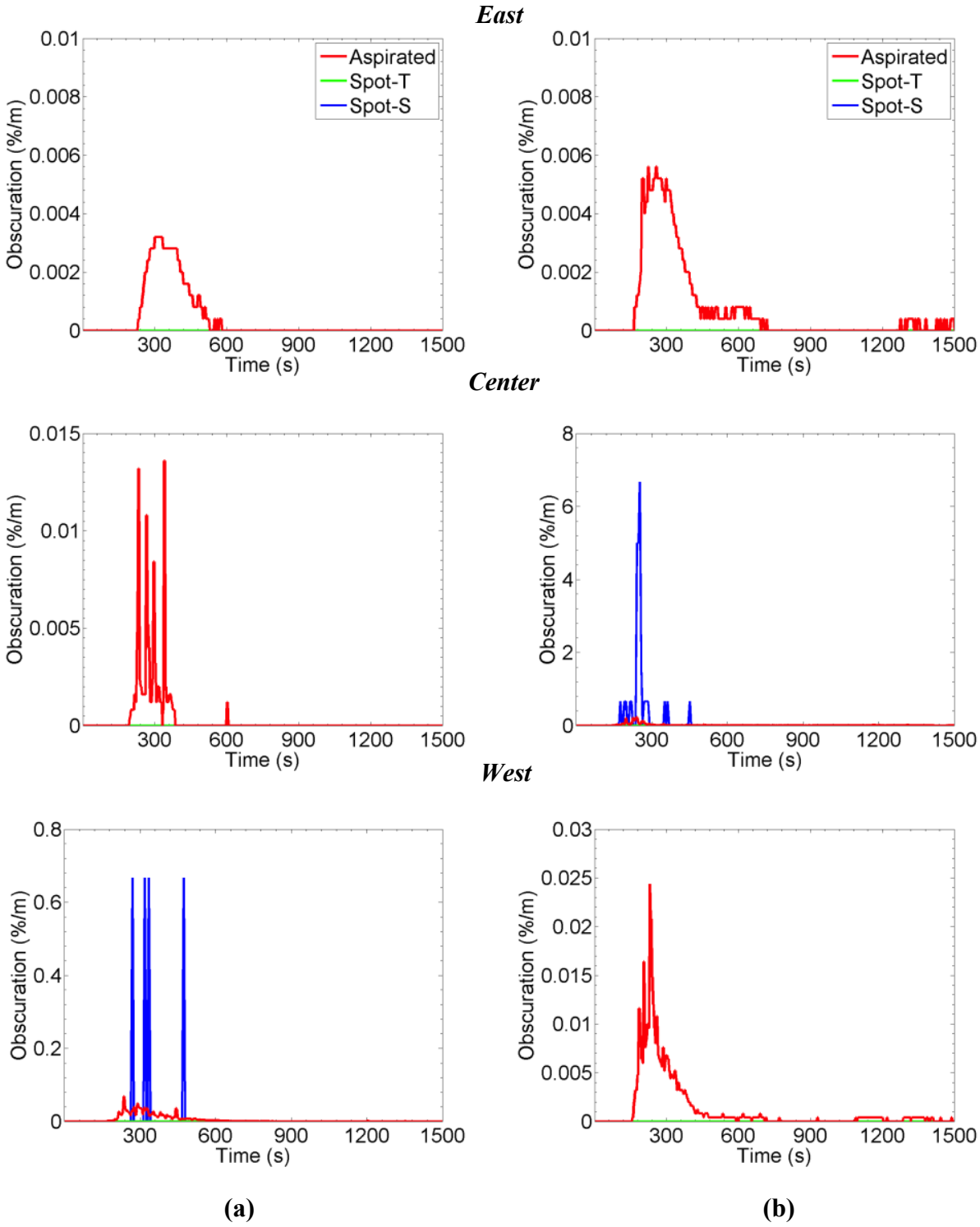

Figure F-8: Detector response in the *Server Room* for the circuit board smoke source placed in the cabinets at air exchange rates of (a) 78 ACH and (b) 265 ACH.

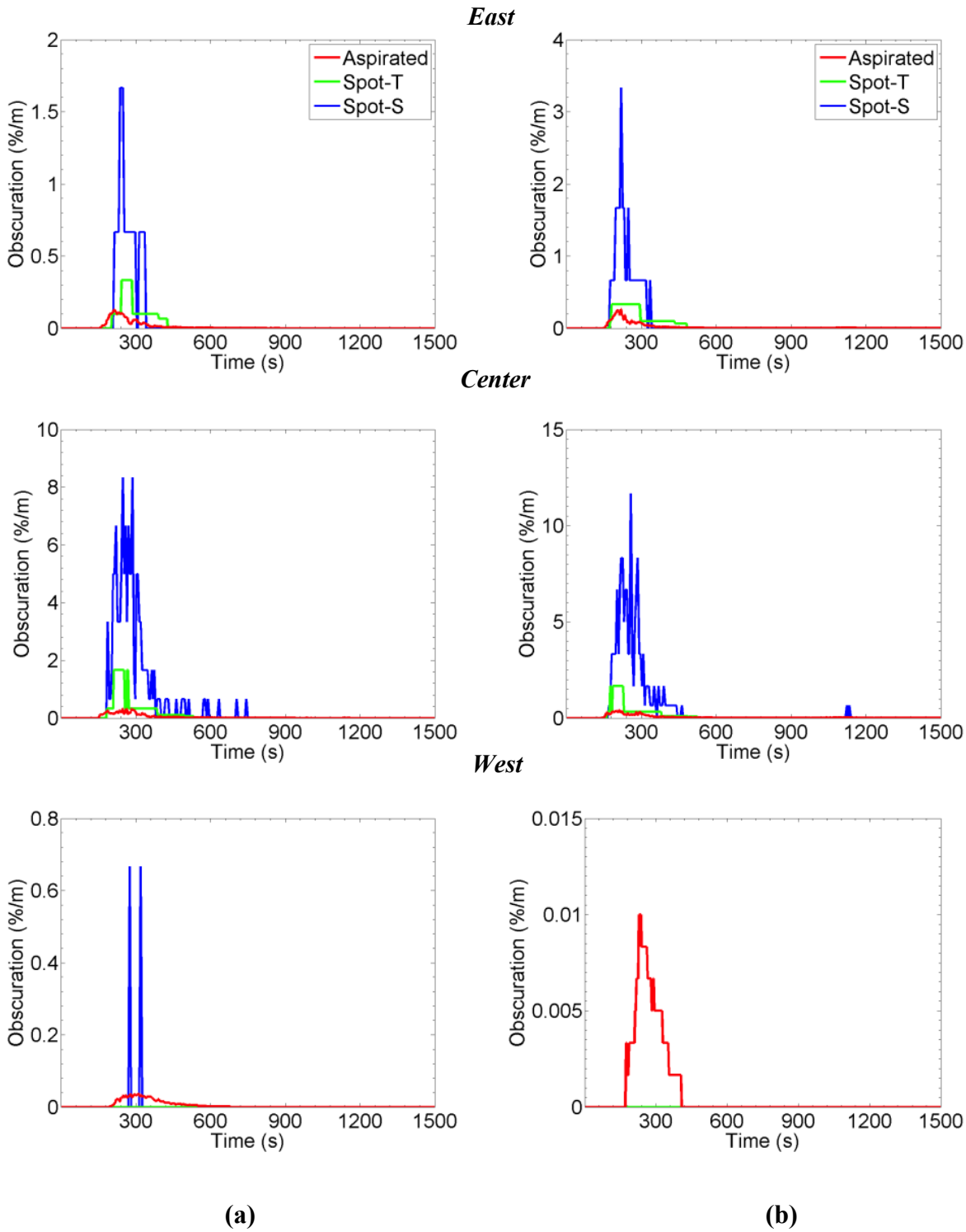

Figure F-9: Detector response in the *Ceiling Plenum* for the circuit board smoke source placed in the cabinets at air exchange rates of (a) 78 ACH and (b) 265 ACH.

F.5 CABLES IN THE SUBFLOOR

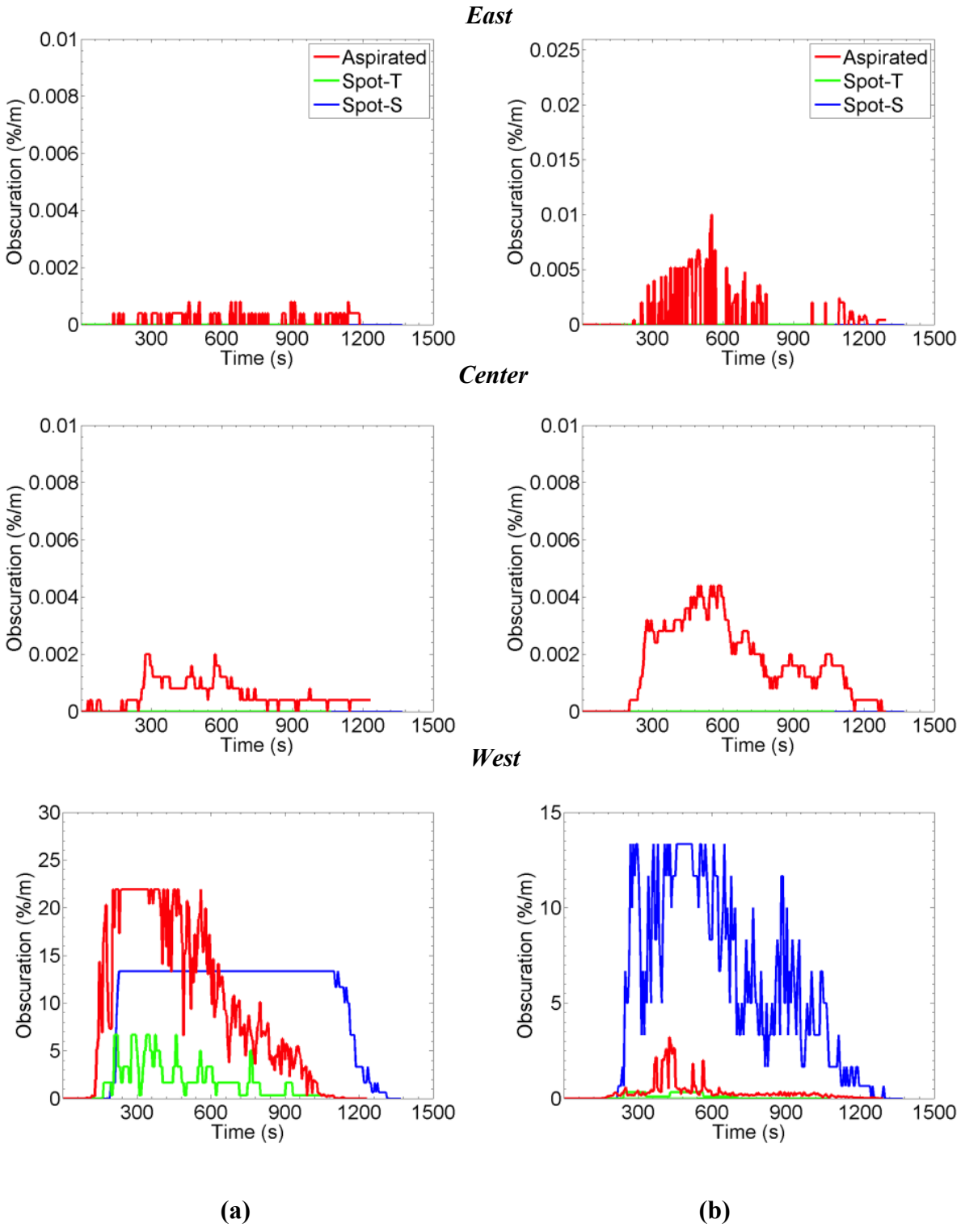

Figure F-10: Detector response in the *Server Room* for the cables smoke source placed in the subfloor at air exchange rates of (a) 78 ACH and (b) 265 ACH.

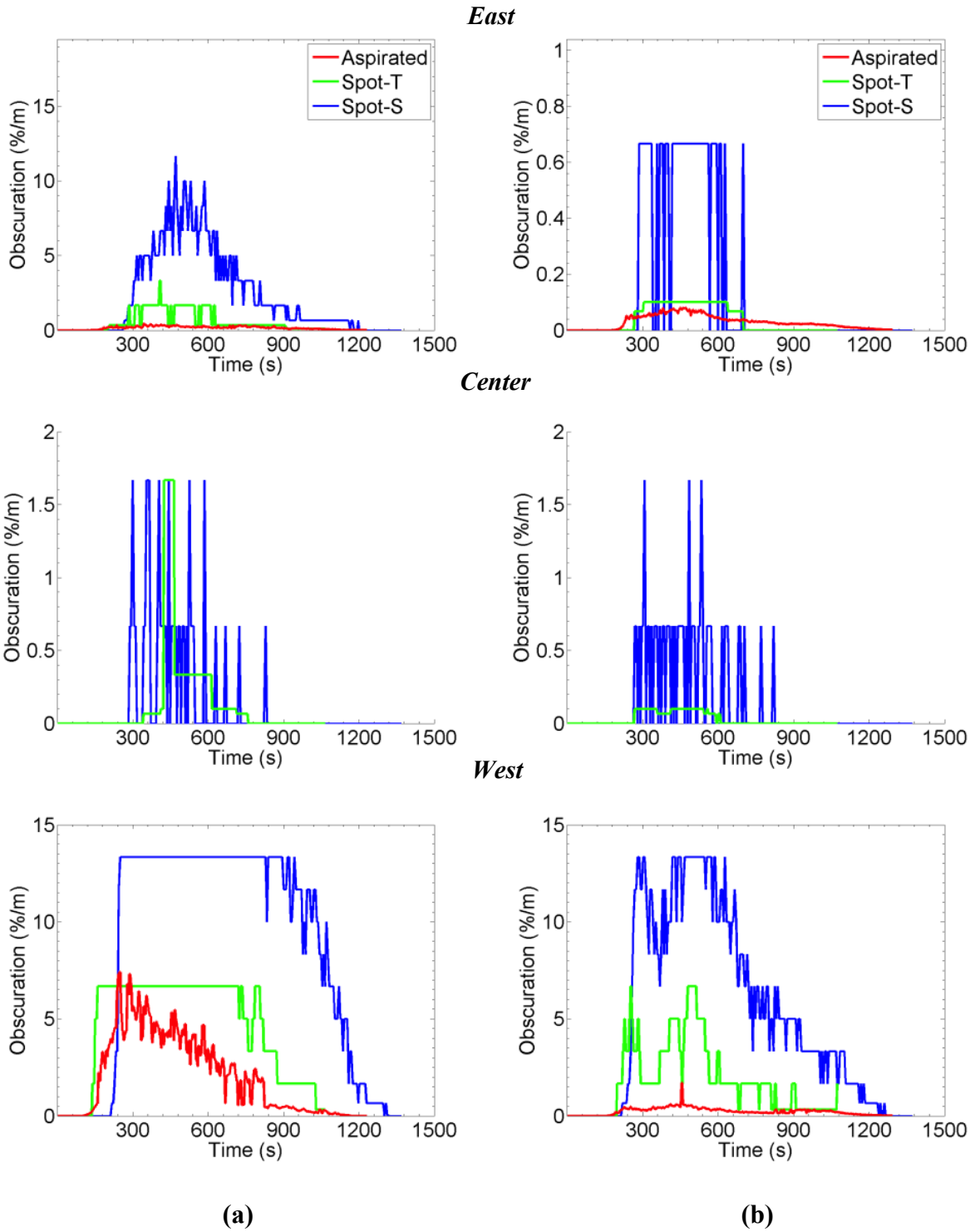

Figure F-11: Detector response in the *Server Room* for the cables smoke source placed in the subfloor at air exchange rates of (a) 78 ACH and (b) 265 ACH.

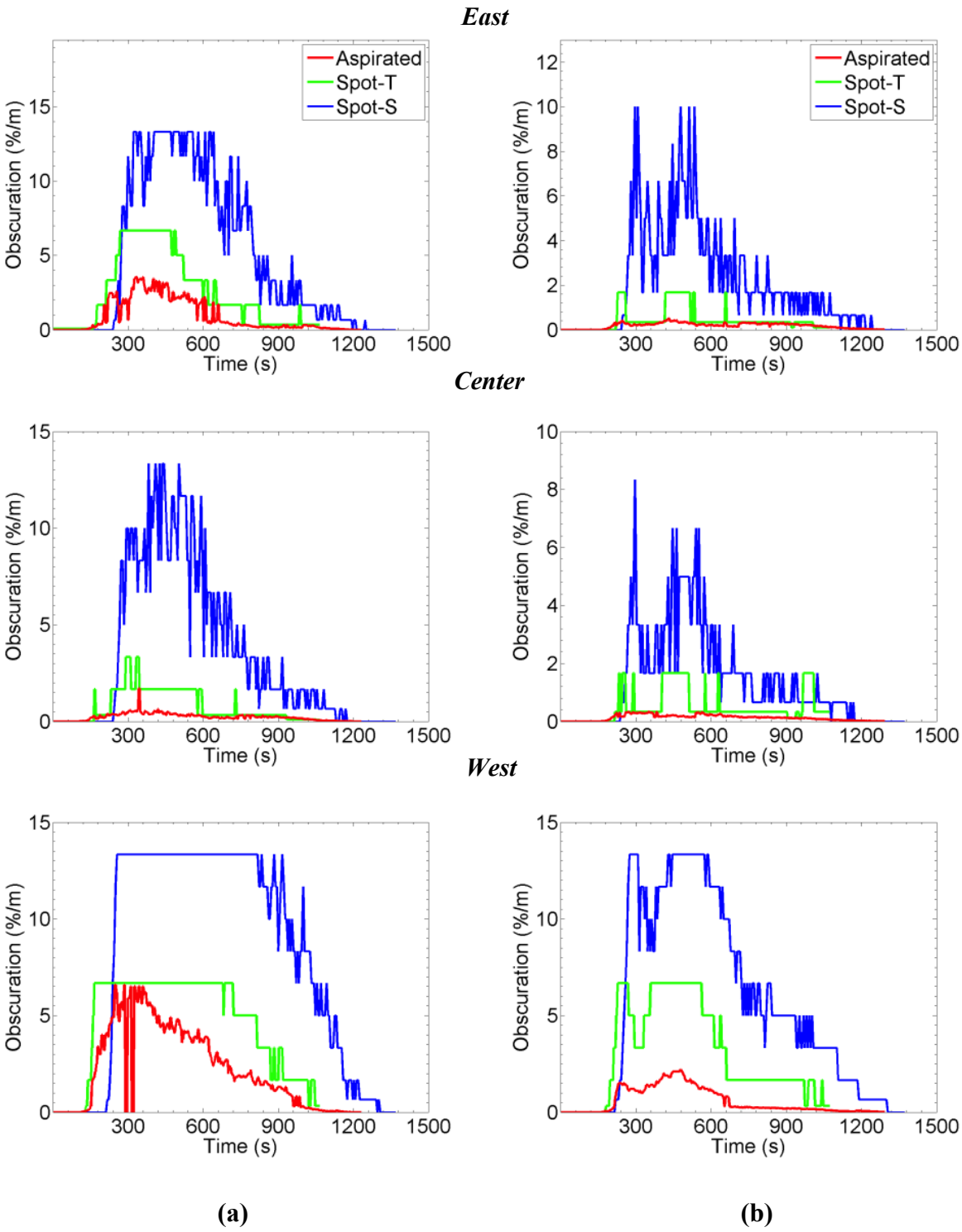

Figure F-12: Detector response in the *Ceiling Plenum* for the cables smoke source placed in the subfloor at air exchange rates of (a) 78 ACH and (b) 265 ACH.

APPENDIX G. ASPIRATED LASER SAMPLING RATE FOR ALL TESTS

Table G-1: Aspirated Laser Sampling Rate

Smoke source type	Smoke source location	Airflow rate (ACH)	Measurement Location	Sampling Rate* (*L/min*)	Sampling Velocity (*m/s*)	Transport Time (s)
Propylene	Hot-Aisle	265	Subfloor	5.67 ± 0.75	0.26 ± 0.03	29
			Hot aisle	25.2 ± 0.75	1.17 ± 0.03	6
			Ceiling plenum	56.6 ± 1.2	2.64 ± 0.06	3
	Hot-Aisle	78	Subfloor	11.5 ± 0.75	0.54 ± 0.04	14
			Hot aisle	10.2 ± 0.75	0.48 ± 0.03	15
			Ceiling plenum	14.3 ± 2.4	0.67 ± 0.11	11
	Hot-Aisle	78	Subfloor	8.94 ± 0.75	0.42 ± 0.03	18
			Hot aisle	11.1 ± 0.75	0.52 ± 0.03	14
			Ceiling plenum	17.1 ± 2.4	0.80 ± 0.11	9
	Subfloor	78	Subfloor	8.54 ± 0.75	0.40 ± 0.03	19
			Hot aisle	12.5 ± 0.75	0.58 ± 003	12
			Ceiling plenum	17.8 ± 2.4	0.83 ± 0.11	9
	Subfloor	265	Subfloor	6.25 ± 0.75	0.29 ± 0.03	26
			Hot aisle	36.3 ± 0.75	1.69 ± 0.03	4
			Ceiling plenum	59.3 ± 1.2	2.76 ± 0.06	3
	Subfloor	265	Subfloor	8.63 ± 0.75	0.40 ± 0.03	19
			Hot aisle	37.5 ± 0.75	1.75 ± 0.03	4
			Ceiling plenum	58.6 ± 1.2	2.73 ± 0.06	3
Foam	Cold Aisle	265	Subfloor	6.64 ± 0.75	0.31 ± 0.03	24
			Hot aisle	36.6 ± 0.75	1.71 ± 0.03	4
			Ceiling plenum	59.7 ± 1.2	2.78 ± 0.06	3
	Cold Aisle	78	Subfloor	9.33 ± 0.75	0.43 ± 0.03	17
			Hot aisle	12.4 ± 0.75	0.58 ± 0.03	12
			Ceiling plenum	19.2 ± 2.4	0.90 ± 0.11	8
Electric cables	Cabinets	265	Subfloor	6.46 ± 0.75	0.30 ± 0.04	25
			Hot aisle	35.9 ± 0.75	1.67 ± 0.03	4
			Ceiling plenum	60.0 ± 1.2	2.80 ± 0.06	3
	Cabinets	78	Subfloor	9.47 ± 0.75	0.44 ± 0.04	17
			Hot aisle	12.9 ± 0.75	0.60 ± 0.04	12
			Ceiling plenum	18.6 ± 2.4	0.87 ± 0.11	8
Cables	Subfloor	265	Subfloor	6.29 ± 0.75	0.29 ± 0.04	26
			Hot aisle	36.5 ± 0.75	1.70 ± 0.03	4
			Ceiling plenum	59.5 ± 1.2	2.77 ± 0.06	3
	Subfloor	78	Subfloor	10.1 ± 0.75	0.47 ± 0.3	16
			Hot aisle	14.1 ± 0.75	0.66 ± 0.03	11
			Ceiling plenum	16.8 ± 2.4	0.78 ± 0.11	9

* Measured in the subfloor and hot aisle with an Omega FMA-1828 mass flow meter and with an Omega FMA-1841 in the ceiling plenum; measurement uncertainty shown in Appendix B.

www.fmglobal.com/researchreports

In the United Kingdom:
FM Insurance Company Limited
1 Windsor Dials, Windsor, Berkshire, SL4 1RS
Regulated by the Financial Services Authority.